Biodegradable Fluidic Microsystems for Cell Cultures and Tissue Engineering

Biodegradeerbare microfluïdische systemen voor celculturen en weefselregeneratie

Diana-Elena Mogosanu

UNIVERSITEIT
GENT

GHENT UNIVERSITY

Promoters
Prof. Dr. Ir. Jan Vanfleteren
Center for Microsystems Technology (CMST)

Prof. Dr. Peter Dubruel
Polymer Chemistry and Biomaterials (PBM)

Members of the Examination Committee

Prof. Dr. Ir. Luc Taerwe Chairman
Ghent University

Dr. Astrid Bakker
Amsterdam University

Dr. Ir. Rik Verplancke Secretary
Ghent University

Prof. Dr. Ir. Heidi Ottevaere
Vrije Universiteit Brussel (VUB)

Prof. Dr. Ir. Peter Bienstman
Ghent University

Prof. Dr. Sandra Van Vlierberghe
Vrije Universiteit Brussel (VUB),
Ghent University

Prof. Dr. Ir. Erwin Bosman
Ghent University

Prof. Dr. Maria Cornelissen
Ghent University

A Dissertation Submitted in Fulfillment of the Requirements for the
Degree of Doctor of Biomedical Engineering
Academic Year 2016–2017

Acknowledgments

The time dedicated to the current PhD work was most rewarding as I experienced both professional and personal growth. First and foremost, I would like to thank my supervisors, Jan Vanfleteren and Peter Dubruel, for giving me this amazing opportunity. I am grateful for their knowledge, guidance and encouragements throughout this period, as well as for the great freedom in planning and following different research ideas. I feel honored to have worked in their research groups, namely Center for Microsystem Technology (CMST) and Polymer Chemistry and Biomaterials (PBM). Special thanks are in order for Rik Verplancke, my guiding post-doc in the technology department. His professional advice and kindness are invaluable and deserve my complete gratitude.

I would also like to thank the jury members for the time and efforts put in reading this book and providing essential feedback. This PhD was financially supported by the Research Foundation-Flanders (FWO, Belgium) which I gratefully acknowledge (Research Grant "Biodegradable fluidic microsystems for cell cultures and tissue engineering", grant number G092511N).

I would like to acknowledge my collaborators: Catherine Verfaillie, Yonsil Park and Ruben Boom for the initial cell tests; Sangram, Mieke, Diana G, Diana D., Giusseppe, Annemie, Kenny, Timothy and Sheila for their help with writing and editing the book chapters I (co-)authored; Thijs, Astrid and Elien for performing the much needed cell tests, and Lucila for the work on the material synthesis during her internship at PBM. Another person I would like to thank is Sandra Van Vlierberghe; although she was not my supervisor, she helped me whenever I needed it.

All my colleagues deserve warm thanks for the stimulating discussions and for all the fun we have had in the last years. I feel I should name all my colleagues, as they all had a certain influence either on my work or on my spirit ☺ at some point. This is not practical within this thank you note, as I have over 90 colleagues (60 in CMST, 33 in PBM). I personally believe that although with some of them I did not exchange many words or I did not spend too much time, they equally contributed to the finality of this thesis

by bringing their own contribution to the groups' management, organization and overall functioning. We are all whole parts of a whole unity.

From CMST, I would like to mention my office colleagues Bjorn, Lieven, Frederik, Thomas, Bart and Philip. They created a nice, enjoyable and much-needed-quiet environment (when compared to the lab/clean room). My sincere thanks also go to Sandeep, who kindly welcomed me in my first day in CMST and helped me by taking me to the UGent administration building and showing me the city of Ghent. Sheila was the first lady I "clung" to when I first arrived in CMST. By then there were only 4-5 women out of a total of around 45 persons. I have enjoyed her company and highly positive and contagious spirit; I thank her for that. I would also like to acknowledge David for his expertise and with whom I had interesting discussions, both professionally and about life in general. I have enjoyed the company of Sandeep, Sanjeev, Nuria, Pankaj, Bram, Imen, Andres, Jindrich, Tom and Jeroen in the frame of organizing activities for the SPIE-UGent student chapter and for their nice company in general. I would like to thank Dieter, Steven, Peter G. and Filip[2] for their assistance with some of the experiments performed; and, of course, Katrien for essential administrative help.

From PBM, I would like to give my thanks to an ex-colleague, Tom Parlevliet whose help in my first weeks of living in Belgium with papers etc. was extremely appreciated. I am sure his kindness will not go unrewarded. Also, Veerle was always extremely nice and helpful even if her workload was at times too much. "My girls", Diana G, Didi, Mamoni, Els, Elke and Myriam, gave me a feeling of belonging for which I am grateful. Warm talks and nice times I also had with Olga and Adelaide. So many memories together! I feel privileged to have met you all. Thank you for being there for me, workwise and otherwise ☺. Geert-Jan, Arn, Jasper and Maxime, my congrats for coping with all the estrogen in the PBM group. I really appreciate the nice and fun moments we had together.

I would like to thank Ismail and Haliima for their support, love and friendship and for offering me a stress-free environment – much needed during a PhD- in which I could recompose myself every time it was necessary.

And last but definitely not least, I would like to acknowledge my parents and my brother for their love and for offering me the appropriate conditions for my development and supporting me throughout life in general. Their guidance and early "push" towards studying led to the current achievements, for which I am grateful.

The PhD topic presented herein also facilitated the reflection on the complexity of human body and life in general. During these four years I have realized the beauty and perfection of life.

GLORIA IN EXCELSIS DEO

Contents

List of abbreviations

2D - 2-dimensional

3D - three-dimensional

^{1}H-NMR - Proton nuclear magnetic resonance

µTAS - micro total analysis system

AEMA - 2-aminoethyl methacrylate

ADF - annular dark-field

AFM - atomic force microscopy

ATR-IR - attenuated total reflectance/Fourier transform infrared

BEC - backscattered electron composition image

BF - bright-field

CAD - computer-aided

CDCl3-d$_6$ – deuterated chloroform

COC - cyclic olefin copolymer

CO_2 – carbon dioxide

CS - chondroitin sulfate

DCM – dicholomethane

DES - drug eluting stents

DMSO-d6 - deuterated dimethylsulfoxide

DSC - differential scanning calorimeter

E - Young's modulus

ECM - extracellular matrix

EDC - 1-ethyl-3(-3-dimethylaminopropyl) carbodiimide hydrochloride

EDX - energy dispersive x-ray analysis

FDA - Food and Drug Administration

FT-IR - fourier-transform infrared

GAGs - glycosaminoglycans

GelB - Gelatin type B

GPC - gel permeation chromatography

hASCs - human adipose-derived stem cells

HepG2 - human liver hepatocellular carcinoma cell line

HFIP – hexafluoroisopropanol

HuH7 - differentiated hepatocyte derived cellular carcinoma cell line

LADs - Liver Assist Devices

LOC - lab-on-a-chip

MeOH – methanol

MEMS - microelectromechanical systems

PBS - phosphate-buffered saline

PC - polycarbonate

PCL - poly (ε-caprolactone)

PDI – polydispersity

PDMS - poly (dimethylsiloxane)

PEG - poly(ethylene glycol)

PES - poly (erythritol sebacate)

PES-DS - poly (erythritol sebacate)-derived with decanediol

PES-PS - poly (erythritol sebacate)-derived with propanediol

PET - polyethylene terephthalate

PGA - polyglycolide

PGS - poly (glycerol sebacate)

PGSC - poly(glycerol-sebacate-citrate)

PGS-DS – poly(glycerol sebacate)-derived with decanediol

PGS-PS – poly(glycerol sebacate)-derived with propanediol

PLA - poly lactic acid

PLGA - poly lactide-co-glycolide

PLLA - poly (L-lactic acid)

PMMA - poly (methylmetacrylate)

PMNs - polymorphonuclear leukocytes

PP - polypropylene

PPS - poly (polyol sebacate)s

PTCA - Percutaneous transluminal coronary angioplasty

PVB - polyvinyl butyral

Ref. - reference

SCA - static contact angle

SEM - scanning electron microscope

SU8 - epoxy-based negative photoresist with 8 epoxy groups

THF - tetrahydofuran

TGA - thermogravimetric analyzer

TE - tissue engineering

T_g - rubber transition temperature

T_m - the melting temperature

T_c - crystallization temperatures

TEM - transmission electron microscopy

UV - ultraviolet

WHO - World Health Organization

XPS - X-ray photoelectron spectroscopy

Summary

In the last two decades, a multidisciplinary approach on the delivery of cells to the body has advanced. On the one hand, the science of polymers focuses on the development of biocompatible materials for cell culturing and tissue engineering applications, while on the other hand (micro-)engineering has an important part in providing a specific topography that directs the cells and provides a more similar architecture to that of tissues. Soft and flexible elastomers have gained more and more interest, especially due to their biodegradability and tunable mechanical properties that can mimic the natural tissue. Herein, we report the design of novel poly(polyol sebacate) elastomers synthesized from monomers found within the human metabolism. The thermoset properties of these polymers as well as their optical transparency make them ideal materials for microsystems technology. Therefore, microfluidic devices were developed out of these polymers in order to facilitate the design of a tissue-engineered organ. A porous membrane was inserted in the microfluidic device to enable co-culture and distribution of nutrients to the cells. Furthermore, the reported polymers and microfluidic structure can serve a multitude of applications, from tissue engineering to point-of-care diagnostics or compound screening.

The field of tissue engineering, pioneered by Robert Langer and his co-workers, combines the principles and methods of engineering and the life sciences towards the development of biological substitutes that restore, maintain, or improve tissue function. The new developments on the various strategies of tissue engineering (TE) are aiming to understand the complexity of tissue remodeling and the inter-dependency of many associated variables. This clearly makes it a highly multi-disciplinary field that combines the expertise of different areas. Material scientists, engineers and biologists, in this regard form an important triad. *Materials science* focuses on the synthesis and characterization of required materials for the *engineers* to design the material in a way that it resembles the internal structure of the respective tissue or organ. Herein, the role of *biologists* becomes important who provide knowledge on how to introduce cells in these systems in order

to support their proliferation and differentiation into a specific tissue. Thus, a (bio)material is developed.

For further construction of bio(materials) as implantable tissue structures, the development of three-dimensional (3D) fluidic microsystems for cell culturing has become a necessity. Microfluidic technology offers a controlled environment, reduced reagent consumption and precision, promising an alternative for conventional biological laboratory methods. These microsystems involve the manipulation of small amounts of fluids using channels with dimensions at a micron level. Their specificity and flexibility is beyond the one of normal well plates or two-dimensional cell culturing films due to the ability to handle co-culture systems or to encompass from millions of cells to single cells, depending on a specific application.

In this context, the aim of the present work is to combine the knowledge of different fields of research in order to pave the way in the direction of 3D biodegradable fluidic microsystems for cell culturing and tissue engineering. The focus is laid on the development of biodegradable 3D microfluidic systems that can eventually sustain cell culturing and proliferation with subsequent tissue formation. Liver tissue is chosen as a model for the developed technology due to its complex structure that contains two main cell types, namely hepatocytes and endothelial cells, displaced in a three-layer architecture. The proposed research aims to overcome the shortcoming of the existing methods or technologies available worldwide, allowing the fabrication of such complex biodegradable microsystems.

The layout of the thesis is divided into different chapters that discuss specific topics towards the achievement of the final research objective. The multi-disciplinary aspect and collaboration between the different fields with varied competences is presented in Chapter 1.

The synthesis and characterization of novel poly(polyol sebacate)-derived elastomers is reported in Chapter 2. Poly(polyol sebacates) are thermoset materials and possess several characteristics such as biocompatibility, biodegradability, optical transparency etc. that makes them a good choice for developing microfluidic bioreactors. These polymers are approved by the

U.S. Food and Drug Administration (FDA) for use in tissue engineering and implant applications. Details on the synthesis and characterization of the obtained pre-polymers are discussed in this chapter. Furthermore, as synthetic biomaterials that mimic the ECM have a wide range of biomedical applications, one of the polymer films was also functionalized with gelatin via a chemical immobilization technique that has never been applied up to now for poly (polyol sebacate)s. This comes as an improvement to the already existing physio-sorbtion methods that lead to protein removal from the material.

Chapter 3 presents the use of the scaffolding technique of electrospinning for the development of porous structures. These scaffolds provide the three-dimensionality cells need in order to differentiate and maintain the specific phenotypic expression, as they mimic the extracellular matrix and are included in a later step of the final microsystem technology. The scaffolds developed in this chapter can stand alone as cell delivering porous membranes and can serve various applications, from soft to hard tissue engineering. Other enabling applications of these types of scaffolds such as cardiovascular tissue engineering are also mentioned.

Microfabrication technology is an interesting tool used to impart a specific topography and is presented in Chapter 4. The technology developed herein comprises of a complex 3D architecture for microfluidic environments that can be potentially used in tissue engineering applications, such as in the design of a tissue-engineered organ. As vital organs contain multiple types of cells, a porous membrane prepared by a classical scaffolding technique (i.e. electrospinning) has been integrated in the microfluidic devices. This strategy would enable not only cell (co-)culture, but also distribution of nutrients and oxygen.

In Chapter 5 the biocompatibility of the developed materials and electrospun structures is evaluated with different cell lines, demonstrating their non-cytotoxicity and potential for liver tissue engineering.

In conclusion, a perspective on the synthesized polymers and their utility in microsystem technology is presented. The presented technology possesses

the ability to relate to a variety of applications and can be easily transferred to all poly(polyol sebacates) present in literature. The unique feature of the developed microfluidic devices is the porous membrane that would impart the 3-dimensionality that cells need to grow, while the microchannels will guide the cells and align them in a specific way as to better mimic the native tissue.

Samenvatting

In de laatste twee decennia is een multidisciplinaire aanpak van de afgifte van cellen in het lichaam opgekomen. Enerzijds is er de polymeerwetenschap die zich richt op de ontwikkeling van biocompatibele materialen voor celculturen en weefselregeneratietoepassingen. En anderzijds is er de (micro)-ingenieurswetenschap die een belangrijke rol speelt in het voorzien van een specifieke topografie. Deze topografie stuurt de cellen en biedt een structuur die gelijkaardig is aan die van weefsels. Zachte en flexibele elastomeren kregen meer en meer belangstelling, vooral door hun biodegradeerbaarheid en afstembare mechanische eigenschappen die het natuurlijk weefsel kunnen nabootsen. In dit proefschrift wordt de ontwikkeling van nieuwe poly-(polyol sebacaat) elastomeren, gesynthetiseerd uit monomeren afkomstig het menselijk metabolisme, beschreven. De thermohardende eigenschappen van deze polymeren alsook hun optische transparantie maken dat ze ideale materialen zijn voor microsysteemtechnologie. Bijgevolg werden microfluïdische systemen ontwikkeld uitgaande van deze polymeren, met als doel het ontwerp van een weefselgeregenereerd orgaan te vergemakkelijken. Een poreus membraan werd aangebracht in het microfluïdisch systeem om co-kweken en de toelevering van voedingsstoffen aan de cellen mogelijk te maken. Bovendien kunnen de beschreven polymeren en microfluïdische structuur dienen voor een brede waaier aan toepassingen, gaande van weefselregeneratie tot 'point-of-care' diagnostiek.

In het veld van weefselregeneratie, met Robert Langer en zijn medewerkers als baanbrekers, worden meerdere principes en methodes uit de ingenieurs-

en bio-wetenschappen samengebracht om biologische substituten te ontwikkelen die weefselfuncties kunnen herstellen, onderhouden of verbeteren. De nieuwe ontwikkelingen binnen weefselregeneratie zijn gericht op het beter begrijpen van de complexiteit die samengaat met de weefselreconstructie, en de onderlinge afhankelijkheid van de vele bijhorende variabelen. Dit maakt het duidelijk een multidisciplinair veld. Materiaalwetenschappers, ingenieurs en biologen vormen in dit verband een belangrijk triade. De *materiaalkunde* richt zich op de synthese en de karakterisering van de benodigde materialen, die de *ingenieurs* op zo'n manier structureren dat ze lijken op de interne structuur van het respectievelijke weefsel of orgaan. Hierin is de rol van de *biologen* niet te miskennen. Zij verschaffen de kennis om cellen in deze systemen te introduceren, en om hun proliferatie en differentiatie te ondersteunen tot een specifiek weefsel zich vormt. Aldus wordt een (bio)materiaal ontwikkeld.

Voor de constructie van (bio)materialen als implanteerbare weefselstructuren, is de ontwikkeling van driedimensionale (3D) microfluïdische systemen voor celculturen een noodzaak geworden. Ze bieden een gecontroleerde omgeving waarin met meer precisie en een verminderd verbruik van reagentia gewerkt kan worden. Zo vormen ze een uitstekend alternatief voor de conventionele methoden die momenteel gebruikt worden in de biologische labo's. In deze microsystemen worden kleine hoeveelheden vloeistof gemanipuleerd via microscopisch kleine kanaaltjes. Hun specificiteit en flexibiliteit overtreft die van gebruikelijke 'well plates' of tweedimensionale films voor het kweken van cellen omdat ze de mogelijkheid bieden om diverse celtypes te co-kweken. Bovendien kunnen ze, afhankelijk van de toepassing, individuele tot miljoenen cellen bevatten.

Het doel van het huidig werk bestaat erin de kennis van de verschillende onderzoeksdisciplines te combineren om de tekortkomingen van de bestaande methoden en technologieën te verhelpen waardoor de constructie van driedimensionale, biologisch afbreekbare microfluïdische systemen voor celculturen en weefselregeneratie mogelijk wordt. Deze systemen zullen dus uiteindelijk celculturen onderhouden en hun proliferatie

stimuleren tot een weefsel gevormd wordt. Leverweefsel werd gekozen als model voor de ontwikkelde technologie omwille van zijn complexe structuur. Dit weefsel bevat twee celtypes, namelijk hepatocyten en endotheelcellen, die in een drielaagse architectuur zijn georganiseerd.

Dit proefschrift bestaat uit verschillende hoofdstukken waarin de specifieke onderwerpen ter verwezenlijking van het uiteindelijke onderzoeksdoel besproken worden. Het multidisciplinair karakter en de samenwerking tussen de verschillende onderzoeksgebieden met hun respectievelijke competenties worden besproken in hoofdstuk 1. Aangezien synthetische biomaterialen, die de ECM nabootsen, een brede waaier aan biomedische toepassingen hebben, werd bovendien één van de polymeerfilms ook gefunctionaliseerd met gelatine. Hiertoe werd een chemische immobiliseringstechniek aangewend die tot nu toe nog nooit werd toegepast voor poly-(polyol sebacaat) polymeren. Dit is een verbetering ten opzichte van de reeds bestaande fysisorptie methoden die leiden tot verwijdering van proteïnen van het materiaal.

De synthese en de karakterisering van nieuwe poly-(polyol sebacaat) afgeleide elastomeren wordt beschreven in hoofdstuk 2. Poly-(polyol sebacaten) zijn thermohardende materialen en bezitten verscheidene eigenschappen zoals biocompatibiliteit, biodegradeerbaarheid, optische transparantie etc., wat hun een goede keuze maakt voor de ontwikkeling van microfluïdische bioreactoren. Deze polymeren werden reeds goedgekeurd door de Amerikaanse Food and Drug Administration (FDA) voor gebruik in weefselregeneratie en implantaten. De synthese en de karakterisering van de verkregen pre-polymeren worden in detail besproken in dit hoofdstuk.

In hoofdstuk 3 wordt het gebruik van de techniek electrospinning besproken voor het ontwikkelen van poreuze draagstructuren. Deze draagstructuren bieden de driedimensionaliteit die cellen nodig hebben om hun differentiatie en specifieke phenotypische expressie te behouden. Ze worden opgenomen in een latere stap van de uiteindelijke microsysteemtechnologie. De draagstructuren ontwikkeld in dit hoofdstuk kunnen op zichzelf staan als poreuze membranen die cellen afleveren, maar kunnen ook van nut zijn voor verschillende toepassingen, gaande van zachte tot harde

weefselregeneratie. Andere mogelijke toepassingen voor dit soort draagstructuren worden ook aangehaald, zoals bvb. cardiovasculaire weefselregeneratie.

Microfabricagetechnologie is een interessant hulpmiddel dat toelaat om de materialen een specifieke topografie te geven. Dit wordt besproken in hoofdstuk 4. De hierin ontwikkelde technologie leidt tot een complexe driedimensionale architectuur voor microfluïdische omgevingen. Deze kunnen dan gebruikt worden in toepassingen zoals weefselmanipulatie, bvb. bij het ontwerpen van een weefselgeregenereerd orgaan. Omdat vitale organen meerdere celtypes bevatten, werd een poreus membraan bereid volgens electrospinning en geïntegreerd in de microfluïdische systemen. Deze strategie zou niet alleen de (co-)cultuur van cellen mogelijk maken maar bevordert ook de toevoer van nutriënten en zuurstof.

In hoofdstuk 5 wordt de biocompatibiliteit van de ontwikkelde materialen en structuren, bekomen via electrospinning, geëvalueerd door middel van verschillende cellijnen. Zowel hun niet-cytotoxiciteit als hun potentieel voor de constructie van leverweefsel worden gedemonstreerd.
Tot slot wordt een perspectief geboden op de gesynthetiseerde polymeren en hun toepasbaarheid in microsysteemtechnologie. De voorgestelde technologie kan aangewend worden voor verschillende toepassingen en kan makkelijk overgedragen worden op alle poly-(polyol sebacaten) die vermeld worden in de literatuur. De unieke eigenschap van de ontwikkelde microfluïdische systemen is het poreuze membraan dat de driedimensionale structuur voorziet die cellen nodig hebben om te groeien, terwijl de microkanaaltjes de cellen kunnen leiden en op een specifieke manier kunnen organiseren om het natuurlijke weefsel beter na te bootsen.

Chapter 1: Introduction

1.1.   Motivation and Objectives

Liver diseases that lead to liver failure are becoming one of the most common causes of death in the world. The World Health Organization (WHO) estimated that by 2016 approximatively 1.800.000 people will die due to liver disease, while by 2030 this number will reach around 2.500.000 [1]. These alarming facts, together with the limited amount of liver organs available for transplantations, led to alternative approaches such as extracorporeal devices [2-4], stem cell therapy [5, 6], or artificial liver devices [7, 8]. Tissue engineering uses cell biology, material science and engineering methods in order to develop biological substitutes to improve, replace or regenerate biological functions [9]. In the case of liver tissue engineering, the investigated cells used are stem cells, hepatocytes [10, 11], endothelial cells [12, 13] and co-culture systems [14, 15]. The materials used to deliver or/and to sustain the growth of these cells have to possess special properties such as biocompatibility, biodegradability and immunological inertness. The material design is also essential as the scaffold architecture offers specific shapes, increased surface area and therefore play an important role in cell survival, morphogenesis, and function [14, 16].

The primary goal of the present work is to develop biodegradable and biocompatible platforms/scaffolds for liver regeneration. For this purpose, a novel three-dimensional microsystem bioreactor is proposed. The bioreactor is desired to be biocompatible, such that it can present the possibility to be implanted in the human body. Biodegradation is another key-aspect of the microsystem. As the final application is the growth of liver tissue inside the bioreactor, a short degradation time of three months is desired. In this context, the steps required to achieve this goal are: the synthesis of new synthetic biodegradable and biocompatible materials that can be processed via microfabrication techniques; the fabrication of a porous membrane that can provide the 3D space in which the liver cells can proliferate and

differentiate; and the development of the final bioreactor from the assembly of above mentioned materials and membranes.

As soft elastomers have become widely used in diverse soft tissue engineering (TE) applications such as liver TE, the synthesis of poly (erythritol sebacate) (PES) is initially considered. This material belongs to the same material class as poly (glycerol sebacate) (i.e. the biorubber) [17], with the difference that the sugar alcohol used is erythritol instead of glycerol. The reaction between erythritol and sebacic acid was previously reported [18], but some important characterization aspects such as degradability and cytotoxicity behavior were lacking. Therefore, the development of derived poly(polyol sebacates) starting from glycerol and erythritol that could offer diverse bulk and surface properties is targeted. This class of elastomers was chosen for its relatively fast degradation time (i.e. two months *in vivo*), biocompatibility, flexibility and optical transparency, the latter requirement being important especially during the microfabrication of the final bioreactor.

Microfabrication and microelectromechanical system technology are micro-engineering methods designed to shape materials such that a good spatial resolution is obtained [19]. Up to now, most of the developed microfluidic bioreactors were created by essentially two ways: either bonding a patterned layer on top of a flat one [20], or by stacking and bonding single-layer microfluidic networks [21]. Microfabrication technology is basically a 2-dimensional (2D) technique that generates patterns on 2D surfaces, and therefore it limits its use in the study of surface morphology effects on cell growth [22]. Another limitation consists in the hypoxic oxygen concentrations that arise from the use of polymer thicknesses over 200 µm and that further restricts the maximum thickness of the engineered tissue [20]. In order to counteract these limitations, the integration of a porous membrane in between two micro-patterned microfluidic layers is proposed. To the best of our knowledge, this unique strategy has not been reported for biodegradable microfluidics.

Electrospinning is the chosen traditional scaffold fabrication technique used to create the porous membrane that is to be placed in between the

patterned microfluidic layers of the final bioreactor. Its purpose is to provide cell support, cell-to-cell interaction thus mimicking the extracellular matrix (ECM). In microfluidic systems, it provides solution to the oxygen diffusion limitations imparted by microfluidic membranes with thicknesses exceeding 200 μm [20]. Electrospun membranes have found applications in microfluidic systems, biosensors and lab-on-a-chip devices [23]. Most of the applications involve point-of-care diagnostics or tissue engineering and regenerative medicine. Up to now, the membranes consisted of polyvinylidene difluoride [24], track-etched polycarbonate [25], polystyrene [26], polyurethane [27], polyvinylpyrrolidone and incorporated into poly (dimethylsiloxane) (PDMS) or poly (methylmetacrylate) (PMMA). In the context of tissue engineering and regenerative medicine, the ability to manipulate the cell microenvironment is important in achieving an *in vitro* organ model. Therefore, it is preferable that the system comprises of materials that are easily biodegradable in order to minimize the foreign body response. Moreover, due to the usual small dimensions of the microsystem bioreactor (i.e. 100 μm width, 100-200 μm height) the electrospun membrane is desired to have a thickness of a few tens of microns (i.e. 20μm) and to be transparent enough for the final alignment in between the patterned microfluidic layers.

In the present dissertation, a biocompatible system is proposed for which both the membrane and the microfluidic materials are biodegradable. The microfluidic devices were fabricated of biodegradable and biocompatible elastomers, poly (glycerol-sebacate) (PGS) and poly (erythritol-sebacate) (PES) that serve as a proof of concept, that the developed technology in this work can be transferred to all poly (polyol sebacate)s. The membrane consisted of either poly (L-lactic acid) or a combination of this polymer with the synthesized elastomer poly (erythritol sebacate). The combination of traditional scaffold fabrication (i.e. electrospinning) and microfabrication techniques is *hypothesized* to provide the needed platform to create complex *in vitro* environments that allow the culture of multiple cell types, and oxygenation and nutrients diffusion to the cells.

1.2. Biomaterials in Tissue Engineering

Nowadays there is a growing interest from the scientific and industrial world for cell culturing and tissue engineering. A stringent need of producing and using more complex tissues with different types of cells and with a more complex 3-dimensional (3D) structure drives researchers to study biomaterials and imprint novel designs using different tools [28-31]. Tissue engineering has different approaches for the development of a biological substitute, such as: the use of cells or the delivery of tissue-inducing substances at the targeted location and growing cells in three-dimensional scaffolds [32]. Amongst these, the latter is one of the most popular as the first mentioned paths present serious restrictions such as shape and size limitation as well as poor control over the cells. The schematic representation of one of the tissue engineering approaches is depicted in Figure 1.1. More specifically, the process starts by isolating cells from a donor that are further cultured under controlled conditions in a biocompatible scaffold. The obtained cell/scaffold construct is then implanted/delivered in the patient's body at the specific location.

According to the European Society for Biomaterials, a biomaterial is a "material intended to interface with biological systems to evaluate, treat, augment or replace any tissue, organ or function of the body" [33]. In nature, the equivalent for a biomaterial is the extracellular matrix (ECM). It is secreted by resident cells and supports tissue and organs. The ECM provides physical support and spatial organization, as well as an interactive microenvironment that supports and promotes cellular functions [34, 35]. Therefore, there is a continuous bidirectional cross talk between the cells and the surrounding ECM [36]. Due to the fact that the ECM contains structural proteins (e.g., collagen and elastin), cell adhesion proteins (e.g., fibronectin and laminin), and glycans (e.g., glycosaminoglycans (GAGs) and proteoglycans), a great number of investigated materials for tissue engineering are natural polymers.

These include protein-based biomaterials such as collagen, gelatin and silk [37] or polysaccharide-based biomaterials like cellulose, chitin/chitosan,

glucose [38, 39]. Although natural materials have been applied to create tissue engineered scaffolds due to their biocompatibility and low foreign body reaction, natural materials possess important limitations such as the difficulty in controlling their mechanical properties and degradation rates. Synthetic biomaterials, on the other hand, are the preferred option because they are cheaper to fabricate in large quantities, have a longer shelf life and they have tunable properties. All these characteristics make the synthetic materials more pliable for a wide range of applications. Synthetic polyesters are well-investigated materials for scaffold production due to the fact that they can be designed into various shapes and pore features [40]. Nevertheless, synthetic materials can pose biocompatibility issues as their ability to induce tissue remodeling or regeneration by themselves is low. For this purpose, this type of polymers can be functionalized with different chemical groups such that either the surface chemistry or the bulk properties are tailored for specific applications.
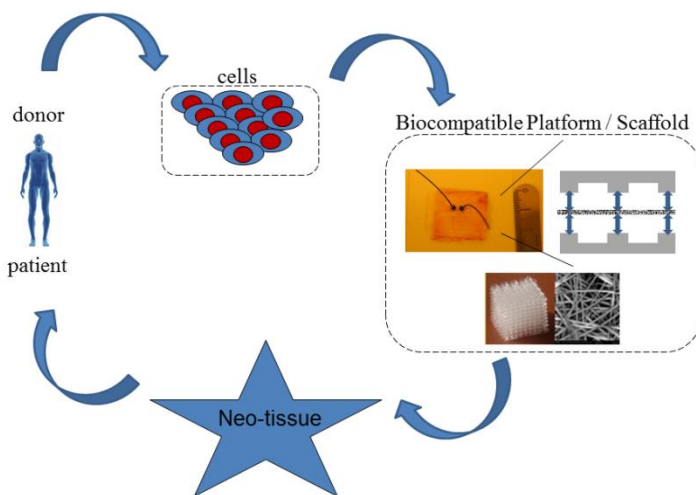

Figure 1.1: Schematic representation of a tissue engineering approach

For liver TE, poly (ε-caprolactone) or PCL is a well-known polymer that has attracted attention from both research world and industry due to its biocompatibility, structural stability and capacity to form blends with a large number of other polymers [41-43]. One of the first bioresorbable polymers

synthesized by Van Natta and his colleagues in the 1930s [44], PCL has appealing properties such as very low glass transition temperature (-60°C), low melting temperature (≈ 60°C) and high thermal stability [45]. These attributes make this polymer suitable for a large range of applications, from the medical and pharmaceutical sectors to packaging and microelectronics [46]. The initial biomedical objectives of PCL were the development of controlled drug release carriers and of absorbable surgical sutures. In the 1980s, the need for polymers with faster degradation rates led to decreased interest towards PCL, which can take up to several years to degrade [47]. Therefore, more easily resorbable polyesters like polyglycolide (PGA), poly lactic acid (PLA) and their copolymers, poly lactide-co-glycolide (PLGA), gained popularity [48]. Their mechanical properties are dependent on molecular weight, polydispersity index and degree of crystallinity, while the degradation rates depend on the monomer composition ratio. For example, PLGA polymers with more lactide units in their composition are more hydrophobic and degrade more slowly due to the methyl side groups in PLA [49]. Higher content of PGA leads to faster degradation, with the exception of PLGA with a monomer ratio of 50/50 which exhibits the fastest degradation [50].
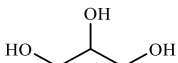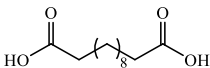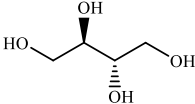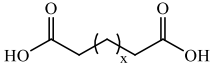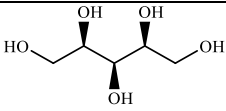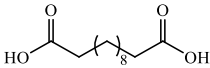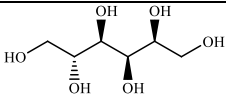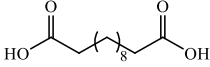
Polyurethanes are other materials with great diversity of chemical compositions and mechanical properties [51]. The polyurethane structure is composed of isocyanates and bi- or poly-hydroxy functional groups. Additional chain extenders can be added to the chemical structure leading to rigid segments. The versatility of these type of materials comes from the fact that they can be either thermoplastics (i.e. becomes soft when heated and hard when cooled) or thermosets (material that, once cured, it irreversibly maintains its form), depending on the chemistry used. The use of components with two functionalities (i.e. diisocyanate and bi-functional polyols) leads to thermoplastic materials, while more than two functional groups lead to three-dimensional chemical crosslinking. Polyurethanes have been studied for soft tissue engineering such as liver TE [52, 53] and cardiovascular TE since the 1990s, but they present disadvantages such as susceptibility to hydrolytic, oxidative and enzymatic degradation in vivo [54].

Although the above mentioned polymers and many others have been evaluated for their suitability to create an implantable tissue engineered liver, in the last decade, synthetic elastomeric materials such as poly (glycerol sebacate), and poly (polyol sebacate)s (PPS) [55] emerged as attractive materials for soft tissue engineering applications due to their biocompatibility and to the tunability of the materials' mechanical properties, that can resemble those of the native tissue [56]. For example, the Young's modulus of one PPS, namely poly(glycerol sebacate), is between that of ligaments (kPa range) and the myocardium (i.e. ranges between 0.02 and 0.5 MPa) and its maximum elongation is similar to that of arteries and veins (i.e. 260%) [56]. Poly(polyol sebacates) are synthesized from an alcohol containing multiple hydroxyl groups (i.e. polyol) and sebacic acid, a dicarboxylic acid endogenous to human metabolism. Preferred polyols for the polyesterification reaction with sebacic acid are sugar alcohols, as they are used both in food and pharmaceutical industry. Table 1.1 below shows some common sugar alcohols and their structure. The reaction that occurs between these monomers is a polycondensation (polyesterification, with removal of water molecules) whereby the primary hydroxyl (–OH) groups react first with the carboxylic groups (-COOH) with a formation of a pre-polymer (i.e. low molecular weight). At this point, the pre-polymer can still be dissolved or processed in different shapes. The next reaction implies curing or crosslinking the –OH groups left unreacted towards the middle of the polyol structure with the free –COOH groups. This results in more ester links and crosslinks between polymer chains and therefore leads to an elastomeric network that cannot be dissolved or remodeled [51].

Poly (glycerol sebacate) is the most studied among all the above presented PPS and the first one developed by Langer and his co-workers [17]. While the other materials presented in Table 1.1 were synthesized and characterized to underline the potential use in tissue engineering, PGS has been studied specifically for cardiovascular [57, 58], neural [59], cartilage [60], and retinal tissue engineering [61]. Its biocompatibility arises from the compatibility of its monomers, both intrinsic to human metabolism [56, 62]. While glycerol is a triol that forms the backbone of triglycerides, sebacic acid occurs naturally (i.e. castor oil). The degradation behavior of PGS is another important feature

when considering biomedical applications. After a number of studies that focused on this subject, it was concluded that the in vivo and in vitro studies cannot be correlated. This is due to the fact that the polymer degrades in PBS only around 17% after 60 days, while the in vivo experiments in rats attest a total resorption of PGS in the same time frame [17].

Table 1.1: Sugar alcohols used for the polyesterification reaction with sebacic acid

Sugar alcohol	Acids used for polyesterification	Abbreviation of resulting polymer	Applications	Ref.
Glycerol	*Sebacic acid*	PGS	Soft tissue engineering scaffolds and microfluidic devices	[57-60]
Erythritol	*x=1-8,10,12*	PES		[18]
Xylitol	*Sebacic acid*	PXS	Tissue engineering with general applications	[55]
Sorbitol	*Sebacic acid*	PSS		

The in vivo characteristics of PGS materials with different crosslinking densities [63] also reported no significant correlation between the polymer mass loss and the crosslinking density (i.e. curing time). It was stated that the in vivo degradation mechanism is probably controlled by an enzymatic surface erosion process [64]. Therefore, introducing new chemical functionalities in the PGS structure might provide a solution for applications that require slower degradation rates [40].

1.1.1. Modification of Polymers: Bulk vs. Surface Modification

Tailored polymers for biomedical and pharmaceutical applications can also be obtained by polymer modification, a flexible alternative to the synthesis of new materials. Modification techniques include a range of transformations such as polymerization reactions, blending, grafting/ functionalization, chain extension, cross-linking, branching, etc. In what follows, a focus will be on the modification of the bulk and surface properties of materials.

Bulk Functionalization

The bulk properties can be changed mainly to target special properties and therefore to tailor a material for a specific application. This is most commonly achieved by either blending different polymers that present complementary properties or by adding an additional functionality to a certain polymer chain.

A typical example of changing the bulk properties is represented by the studies of variations in the composition of the PGS elastomer, with the hope of finding new and better materials with various applications. A blend of PGS with citric acid in molar ratios of 4/4/1 and 4/4/0.6 (glycerol/sebacic acid/citric acid) and its effect in controlling the curing times was investigated [65]. This had the goal to render more mechanical strength and to shorten the curing time for the PGS elastomer. The authors state that the mechanical properties had improved as the Young modulus increased from 0.9 to 5.3 MPa and elongation at break increased from 33% to 117%.

In another attempt to improve the mechanical properties of this type of material, poly(glycerol-sebacate-citrate) (PGSC) was reinforced with nano-fumed silica [66]. It is stated that the obtained elastomers had improved mechanical properties due to the filler-polymer interaction and that a weakened cytotoxicity was observed, making the materials suitable for biomedical applications. The creativity of researchers also led to blending PGS elastomer with thermoplastic materials such as poly(L-lactide) or polycaprolactone. Therefore, poly(glycerol-sebacate-L-lactide) copolymers were synthesized via a ring-opening polymerization of L-LA initiated by Sn(Oct)$_2$ and PGS. These branched copolymers exhibit higher molecular

weights than PGS alone and lower onset decomposition temperatures than PLLA [67, 68].

Surface Modification

The first contact between an implantable biomaterial and the body is essential and determined by the surface properties of the material. Implantation of a biomaterial can lead to a sequence of events if it is rejected by the body. Danger signals are released from the damaged tissue around the biomaterial and the first response of the immune system to injury starts with acute inflammatory response. Acute inflammation is dominated by the action of polymorphonuclear leukocytes (PMNs) that corrode the biomaterial surface [69]. This is followed sometimes by chronic inflammation where, by the activation of macrophages, the biomaterial will be engulfed. Cell infiltration can occur when inflammatory cells such as lymphocytes, macrophages, etc. infiltrate around the blood vessels. The fusion of the macrophages leads to giant cells (multinucleated), which try to degrade the biomaterial. If the giant cells are not able to degrade the biomaterial ("frustrated phagocytosis"), then collagen is secreted and encapsulates the biomaterial, isolating it from the body environment (i.e. foreign body reaction). Successful tissue repair requires both inflammation and solving the inflammation. In the resolution phase of the inflammation there is an increase in the inflammatory mediators, a decrease of leukocyte endothelial adhesion and the removal of inflammatory cells (lipoxins, resolvins, protectins) is stimulated [70].

Therefore, in order to surpass the common limitation of the synthetic biomaterials (i.e. biological recognition) surface modification strategies are required. Up to now, a wide variety of surface modification techniques have been developed to improve the surface properties of polymer, via an either physical or chemical route [71, 72]. Various biomolecules inspired from the extracellular matrix were absorbed on the material surface through physical procedures [73-75]. However, for long time cell culturing, the physical adsorption method has the disadvantage that the protein might diffuse away and become unavailable for cellular interactions [76]. More stable coatings are provided through chemical approaches, where an active biomolecule can

also be covalently immobilized on the substrate surface [77]. The general scheme of surface bio-functionalization is depicted in Figure 1.2. Due to the inert nature of most polymers used in tissue engineering, the surface has to be firstly functionalized before the attachment of the biomolecule [77].
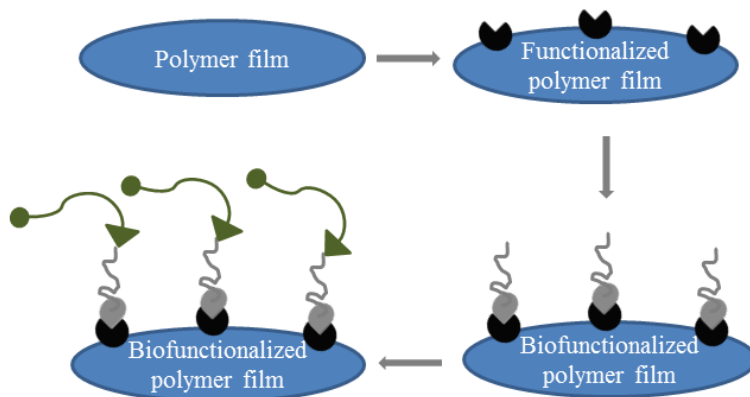
Figure 1.2: General representation of polymer surface modification with a biological compound

After this step, the optimization of the surface functionalization is required in order to introduce the specific type and quantity of reactive functional groups. An intermediary step might be needed depending on the specific case. Surface modification of polymer surfaces can be achieved by either dry or wet chemical methods.

The dry methods include low temperature plasma [106-109], corona discharge [110, 111], flame treatment [112, 113] or UV [114, 115], while the wet methods include salinization [116, 117], polymer adsorption, polymer grafting or grafting polymerization. As the literature on this subject is extremely vast, the goal of the above discussed surface modification methods is to contribute to the development of specific applications within a wide range of scientific disciplines. Therefore, some of the main applications of polymer surface modification via the attachment of bioactive compounds on some representative polymers are presented in Table 1.2.

Table 1.2: Main polymers that are surface modified with biomolecules for tissue engineering and biosensor applications

Polymer	Immobilized Bioactive molecules	Applications	Ref.
Poly(α-hydroxyacids): Poly(lactic acid) Poly(glycolic acid) Poly(lactic-co-glycolic acid) Poly(ε-caprolactone)	Enzymes peptides polysaccharides antibodies	Tissue engineering Drug delivery	[49, 56, 78, 79]
Polyurethanes		Tissue engineering Medical devices	[51, 54]
Poly(polyol sebacates): Poly(glycerol sebacates) Poly(erythritol sebacates) Poly(xylitol sebacates)		Tissue engineering	[17, 56]
Poly (diol citrate) Poly (1,8-octanediol)citrate		Tissue engineering Biosensors MEMS	[80, 81]
Poly(methyl methacrylate)		Tissue engineering Microarrays Biosensors Immobilized enzymes MEMS Packaging materials	[82-90]
Polystyrene		Bioanalytical assays Antimicrobial surfaces Tissue culture	[91-94]
Poly(tetrafluoroethylene)		Biosensors, MEMS	[95-97]
Poly(ethylene terephthalate)		Biocompatible/hemocompatible materials Antimicrobial surfaces Textiles Tissue engineering	[75, 98-101]
Poly(dimethyl siloxane)		Biosensors MEMS	[102-105]

1.2. Processing Techniques and Microfabrication

1.2.1. Classical Scaffolding Techniques

Medicine requires an increasing number of implantable materials and medical devices for tissue repair or regeneration, synthetic scaffolds or three-dimensional constructs provide a solution for a wide range of medical problems [40]. Polymeric scaffolds offer support for cells to proliferate and maintain their differentiated function. In the same time it supplies proper mechanical function and mass transport for biological delivery and tissue regeneration due to the internal architecture and physico-chemical properties. The most common classification of scaffolds architecture is in two-dimensional (2D) structures, defining mostly sheets or films, and three-dimensional structures, such as porous solids, hydrogels, foams, or sponges characterized by a high porosity [118]. Some typical examples of classical scaffolding techniques include salt leaching, membrane lamination, phase separation, freeze drying procedures, rapid prototyping or electrospinning and are briefly described in the next paragraphs [119, 120].

Particulate leaching uses a template (e.g. particles) that is dispersed within a polymeric or monomeric solution, which is then fixed or gelled; removal of the template results in porous scaffolds [121, 122].

Phase separation techniques involve the separation of a polymer solution into two phases, a polymer-rich phase and a polymer-lean phase. After the solvent is removed by extraction, evaporation or sublimation, the polymer-rich phase is solidified, rendering porous membranes and scaffolds to be used in biomedical applications [32, 121, 122].

Electrospinning is a versatile technology that has the main advantage of creating scaffolds with high porosity as well as high surface area-to-volume ratio [123]. In the electrospinning process, a polymer solution is converted to a fibrous structure via electrostatic forces. The polymer solution is delivered through a needle while a high voltage (1-30 kV) induces charges in the fluid and thus stretches the polymer droplet into fibers. Thus resulted fibers are collected on a grounded collector under the form of nonwoven

fibers. This process is affected by polymer characteristics, polymer solution parameters, process parameters, collector conditions and ambient parameters. By varying these parameters it is possible to obtain electrospun fibers and structures with various morphologies and properties.

Solid free-form fabrication techniques and Rapid Prototyping enable the development of scaffolds by selectively depositing materials in a layer-by-layer approach. Each layer is designed with a computer software. These provide scaffolds with a highly reproducible architecture and compositional variation across the entire matrix [122]. Different rapid prototyping techniques such as stereolithography, 3D printing and extrusion based systems (i.e. Fused deposition modeling) are described in literature [121, 122, 124].

Stereolithograpy uses a focused laser light to scan the surface of a photo-sensitive material and to produce 2D patterns of polymerized material. The build-up of a 3D construct is made using a layer-by-layer approach, whereby the fabrication platform moves stepwise in the Z-direction after a 2D layer is finished. The step height of the fabrication platform is typically smaller than the curing depth, ensuring good adherence of subsequent layers [120-122].

3D printing is used to create a three dimensional scaffold from a digital model (i.e. a CAD representation), by adding a material layer-by-layer [40]. Three-dimensional objects can be printed in different shapes or geometries and are investigated for various applications, including bone, cartilage, retinal, cardiovascular tissue engineering [125]. 3D scaffolds are desired to be highly porous, have interconnected pore networks and adequate pore size for cell migration and infiltration.

Fused deposition modeling implies the extrusion of a thermoplastic material in a temperature-controlled manner and the deposition of the semi-molten polymer on a platform in a layer by layer process. A computer-aided (CAD) model is used in this process. The parameters depend on the specific application. The filaments are fused together upon cooling [121, 122, 126].

1.2.2. Microfabrication Techniques and Microfluidics

Microfabrication techniques and microfluidics are increasingly becoming part of modern science and technology. They appeal to both science and industry due to the ability to develop systems with compact dimensions in the range of micrometers to millimeters. Such microsystems present a multitude of advantages such as the obvious size reduction that not only ensures low amounts of reagents but also lower amounts of waste. Another important aspect of these systems is that they can have multiple components with different functionalities, allowing a high degree of automation and parallelization of processes that otherwise would consume more time and resources [127]. This approach led to the appearance of terms such as "lab-on-a-chip" (LOC) or "micro total analysis system (μTAS)".

Although microfabrication has emerged out the need for better microelectronics devices, in the last decades applications of micro-engineered systems such as microanalysis [128], microelectromechanical systems (MEMS) [129] and tissue engineering [130] gained increasing interest. With a market that is estimated to grow to $32 billion by 2018, tissue engineering is dealing with mimicking the complexity of tissues in vitro. Providing 3D micro-features within a scaffold has become a new challenge for the field of microfabrication.

Materials in Microfabrication

Specific geometric features are produced via suitable fabrication techniques provided that the material properties apply to the constraints of the fabrication methods. Therefore, the material choice is of utmost important and should be considered before attempting to imprint a specific design. Some of the most used materials in microfabrication are briefly presented in the next paragraphs.

Silicon is the base material of MEMS and it has a long tradition in semiconductor and MEMS fabrication. It is used as single-crystal wafer with diameters of 75–200 mm and thicknesses of 0.25–1.0 mm. In addition it has excellent electrical properties and high strength that allows higher strain levels [131].

Glass has the advantage of optical transparency. Although glass wafers come in various compositions and sizes they are brittle and the surface chemistry is difficult to manipulate [131].

Polymers such as PDMS and PMMA have been amongst the most preferred materials. Their advantages consist of being inexpensive, flexible, and transparent to visible/UV. More recently introduced in microfabrication are soft materials like hydrogels and elastomeric PGS due to their surface properties that can be more easily modified and their improved biocompatibility and bioactivity over the other materials. These are mostly used in biotechnology and microfluidics applications [131].

Thermoset polymers are materials in a soft solid or liquid state that once subjected to a process called curing they irreversible harden and form a polymer network that cannot be reheated and melted to be shaped differently. Examples of thermoset materials include PGS, PI, epoxy and phenolic resins.

On the other hand, thermoplastic polymers become moldable above a specific temperature and solidify upon cooling. In comparison with thermosets that contain irreversible chemical bonds after curing, thermoplastics can be reshaped as many times as needed. PLA, PCL, PVC, COC, PP, PC are just a few examples of thermoplastic materials used in microfabrication.

Nevertheless, for tissue engineering applications and especially for implantation within the human body, there is a constant need of new biocompatible and biodegradable materials that can be processed via microfabrication techniques in order to have the desired topography for the specific application.

Microfabrication Techniques

Soft lithography represents a group of techniques that uses stamps, molds, and masks for pattern transfer on a substrate material. The work "soft" comes from the use of an elastomeric soft stamp to transfer a pattern into materials. The most common material used as a stamp is PDMS, a flexible

transparent material that is nontoxic, impermeable to water but permeable to gasses. Thermoplastic materials such as PMMA or COC are also successfully used as molds due to the fact that they are less fragile and susceptible to deformation than PDMS [132]. Although metal molds made of (stainless) steel or aluminum and metallic micro-parts (i.e. parts with a maximum size below 10 mm and features in the micron range) have been used in the field of micro-electronics, micro-machinery, their application in tissue engineering seems to be mostly for thermoplastic materials such as ultra-high molecular weight polyethylene and bone (i.e. hard) tissue engineering (TE) applications [133, 134]. In the context of liver TE or soft TE, PDMS microfluidic environments were created for high density hepatocyte culture using soft lithography and replica molding. This microfluidic system enabled HepG2/C3 cells to be assembled in close proximity to each other without nutrient limitation (Figure 1.3). The authors state that this design mimicked the natural liver tissue configuration, where a high density of hepatocytes is in close contact with the microcirculation [135].
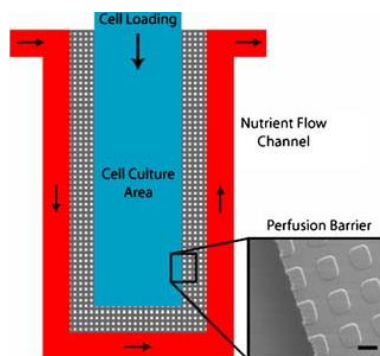
Figure 1.3: (a) PDMS Microfluidic culture unit design. The microfluidic unit consisted of three parts: a 150 µm wide by 440 µm long cell culture area (blue), a microfluidic perfusion barrier (gray), and a medium flow channel (red). Inset shows SEM micrograph of the perfusion channels. Scale bar represents 5 µm. Figure reprinted and adapted from [135] with permission.

Replica molding reproduces geometric features from a mold into a material by first coating the mold, followed by solidification of the material. Compression molding targets both thermosets and thermoplastics and can impart a specific shape on opposing sides of a material. For biodegradable thermoset materials such poly (glycerol sebacate), replica molding is used to

fabricate porous scaffolds with thickness of 45 µm for retinal cells grafting (Figure 1.4), as possible treatment of treating blinding disorders [136].
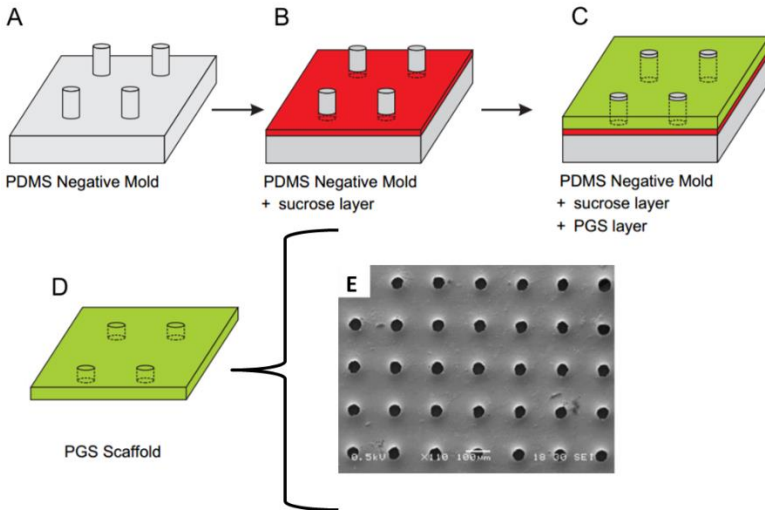
Figure 1.4: Replica molding of a soft elastomer, PGS, for retinal tissue engineering applications. Figure reprinted and adapted from [136] with permission of Elsevier.

Hot embossing can be applied to almost any thermoplastic material (e.g. PC, PMMA, PVB, PET, etc.) and is based on heating and plastic deformation while a load is applied to the material. After the removal of heat and pressure, the molded thermoplastic retains its new shape [137]. Different plastic materials such as PC, PMMA, PS, COC and PDMS were processed via hot embossing for advanced microfluidic cells and tissue culture models as seen in the below Figure 1.5.

Photolithography is a process used in microfabrication to selectively remove parts of a thin film from a substrate. The process flow requires a substrate that is coated with a light-sensitive chemical called photoresist (i.e. resist). Deposition of the photoresist on a wafer is done by spin coating, lamination, spray coating or electrodeposition.
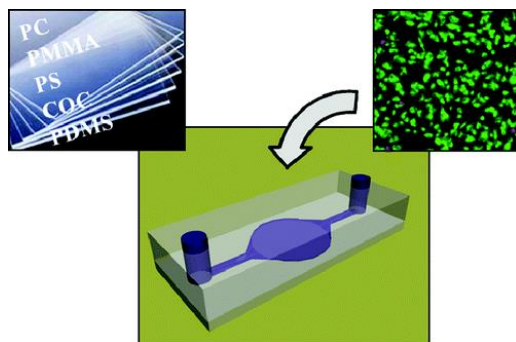
Figure 1.5: Hot embossing of different plastics cultured with human hepatoma (HepG2) cells. Reprinted adapted with permission from van Midwoud, P.M., et al., Comparison of Biocompatibility and Adsorption Properties of Different Plastics for Advanced Microfluidic Cell and Tissue Culture Models. *Anal Chem, 2012. 84(9): p. 3938-3944.[137]. Copyright 2012 American Chemical Society.*

The pattern is transferred from a mask to the resist by light irradiation. The mask is usually chrome or a transparency mask that allows light to shine through in a defined pattern. Depending if the resist used is positive or negative, the light will either harden the exposed are or not. By removing the remaining unnecessary resist, the pattern is transferred and the mold is therefore developed [138]. For tissue engineering, this technique has been used to create microfluidic channels mimicking blood vessels bifurcated networks from amino alcohol-based poly(ester amide) elastomers (Figure 1.6) [139].

Subtractive processes refer to wet and dry etching techniques. Etching is considered to be the second most basic type of microfabrication process after photolithography [140]. Subtractive processes are used to create cavities such as microchannels, wells, orifices. In wet etching, the material is attacked by a liquid chemical (i.e. etchant) and removed order to create channels or cavities. In the case of the dry etching process, the substrate is not immersed in liquid. The most common method of dry etching is in a plasma (either direct current or radio frequency), which consists of high-energy ions and electrons, as well as neutral particles. An important parameter for plasma etching is the pressure used, as it can affect the etch profile and the surface roughness.
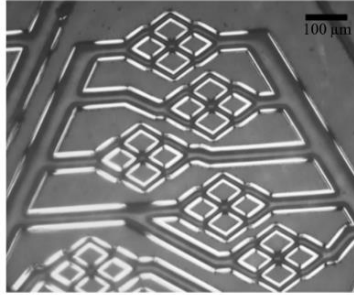
Figure 1.6: Microfluidic channels from amino alcohol-based poly(ester amide) elastomers for soft tissue engineering applications. Printed with permission from [139].

Additive processes consist of vapor deposition, plating, and printing. While for subtractive processes the directionality of material removal can be classified as isotropic (i.e. uniform in all direction) or anisotropic (i.e. preferential), for additive processes the profile of added material is either conformal (i.e. material continuity is preferred) or nonconformal (i.e. line-of-sight directionality) [140].

Microfabrication techniques such as the ones described above have emerged from automotive, microelectronics and aerospace industries to be successfully integrated into the field of tissue engineering [141]. For soft tissue engineering applications and the specific characteristics of the herein proposed biodegradable and biocompatible microfluidic system, techniques such as soft-lithography, replica molding, photolithography and hot embossing are amongst the most suitable.

1.3.   Cell Biology and Liver Tissue Engineering

Cell-based tissue-engineering techniques are important in diverse clinical applications. Material/ polymer science and engineering both work towards providing a proper environment for cells to proliferate and differentiate into a specific tissue/organ. Therefore, manipulation of cells through their extracellular environment (i.e. scaffolds, engineered templates) or even genetically to develop biological substitutes represents the final goal of tissue engineering [142].

For hepatic tissue engineering, the ideal biological liver substitute should perform most of the liver-specific detoxification, synthetic and biotransformation functions [143]. The first step for acute liver failure treatment was the development of extracorporeal devices [144]. Therefore, Liver Assist Devices (LADs) are temporary solutions that use hepatocytes to sustain the patient's liver function until a transplant is possible. In this device, there is an exchange of nutrients, wastes, and gases occurs while cells undergo metabolism, protein production, and synthesis of hepatic products [14]. The schematic principles of LADs are presented in Figure 1.7. Nevertheless, the long term goal is to have a functional liver tissue to be implanted and replace these laborious devices.
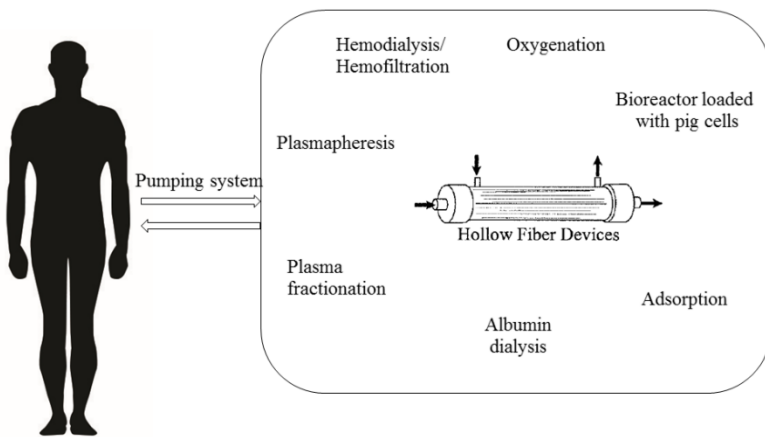
Figure 1.7: Schematic principles of extracorporeal systems for the treatment of liver failure, adapted from [134].

1.3.1. Liver Structure and Function

The liver performs many essential functions related to digestion, immunity, and the storage of nutrients within the body metabolism. In addition to these, liver is essential to toxin removal and metabolic activity such as cytochrome P-450 activity, glycogen storage, urea production, and release of proteins, carbohydrates, lipids, and metabolic wastes [14].

The liver is part of the digestive system and has as a morphological unit the hepatic lobule. In total, the liver contains up to 100 000 hepatic lobules that

are comprised by hepatocytes in a proportion of 60%, a complex array of vasculature (i.e. sinusoidal capillaries, endothelial cells) and other parenchymal cells (i.e. stellate cells, kuppfer cells, epithelial cells, biliary epithelial cells, and fibroblasts) [145, 146]. A simplified representation of the liver and the alignment of cells inside a hepatic lobule is depicted in Figure 1.8.
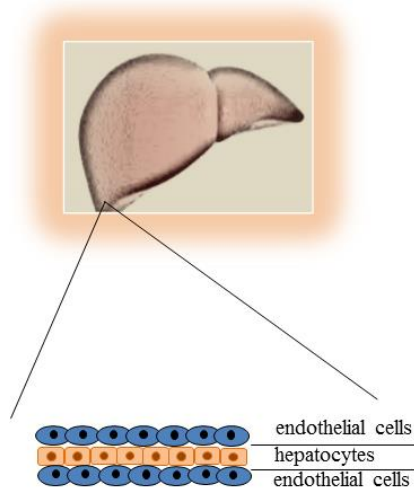
Figure 1.8: Schematic representation of liver and its inner structure

The high complexity arrangement of the liver cells allows communication and attachment between cells, as well as interaction with the surrounding extracellular matrix [14]. Cells communicate directly through cellular and gap junctions and via chemical signals present in the biomolecules of the surrounding ECM [143].

Therefore, it is fundamental for the cells from a liver engineered construct to have the same function as in the natural liver. Due to the liver's 3D structure and the need of the cells to interact, co-culture systems have been more than often considered. Increased hepatocyte differentiation and proliferation was noticed when epithelial cells, mesenchymal cells, endothelial cells or fibroblasts were part of the co-culture system [14, 147, 148].

1.3.2. Representative Cells for Liver Tissue Engineering

The choice for representative cells and cell sources is an important parameter for the study and growth of liver tissue. Up to now, the most used cells for this application were hepatocytes, stem cells, oval progenitor cells and hematopoietic cells [14, 149]. For stem cells, it is widely known that they can differentiate into a desired cell type, provided that the proper growth factors, extracellular matrix, signals and cues are supplied. Studies where bone marrow stem cells were delivered to patients with liver cirrhosis through perfusion of the peripheral vein or the hepatic artery showed a statistical improvement of their clinical condition [150, 151]. Hepatic progenitor cells, also called primary hepatocytes, are the precursor cells of mature hepatocytes. Up to now mostly rat and porcine primary hepatocytes have been isolated and grown in culture [12, 152, 153]. Human hepatocytes possess some challenges in this regard such as difficulty to be maintain in culture and inability to perform normal functions or undergo differentiation [146, 154].

Currently, one of the most used cell lines for liver tissue engineering is represented by HepG2. These human cells are derived from metastatic tumors and have demonstrated a good capacity for growth *in vitro.* However, due to their carcinogenic nature, they are mostly used to assess the cytotoxicity of the scaffold or the designed culture material and not for transplantation in humans. This is also the case for rat and even porcine hepatocytes. Although the latter presents similar qualities and effects as human hepatocytes, the risk of animal virus transmission and immune rejection by the patient are obstacles that are not easily transcended.

Therefore, human hepatocytes are to be considered for human transplantation although scarcity and difficulty in handling or culturing them might arise. In this context, stem cells seem to be a good compromise as they divide asymmetrically to produce a new stem cell and a progenitor cell that subsequently undergoes differentiation and maturation to form functional tissues [155].

1.4. Outlook and Thesis Perspective

The recent advances in the fields of materials science, engineering and biology show great promise for hepatic tissue engineering and for working towards an implantable organ. New materials or scaffolds that mimic the ECM by their innate structure or by grafting growth factors, enzymes and other mediators show great potential for cell attachment and proliferation. Nevertheless, the liver is a complex vascularized organ and all research should start having in mind its 3D architecture that encompasses multiple cell types and their interaction. Appropriate safe cell sources should be used, as well as standard procedures for their storage and culturing.

The present thesis aims at building such complex hepatic model that considers both a 3D architecture and the possibility to have a co-culture system as to provide cell-to-cell interaction and, therefore, increase the chances of having functional hepatocytes. The herein developed model can also serve other tissue engineering application due to fact that the above mentioned features are also characteristic to other organs.

Chapter 2: Biodegradable Poly (polyol sebacate)s

This chapter discusses the development of biodegradable and biocompatible materials for soft tissue engineering applications such as liver and cardiovascular tissue engineering. The work presented in this chapter was previously published in Macromolecular Bioscience [156].

2.1. Introduction

Biocompatible materials are necessary for the purpose of the present thesis, as they will constitute the major part (i.e. the patterned layers) of the microfluidic bioreactor. One the one hand, the materials are required to be transparent and be able to be shaped in different forms so they can be assembled into the final device. Other important characteristics are biodegradability and the ability to maintain their topography until the new tissue is formed. For liver regeneration and tissue formation, the materials should to have a degradation rate of around three months, as it is well known that liver is an organ with a high regeneration rate (i.e. 1-2 months for normal liver and 3-5 months for injured liver [157]).

The field of tissue engineering has focused its efforts on the regeneration of living tissues by culturing cells on biocompatible scaffold materials [5, 50, 158-160]. The state of art regarding biomaterials has increased in the last decades as many scientists have struggled to guide the process of tissue regeneration. Until now, the scientific world tried to obtain the properties of native tissue using natural and synthetic derived materials. Natural materials present important properties like biological recognition, but also important limitations such as difficulty in controlling the mechanical properties and fast degradation rates. Synthetic biomaterials, on the other hand, are cheaper to fabricate, can be produced in large quantities and they can be tailored to meet strictly the needs of specific applications.

Among these synthetic biomaterials, poly(polyol sebacates) are an important class of biomaterials in the field of tissue engineering. These thermoset

elastomers, amongst which poly (glycerol sebacate) (PGS) [55] is well known, have become most favored materials for tissue engineering [17]. Their biodegradability and biocompatibility derives from the two building blocks of the polymer, namely glycerol and sebacic acid, both being endogenous monomers found in human metabolism. While glycerol is part of the backbone of fats such as triglycerides, sebacic acid is a natural intermediate in the metabolism of fatty acids [62]. Other polyols, such as xylitol, sorbitol and, most recently, erythritol belong to the class of sugars and are used in different areas, from food industry to pharmaceuticals. The first reported synthesis of such an elastomer involved mixing equimolar quantities of the monomers under inert atmosphere (at 120°C) for 24h, followed by a vacuum condition from 1 torr to 40 mtorr for another 5 hours [17]. The result is a slightly yellowish pre-polymer that can be dissolved in most organic solvents and can be molded in different forms according to the desired application. By a subsequent crosslinking step (i.e. curing step), using high temperatures and vacuum, the final elastomer is obtained. Extensive research has been done on varying parameters such as molar ratio, type of reagents, and/or curing temperature and time [161-168].

Poly (erythritol sebacate) (PES) is another soft elastomeric material, less known in literature but similar to poly (glycerol sebacate), with the difference that the sugar used is erythritol instead of glycerol. Both monomers are, as stated above, endogenous to human metabolism and approved by the U.S. Food and Drug Administration (FDA). It is one of the poly(erythritoldicarboxylate)s previously reported by Barrett et al. [18], but in their study some important characterization aspects such as degradability and cytotoxicity behavior are lacking which will be, amongst others, tackled in the present thesis.

In the present work, a comparison between bulk and microwave polymerization of PGS- and PES-derived polymers is performed. The motivation behind choosing these two starting materials for synthesis and further modification was their potential as platforms for soft tissue engineering (TE). In addition, for the current application, there is a need for new materials derived from the mentioned poly(polyol sebacate)s that have

longer degradation rates, as the current available PGS materials are completely resorbed within 60 days [17, 56].

The need of the modern world in which time is of the essence is addressed by using a microwave-assisted polycondensation process for the development of the novel poly(polyol sebacate)s. Microwave irradiation has become a viable alternative heat source for different types of polymerizations such as radical polymerization [169], cationic polymerization [170] and polycondensation [171]. Although its key advantage is the acceleration of the reaction rates due to the direct heating of the molecules present in the reaction mass, microwave irradiation also offers a highly reproducible and homogeneous synthesis process. To the best of our knowledge, this is the first report which describes the synthesis of the above stated poly(polyol sebacates)-derived polymers via microwave irradiation.

In order to surpass the common limitation of the synthetic biomaterials (i.e. biological recognition), a new surface modification strategy of the polymer films is also reported in the present chapter. For this purpose, PGS was chosen as a representative material for all poly (polyol sebacates) and their derivatives. The strategy implied the chemical immobilization of gelatin on the 2-dimensional (2D) PGS surfaces. Until now only physical adsorption of gelatin has been reported on PGS [161]. However, for long time cell culturing, the physical adsorption method has the disadvantage that the protein might diffuse away and become unavailable for cellular interactions [76]. Furthermore, this protein has proven to bind to other bioactive molecules like fibronectin, leading to increased cellular activity [109, 172, 173].

In addition to the main purpose of using the newly synthesized materials as platforms for liver tissue engineering, in the last part of the present chapter another enabling application (i.e. cardiovascular TE) of the herein developed materials is presented.

2.2. Materials and Methods

Sebacic acid, glycerol (99.6%), meso-erythritol (99.9%), 1,3-propanediol, 1,10-decanediol, 1-ethyl-3(-3-dimethylaminopropyl) carbodiimide

hydrochloride (EDC), $CDCl_3$-d_6 and tetrahydofuran used were purchased from Sigma-Aldrich; dimethylsulfoxide-d_6 and 2-aminoethyl methacrylate (AEMA) were purchased from Polysciences. Gelatin type B (GelB) isolated from bovine skin was kindly supplied by Rousselot, Ghent, Belgium. All chemicals were used as received unless otherwise mentioned.

2.2.1. Poly (polyol-sebacate) Pre-polymer Synthesis and Characterization

Microwave Polymerization

Typically, equimolar (0.01 moles) quantities of glycerol or meso-erythritol and sebacic acid were placed in a flask and introduced in the microwave system (CEM focused, model Discovery, Synergy version 1.38). The reaction mass was heated, under continuous stirring, at either 180°C or 200°C for the times shown in Table 2.1. After subjecting the reaction mass to microwave irradiation, the flask was removed and heated at 150°C for an additional 1hour, under vacuum, to remove the by-product (i.e. water). For the poly (polyol sebacate)-derived polymers, either 1,3-propanediol or 1,10-decanediol were added together with the other monomers in the microwave reactor. The different molar ratios were 1/0.4/0.6 and 1/0.6/0.4 corresponding to sebacic acid/polyol/diol.

Bulk Polymerization

Poly (glycerol sebacate) and derived polymers

For comparative reasons, the reaction was carried out also under conventional heating, according to previous published methods [17]. Briefly, equimolar (0.01 moles) quantities of glycerol and sebacic acid were reacted at 130°C, under N_2. The inert atmosphere was replaced after 24 hours with a vacuum line which was applied for another 3 hours. For the derived polymers, the short and long chain diols were added in the same molar rations as for the microwave polymerization.

Poly (erythritol sebacate) and derived polymers

Equimolar quantities of meso-erythritol and sebacic acid were reacted at 150°C, under N_2. The inert atmosphere was replaced after 2 hours with a vacuum line for another 4 hours. In the case of the poly (erythritol sebacate)-derived polymers, the diols were added in the same time as the other monomers and the reaction proceeded as for the poly (erythritol sebacate) polymer.

Gel permeation chromatography (GPC) was used to measure the number average molecular weight (M_n), the weight average molecular weight (M_w) and the polydispersity index (PDI) of the pre-polymers. The measurements were recorded with a Waters device equipped with a refractive index detector, a mixed-E column and with tetrahydrofuran as eluent.

Proton nuclear magnetic resonance (^1H-NMR) spectra were recorded in dimethylsulfoxide-d_6 (Bruker500 MHz) for the poly(erythritol sebacate)-derived polymers and in $CDCl_3$ for the poly(glycerol sebacate)-derived polymers.

Fourier-transform infrared (FT-IR) analyses were performed with a Bio-Rad FTS 575C spectrometer to study the chemical composition of the developed materials.

2.2.2. Development and Characterization of Elastomers

All products were white-yellowish pre-polymers that could be molded and cured into the final crosslinked elastomer. The pre-polymers were melted on dextran (T70, Amersham Pharmacia, Sweden) coated glass plates and cured into the final elastomer at 135ºC in a vacuum oven. Therefore, a dextran solution in water (12.5% w/v) was spin-coated at 800 rpm for 30 seconds on clean glass plates, dried at 120°C serving as a release layer for the polymer films. Thus formed films were delaminated from the glass plates by incubation in MilliQ water (obtained by a Millipore water purification systems, Merck, Overijse, Belgium, 27.2 nS/cm) and then subjected to increasing concentrations of ethanol solutions in MilliQ in order to remove the residual monomers.

Static contact angle (SCA) measurements were performed on polymer films with a goniometric OCA 20 device (Dataphysics). SCA values were determined using the sessile drop method and distilled water as the dispensing liquid. Young-Laplace procedure was used as processing method. The device was equipped with a video camera able to record a 30 s video (25 frames/s) of each drop. An average value of at least three drops (0.5 µL) per sample was considered.

Swelling experiments were performed by incubating samples of 8 mm diameter and 2 mm thickness in MilliQ water, PBS pH 5.5 and PBS pH 7.4 (10 mM PBS, 137 moles/L NaCl, 2.7 moles/L KCl, 10 moles/L Na_2HPO_4 and 2 moles/L KH_2PO_4)), at 37ºC in an incubator. At different time points the samples were removed from the medium and weighed after the excess of medium was removed. The swelling degree was calculated according to the formula (1) below:

$$swelling\ (\%) = \frac{m_w - m_i}{m_w} \times 100 \qquad (1)$$

where: m_i and m_w are the initial and wet masses of the samples, respectively.

The thermal properties of the polymer were investigated using a thermogravimetric analyzer (TGA, TA Instruments Q50) and a differential scanning calorimeter (DSC, TA Instruments Q2000). The TGA scans were recorded at 10 °C/min, from room temperature to 800 °C. The DSC scans were performed with a heating and cooling rate of 10ºC/min, in an interval of -50ºC to +150ºC.

Mechanical tensile tests were performed on dog bone-shaped PES specimens using an Instron testing machine equipped with a 50 N load cell. The elongation rate was maintained at 10 mm/hour, and the samples were elongated to failure. The Young modulus (YM) was calculated from the initial slope of the stress-strain curve. At least four tests were carried out for each sample type.

The crosslink density (n) was estimated based on the theory of rubber elasticity, using Eq. (2) [17].

$$n = \frac{E}{3RT} \qquad (2)$$

where n is number of network chain segments per unit volume (mol/m^3), E is the Young's modulus (Pa), R is universal gas constant (8.3144 J/mol K), T is the absolute temperature (25°C =298.15 K).

The in vitro degradation behavior of the obtained polymers was evaluated for a period of 4 months. The degradation rates via hydrolysis of the disc shaped polymer samples (8 mm diameter, 2 mm thickness) were studied in PBS pH 5.5 and PBS pH 7.4, at 37°C in an incubator. At designated time points, the samples were removed, washed with MilliQ water and dried in an oven at 90°C for 3 days. The mass loss was calculated from the dry mass at point p (m_p) and the initial dry mass (m_0) of the sample, according to formula (3) shown below:

$$mass\ loss\ (\%) = \frac{(m_0 - m_p)}{m_0} \times 100 \qquad (3)$$

2.2.3. Surface Modification of Polymer Surfaces

PGS films were punched into small disc samples (10 mm diameter and 0.1 mm thickness) and reactive functional groups were introduced on the surface by applying an Argon plasma. The treatment was performed in a cylindrical dielectrical discharge plasma reactor (Model Femto, version 3, Diener Electronic, Germany) for 30 s, under a pressure of 0.8 mbar and with an applied power of 100W. The plasma-treated surfaces were subjected to ambient atmosphere for 5 minutes in order to generate hydroperoxides and peroxides, that were used as initiating groups in the subsequent UV-induced graft polymerization [174, 175]. The basic principle of graft radical polymerization is depicted in Figure 2.1. Initiation starts by UV irradiation (i.e. generation of radicals, RO$^\bullet$), which is the first step of the radical polymerization mechanism. Afterwards, the AEMA grafting follows in the propagation step until the growth of the chain is terminated.
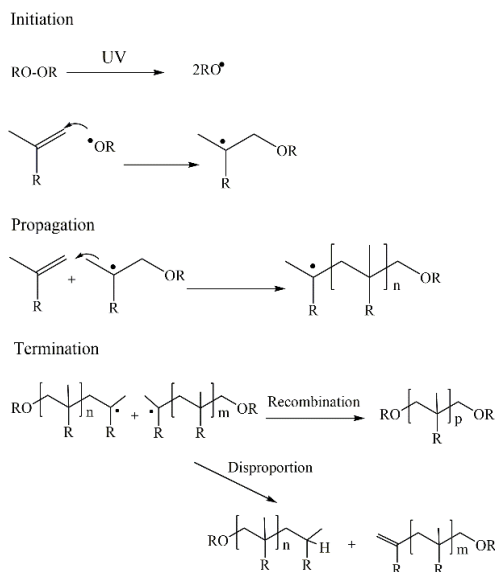
Figure 2.1: Radical polymerization basic principle

The discs were placed in glass well plates and a fresh solution of AEMA 1 M was added. The solution was prepared with degassed deionized water. A quartz cover was placed on the well plate and introduced for 1 hour under a home-made UV device, equipped with four UV-lamps (Sylvania, F15W/350, λ_{max} = 350 nm). The samples were rinsed with deionized water, incubated in deionized water overnight and then dried overnight, at room temperature, in a vacuum oven. Thus obtained samples will be referred to as PGS-AEMA samples.

The final step of the surface modification procedure was to covalently immobilize GelB. The PGS-AEMA samples were immersed for 1 hour in 2 ml of GelB solution (1 mg/ml) in deionised water. EDC (100 µl of a 1 mg/ml solution) was added to each sample and the reaction was maintained for another 4 hours at room temperature. Finally, the samples were rinsed with deionized water, incubated in deionized water overnight at 37ºC, dried at room temperature and stored in a dessicator until further use. In the rest of the present work, we will refer to the modified samples as PGS-GelB. After the immobilization of GelB on the polymer samples, the release profile of the

unbound GelB from the polymer surface was analyzed for a period of five days.

2.2.4. Characterization of Modified Polymer Surfaces

Staining Test

A qualitative Coomassie Blue test was performed in order to determine the presence of amine groups on the surface of the PGS-GelB samples. Formation of the protein/dye complex stabilizes the negatively charged anionic form of the dye, producing a blue color on the samples. Plain PGS samples were also tested and served as blank samples. A solution of 1% (w/v) Coomassie in methanol was prepared and will be referred as solA. A second solution containing 20 (v/v) % methanol and 7% (v/v) acetic acid in deionised water was prepared and will be referred as solB. Both PGS and PGS-GelB samples were incubated for 30 min in 5% solA in solB (v/v). The samples were then incubated for 1.5 hours in solB in order to remove the excess of Coomassie dye. All samples were prepared in triplicate.

IR Mapping

Fourier transform infrared (FT-IR) imaging system (Spotlight 400, Perkin Elmer) equipped with a mercury cadmium telluride (MCT) detector was used to assess the homogeneity of the GelB coating on the PGS surface. For comparison, GelB and PGS samples were also analyzed. The system was operated in a reflectance mode over the range 4000–740 cm^{-1}. An appropriate sample area was selected, and the reflectance IR spectra were collected successively from the actual analysis area by a mapping process.

X-ray Photoelectron Spectroscopy (XPS)

XPS measurements were performed on an ESCA-probe VG monochromatised spectrometer equipped with an Al Kα X-ray source (1486 eV). Survey spectra were collected for both PGS and PGS-GelB films. All samples were analyzed in triplicate (three surveys per sample) in a vacuum of at least 10^{-9} Pa. All elemental compositions obtained will be expressed as atomic percentages.

Atomic Force Microscopy Measurements

The samples roughness was investigated by atomic force microscopy (AFM), using a multimode scanning microscope (Digital Instruments, USA) equipped with a Nanoscope IIIa controller. Scans of 10 and 50 μm were recorded in the "tapping" mode under ambient conditions using a silicon cantilever (OTESPA, Veeco). Nanoscope software version 4.43r8 was used to obtain the root-mean-square roughness (R_q) values from the recorded images, after an XY Plane Fit Auto correction and Flattening procedure. The R_q is defined as the average of peaks and valleys of a surface and can be calculated as follows:

$$R_q = \sqrt{\frac{(Z_i - Z_{ave})^2}{N}}$$

where Z_{ave} is the average Z height value within a given area, Z_i is the current Z value and N is the number of points within the given area.

Quantification of GelB

Radiolabelled Gelatin was used in order to quantify the GelB covalently bonded on the surface of PGS films. Radiolabelled GelB was produced by firstly preparing a stock solution of 5% (w/v) Bolton-Hunter gelatin (BHG) subsequently radiolabelled with ^{125}I (GE/Amersham Health, Einhoven, Holland) by means of the Iodogen-method, according to previously described methods [172]. The concentration of BHG in the final GelB solution was adjusted to 1 mg/ml in MilliQ water. Each PGS-AEMA sample was incubated in 2 ml of this solution for an hour, after which 100 μl EDC (1mg/ml) was added. The vials were incubated at room temperature for 4 hours, washed with MilliQ and incubated at 37°C overnight in MilliQ. The quantification of the radiolabelled gelatin deposited on the PGS surface was done by measuring the radioactivity of the sample using a dose calibrator (CAPINTEC CRC-15R, USA). Stability tests in PBS pH 7.4 were performed for 10 days. All samples were analyzed in triplicate.

2.2.5. Other Enabling Applications – Proof of Concept Application: Stent Coating by Electrospraying and Dip-coating

316L stainless steel (28.0 mm length and 6 cells) were kindly provided from Aeromedicals S.A. (Buenos Aires, Argentina) and used as specimens for coating application. The stents were cleaned with acid pickling solution according to a standard procedure [176] (1 ml HF + 9 ml HNO_3 + 90 ml H_2O) in an ultrasonic cleaner at 45°C and then washed with bi-distilled water to remove the reagents. For the electrospray coating technique a 20% solution (w/v) of PS-PES in hexafluoroisopropanol (HFIP) was used in a typical electrospinning setup. The polymer solution was sprayed through a syringe with a 20 gauge needle connected to a pump (New Era Pump Systems LLC). Each stent was placed on a rotating mandril and optimized experimental conditions were obtained with 10 ml/h flow rate, 18 kV and 14 cm distance between the stent and the needle. For the dipping technique, a solution of 10% (w/v) PS-PES in HFIP was prepared and used to dip the stents. For curing purposes, the coated (electrospray and dip) stents were placed in a vacuum oven at 135°C for 3 days.

The surface morphology of the coated stents was evaluated using a scanning electron microscope (SEM) JEOL JSM 5600 instrument, equipped with a secondary electron detector.

2.3. Results and Discussions

2.3.1. Poly (polyol sebacate)s Synthesis: Bulk vs. Microwave Polymerization

In the present project, novel poly (polyol sebacate)-derived polymeric materials with tunable mechanical properties and good biocompatibility for tissue engineering applications have been successfully synthesized (Figure 2.2). The derived elastomers of poly (glycerol sebacate) and poly(erythritol sebacate) were synthesized by adding two different monomers to the reaction, namely 1, 3-propanediol and 1,10-decanediol. 1,3-propanediol is a known monomer in the synthesis of polyesters and polyurethanes and has a

very high market value [177]. 1,10-decanediol is another intermediate in the synthesis of polyesters and is widely used from cosmetics to pharmaceuticals [178, 179]. The two monomers have the goal of chain extenders, increasing the molecular weight and obtaining a variety of different mechanical properties and different degradation rates.
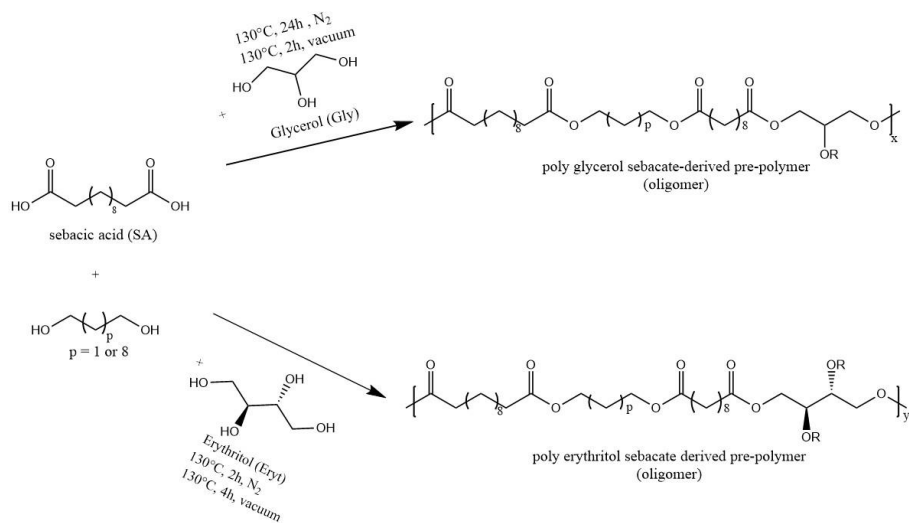
Figure 2.2: Thermal polyesterification of sebacic acid and different polyols

For comparison reasons the syntheses were performed via two methods: conventional bulk polymerization and microwave polymerization. The use of microwave synthesis for polymerization reactions is more than justified by the acceleration of the reaction rate and the uniformity of the heating. While conventional heating is done by conduction, there might be a temperature difference between the core of the reaction mass and the glassware. Microwave irradiation is based on the dielectric (molecular) heating. This implies that monomer molecules will try to align to the applied electromagnetic field, will collide and the desired pre-polymer will be obtained [180]. The enhanced reaction rate is also due to the fact that the synthesis is performed in a closed (pressurized) cap vessel that allows the use of higher temperatures. Based on the outcome of this comparative study, a selection of one of these methods will be made for further characterization and biocompatibility evaluation.

2.3.2. Poly (polyol sebacate) Pre-polymers Synthesis and Characterization

The development of all elastomers involved a two-step procedure. Firstly, oligomers or low molecular weight polymers are synthesized via either bulk polymerization or microwave irradiation. Once these pre-polymers are obtained they are thermally cured into the final elastomer. In the thermal curing step of the pre-polymers, the presence of the remaining unreacted – OH groups allows further crosslinking between polymer chains. More specifically, the curing implies that the pre-polymer is subjected to a temperature of 135°C for 2 or 4 days, in a vacuum oven, or alternatively overnight in a nitrogen flushed oven. Via this way, the final elastomers are obtained.

To the best of our knowledge, until now the poly (erythritol sebacate) has never been synthesized by the microwave method we report [18]. We also propose herein a method of synthesis for PES via bulk polymerization, adapted from the one previously reported, that rendered much higher molecular weights and elastomeric films with higher hydrophilicity. For the poly (glycerol sebacate) elastomer, Aydin et al. reported in 2013 the first microwave synthesis for the pre-polymerization step [181]. Although they reported a total pre-polymerization step of 3 minutes, the method uses a domestic microwave that leads to lack of reproducibility and safety of the experiments. In addition there is no temperature control over the reaction. Therefore, a standardized method would be preferred to increase its reproducibility and safety. In the present thesis a reproducible microwave-assisted polycondensation process of poly(polyol sebacate) polymers is reported.

In the microwave polymerization technique, temperatures higher than in the reported conventional synthesis [17] were used, namely 180° and 200°C. The microwave system was set to a constant temperature mode, a pressure of 5 bar being maintained. Due to the absorbance of microwaves by the starting materials, the power did not reach the set value (200 W) and varied between 50 and 60 W. The effect of the reaction time on the molecular weight of PGS, PES and their derivate elastomers is presented in Table 2.1.

*Table 2.1: Effect of bulk polymerization and microwave irradiation on the properties of the PGS and PES derived pre-polymers. * Determined using ^{1}H-NMR, ** theoretical molar ratio*

Material	Reaction time (hours)	Synthe-sis route	M_n (g/mol)	M_w (g/mol)	PDI	Molar ratio* SA/polyol/diol	Molar ratio ** SA/polyol/diol
PGS	24	Bulk	2208	2650	1.2	1.1/1	1/1
	0.5	Micro-wave	2400	2600	1.1	1/1	
	1		2400	2600	1.1	1/1	
	2		2400	2700	1.1	1.1/1	
	4		2600	2800	1.1	1.1/1	
PGS-PS	24	Bulk	12700	14000	1.1	1/0.61/0.39	1/0.6/0.4
	0.5	Micro-wave	2000	2200	1.1	1/0.57/0.43	
	1		2500	2900	1.1	1/0.57/0.43	
	2		2700	3000	1.1	1/0.6/0.4	
	4		2900	3000	1.1	1/0.6/0.4	
PGS-DS	24	Bulk	7100	8500	1.2	1/0.6/0.4	
	0.5	Micro-wave	2500	2800	1.1	1/0.6/0.4	
	1		2800	3000	1.1	1/0.6/0.4	
	2		3100	3200	1.1	1/0.6/0.4	
	4		3000	3300	1.1	1/0.6/0.4	
PES	24	Bulk	2800	4200	1.5	1.06/1	1/1

	0.5	Micro-wave	1800	2200	1.2	1.1/1	
	1		2000	2800	1.4	1/1	
	2		2200	2500	1.1	1/1	
	4		2700	3600	1.3	1.28/1	
PES-PS	24	Bulk	16500	18000	1.1	1/0.6/0.4	1/0.6/0.4
	0.5	Micro-wave	1900	2000	1.1	1/0.6/0.4	
	1		2200	2300	1.1	1/0.6/0.4	
	2		3200	3700	1.1	1/0.5/0.4	
	4		3300	3600	1.1	1/0.6/0.4	
PES-DS	24	Bulk	6700	8700	1.3	1/0.6/0.4	
	0.5	Micro-wave	2000	2200	1.1	1/0.6/0.4	
	1		2300	2600	1.1	1/0.6/0.4	
	2		3700	4100	1.1	1/0.6/0.4	
	4		3800	4300	1.1	1/0.6/0.4	

Although the microwave polymerization was also performed at 130°C (i.e. the usual reaction temperature used for bulk polymerization), for reaction times between 0.5 and 4 hours, no pre-polymer was obtained. In this case sebacic acid crystals could still be seen and the reaction mass was visibly not homogeneous. This could possibly be attributed to the fact that the microwave reaction took place in a closed vessel and the water by-product could not be removed so quickly at such a low temperature; or to the possible too low reaction times. On the other hand, under bulk polymerization at reaction times of 0.5 to 4 hours and reaction temperatures of 180°C, the reaction mass was from slightly homogeneous for lower times (i.e. the

glycerol could still be seen apart from the rest of the reaction mass) to a homogeneous but non-viscous reaction mass. In addition, temperatures as high as 180° and 200°C could not be uniformly reached throughout the sand bath in which the bulk polymerization took place, making this process more prone to irreproducibility issues (i.e. molecular weight, etc.).

For the microwave synthesis at reaction temperatures of 180° and 200°C, an initial visual inspection showed a clear reaction mixture color difference, between the 0.5, 1, 2 and 4 hours reaction times. Figure 2.3 shows this finding for the PGS pre-polymer, but the observation was valid for all the pre-polymers synthesized via microwave irradiation. As the reaction time increased, the pre-polymers changed color from white-yellowish after 1 hour to brownish after 4 hours. This change was consistent with a slight increase in molecular weight. For the PGS-derived and PES derived polymers, this coloration was not so intense as the reaction time was enhanced, but was still noticeable. Contrary to what was expected, the ^{1}H-NMR spectra revealed no degradation peaks for the pre-polymers synthesized for 4 hours in the microwave reactor.
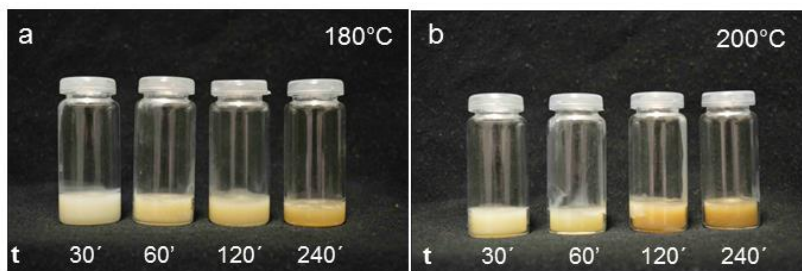
Figure 2.3: Color difference between PES-derived pre-polymers synthesized via microwave irradiation for 30 min, 1, 2 and 4 hours for a) 180°C and b) 200°C

Although the reason for this coloration is not clearly known, other research groups also reported a color change while increasing the reaction time of a microwave-assisted polyesterification [182]. In their study, Velmathi et al. obtained a coloration of their microwave polymerized poly (butylene succinate) when irradiated for 60 min (i.e. the maximum reaction time used by the authors) [182]. Nevertheless, the reaction is a reversible polyesterification where the by-product, water, can break again some of the

oligomer chains. As it is not removed during the microwave irradiation process due to the use of a closed capped-vial, it can lead to hydrolysis. Consequently, one can only obtain a limited molecular weight via the microwave polymerization process. This statement can be supported by the observation in Table 2.1 of the PGS- and PES-derived polymer molecular weights that are higher for the bulk polymerization process than for the microwave technique. Experiments were performed in an attempt to increase the molecular weight of the microwave synthesized materials. In this regard, a drying agent (i.e. $MgSO_4$) was used in order to remove the resultant water during the microwave process. As it was experimentally observed, the removal of this agent from the pre-polymer mass proved not to be feasible. A second reason for not selecting the microwave route included the fact that 10 fold lower quantities of pre-polymer could be synthesized in one batch via the microwave polymerization process (i.e. 3 g microwave vs 30 g bulk process). This was due to device constraints (i.e. small reaction tubes that can hold small amounts of reagents). It was therefore decided to further work with the PGS- and PES-derived pre-polymers obtained via bulk polymerization.

The further characterization of the PGS and PGS-derived (pre-) polymers was performed using different methods. First, the FT-IR spectra were recorded. As shown in Figure 2.4, the characteristic absorptions for these polyesters were noticed: the broad band at 3455 cm^{-1} indicates the O-H stretch was more intense for the pre-polymers than for the cured films. The peaks at 2850-2917 cm^{-1} were attributed to symmetric and asymmetric stretching of C-H in the alkene CH_2 groups, respectively. The C=O stretch at 1731 cm^{-1} sharpened with the increase of crosslinks, while the CH_2 band was present between 1445 and 1485 cm^{-1}. The -COO- ester bonds at 1158 cm^{-1} were more pronounced for the polymer films and the $(CH_2)_n$ (i.e. where n is 4 or more) C-C deformation band at 724 cm^{-1} was present in all cases.
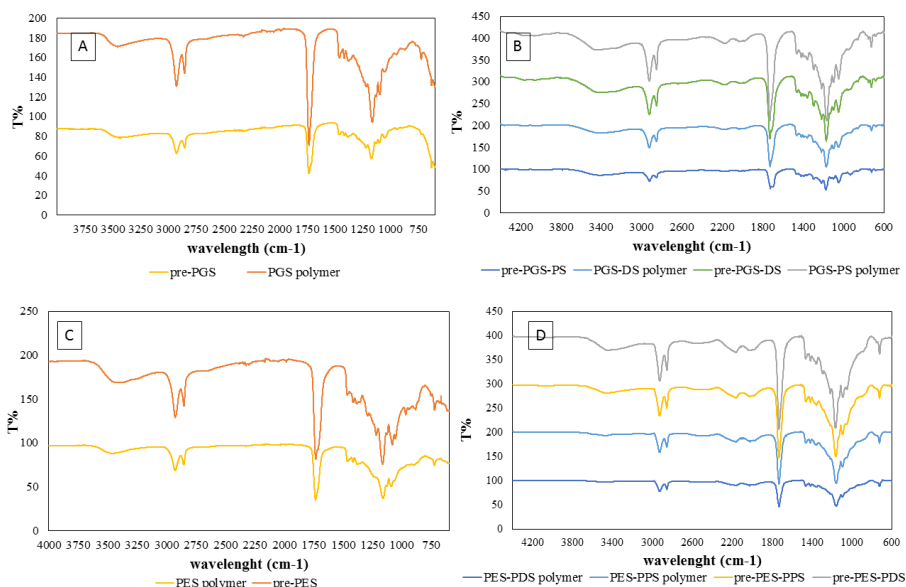
Figure 2.4: FT-IR spectrum of pre-polymers and cured elastomers. A) spectra of PGS pre-polymer and cured elastomer; B) spectra of PGS-derived polymers; C) spectra of PES pre-polymers and cured elastomer; D) spectra of PES-derived polymers.

Secondly, the proton NMR spectra of the obtained polymers were recorded. Both conventionally and microwave synthesized pre-polymers presented typical signals: three signals belonging to the sebacic unit between 1.3 and 2.5 ppm; signals for the methylene protons of glycerol between 3.5 and 4.4 ppm; and signal for the methine protons of the 3 glycerides between 4.8 and 5.5 ppm, as it can be seen in Figure 2.5. All chemical shifts are in agreement with previous studies [167, 183]. The addition of 1,3-propanediol leads to the presence of multiplets corresponding to its methylene protons between 1.8 and 2 ppm. A peak corresponding to the 1,10-decanediol lateral methylene protons was also noticed at 4.06 ppm. In conclusion, all data suggests that the diols were successfully incorporated in both pre-polymers (Figure 2.5).

For the PES pre-polymers, ^{1}H-NMR spectra were recorded in deuterated DMSO-d_6 that rendered a quintet at 2.5 ppm. The peak assignment for the obtained pre-polymers are as follows: ^{1}H NMR for PGS (300 MHz, CDCl$_3$-d) δ ppm 1.22 - 1.38 (m, 20 H) 1.52 - 1.69 (m, 10 H) 2.23 - 2.40 (m, 10 H) 3.68 -

3.76 (m, 2 H) 4.07 - 4.24 (m, 6 H); ^{1}H NMR for PGS-PS (300 MHz, CDCl$_3$-d) δ ppm 1.26 - 1.42 (m, 19 H) 1.54 - 1.71 (m, 10 H) 1.84 - 2.00 (m, 3 H) 2.24 - 2.40 (m, 9 H) 3.64 (d, J=6.22 Hz, 1 H) 3.67 - 3.76 (m, 2 H) 3.82 - 3.90 (m, 1 H) 4.09 - 4.25 (m, 6 H); ^{1}H NMR for PGS-DS (300 MHz, CDCl$_3$-d) δ ppm 1.24 - 1.41 (m, 5 H) 1.24 - 1.41 (m, 21 H) 1.51 - 1.67 (m, 10 H) 2.23 - 2.39 (m, 6 H) 3.60 - 3.70 (m, 1 H) 3.65 (t, J=6.59 Hz, 2 H) 4.04 (s, 1 H) 4.04 - 4.13 (m, 3 H) 4.19 (dd, J=6.40, 5.27 Hz, 1 H); ^{1}H NMR for PES (300 MHz, DMSO-d$_6$) δ ppm 1.16 - 1.33 (m, 14 H) 1.38 - 1.55 (m, 7 H) 2.19 (t, J=7.35 Hz, 3 H) 2.23 - 2.32 (m, 4 H) 2.50 (dt, J=3.63, 1.86 Hz, 8 H) 3.26 - 3.42 (m, 7 H) 3.45 - 3.58 (m, 3 H) 3.95 (dd, J=11.21, 7.06 Hz, 2 H) 4.18 (dd, J=11.21, 2.92 Hz, 2 H); ^{1}H NMR for PES-PS (300 MHz, DMSO-d$_6$) δ ppm 1.16 - 1.32 (m, 15 H) 1.41 - 1.58 (m, 7 H) 1.87 (dd, J=6.59, 6.22 Hz, 1 H) 2.15 - 2.32 (m, 7 H) 2.50 (dt, J=3.72, 1.81 Hz, 3 H) 3.28 - 3.41 (m, 6 H) 3.33 (s, 6 H) 3.45 - 3.61 (m, 2 H) 3.93 - 4.09 (m, 3 H) 4.19 (dd, J=9.89, 1.41 Hz, 1 H); ^{1}H NMR for PES-DS (300 MHz, DMSO-d$_6$) δ ppm 1.11 - 1.28 (m, 16 H) 1.31 (br. s., 2 H) 1.42 - 1.59 (m, 8 H) 2.15 - 2.32 (m, 6 H) 2.51 (dt, J=3.77, 1.88 Hz, 3 H) 3.38 (d, J=4.52 Hz, 3 H) 3.33 (s, 7 H) 3.45 - 3.54 (m, 1 H) 3.54 - 3.68 (m, 1 H) 3.90 - 4.04 (m, 3 H) 4.16 (br. s., 1 H).

The presence of $-CH_2-$ signals between 4 ppm and 5 ppm indicate the formation of the esters, while the ones between 1.1 ppm and 2.4 ppm indicated the methylene protons of sebacic acid. The assignments of the chemical shifts in Figure 2.5 are in agreement with the data of Barrett et al [18]. The ratios between the sebacic acid/diols/polyols were calculated by determining the ratio between the methylene protons within the different polyols and sebacic acid (Table 2.1).

2.3.3. Development and Characterization of Elastomeric Films

All pre-polymers obtained via bulk polymerization were further crosslinked (i.e. cured), in a vacuum oven at 135°C for 2 to 4 days. Although studies report curing times between one and four days for pre-polymers like PGS [56, 184], in the present work the pre-polymers subjected to vacuum for one day did not lead to film formation. It was therefore noticed that the herein

developed pre-polymers can only form films after a minimum curing time of two days.
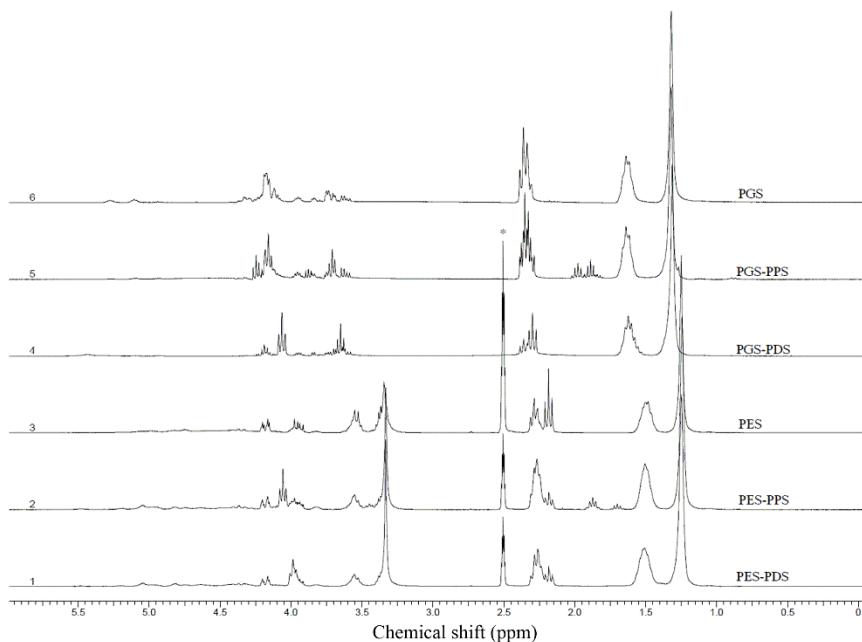
Figure 2.5: *¹H-NMR spectra for the polyesters obtained by bulk polymerization.*

The thus cured obtained polymers (i.e. elastomers) were delaminated from the glass plates by incubation in water, followed by removal of the residual unreacted compounds by incubation in ethanol. As these are the final materials to be applied for cell culturing and tissue engineering applications, intensive characterization from a thermal and mechanical perspective was performed. Furthermore, biodegradability and biocompatibility aspects were also considered.

The static contact angle (SCA) was registered as it enables detection of small wettability differences in the outmost surface layer (i.e. 0.5-1 nm) of a substrate [185]. Although previous research studies reported various contact angles for PGS films, from 32° to 65° [17, 186, 187], our findings indicate that after the curing step, very few free hydroxyl groups were present on its outmost surface. The test revealed that the PGS-derived materials are hydrophobic, with a static contact angle of around 70°, lower than the PGS

reference material (93°). Table 2.2 presents these results. The SCA for PES-derived elastomers (22° and 37°) suggest that these materials are more hydrophilic than the previously reported PES films (59°) [18]. The introduction of diols, in both starting materials, PGS and PES, leads to a decreased water contact angle. This finding can be attributed to the presence of a higher number of hydroxyl units, being hydrophilic in nature.

The swelling properties of the obtained polymers in aqueous media offer valuable information, especially considering that these materials are to be applied in various media for cell culturing purposes. Therefore, three media were investigated in this study, namely water, PBS pH 5.5 and PBS pH 7.4 (Table 2.2). After 8 hours of medium incubation, the polymers' swelling reaches a plateau which represents the maximum medium uptake. The starting polymers (i.e. PGS and PES) exhibited a similar swelling degree (i.e. 3%), while the derived polyol sebacates presented lower swelling capacities (Table 2.2). The change in swelling degree is correlated with the hydroxyl units within the polymer networks. A decrease in crosslinking degree was noticed when comparing the decanediol-derived polymers to the reference ones (i.e. PGS $4.4 \times 10^{-4} \pm 0.2$ mol/cm^3 vs. PGS-DS $3.5 \times 10^{-4} \pm 0.2$ mol/cm^3). Indeed, the addition of the propanediol and decanediol leads to less hydroxyl groups available within the crosslinked network. This indication is also reflected by the gel content within the crosslinked network of the derived polymers which decreased for all materials containing the short and long alkyl chained diols. These observations are in agreement with Patel et al. who noticed the same trend when adding polyethylene glycol to the PGS backbone structure [188] .

The herein developed polymers ranged from flexible to more rigid elasticity which is verifiable through the Young's modulus (YM) that varies between 0.6 MPa and 13.1 MPa (Table 2.2). The mechanical properties were investigated for polymer films cured for 2 and 4 days. The tunability of the elastomers is demonstrated when altering parameters such as the curing time, the curing temperature and the monomer molar ratio. This statement is in agreement with previous reports [60].

In the present experiments, prior to tensile testing, the films were incubated at 37°C in MilliQ water and in a buffer solution pH 7.4 for 24 hours. At least 4 measurements were performed for each sample. Figure 2.6 summarizes the results of the tensile tests performed. The plasticizing effect of the incubation medium on the cured elastomers can be noticed in Figure 2.6A and B. This is in agreement with previous studies of PGS materials [189].

Table 2.2: Thermal and physico-mechanical properties of the various cured materials.

Material	T_g /T_m/T_c (°C)	Gel content (%)	Swelling [a] (%)	SCA (°)	Young's modulus [b] (MPa)	Crosslinking degree [c] x 10^{-4} (moles/cm³)
PGS	T_g: -27	99.1±1.7	3.0±0.5	93±6	1.5±0.2; 3.2±0.2	1.8±0.4; 4.4±0.2
PES	T_g: -10	99.0±0.7	3.0±0.1	24±2	0.6±0.1; 3.7±0.3	0.8±0.1; 4.8±0.3
PGS-PS	T_g: -36	96.4 ±0.5	1.3±0.3	70±2	1.3±0.3; 3.3±0.3	1.7±0.4; 4.4±0.5
PGS-DS	T_c: 2 T_{m1}: 23	93.9±0.4	1.3±0.3	69±4	13.1±1.4; 2.6±0.1	n/a ; 3.5±0.1
PES-PS	T_g: -25	96.6±0.4	0.3±0.1	22±5	1.7±0.2; 3.8±0.1	2.2±0.2; 5.1±0.2
PES-DS	T_g: -31	97.6±1.3	0.2±0.01	37±9	1.3±0.1; 3.0±0.3	1.8±0.1; 4.0±0.4

[a] in water; [b] tensile tests were performed on polymer films that were cured for 2 days and 4 days at 135°C; the polymer films were incubated in water prior to the testing; [c] crosslinking degree calculated for a 2 and 4 days cured elastomer.

As anticipated, the Young modulus increases with an increasing curing time (Figure 2.6C). For example, a value of 1.6 ± 0.15 MPa was obtained for PES-PS cured 2 days, while the polymer cured for 4 days rendered a value of 3.7 ± 0.07 MPa. The polymers exhibited the shape of the stress-strain curves as for other elastomers (Figure 2.6A, B). However, PGS-DS displayed a higher Young modulus and irregular stress–strain curves when compared to the other elastomers (Figure 2.6D). Its curve had a local maximum (= yield point), then a local minimum, and a final increase before break. This irregular shape

of the semi-crystalline thermoset is most likely caused by the presence of semi-crystalline zones within the elastomeric network.

Determination of the Young's modulus enabled the calculation of the crosslinking density, which is expressed in moles of active network chains per unit volume. As an example, a value of 2.2 x 10^{-4} ±0.2 moles/cm^3 was obtained for the PES-PS cured for 2 days whereas a value of 5.1 x 10^{-4} ±0.2 moles/cm^3 was obtained for the polymer cured for 4 days. As mechanical properties provide an important insight into the possible applications of materials, we can conclude that the YM range and the corresponding crosslinking densities for the obtained elastomers enables their use for soft tissue engineering applications.
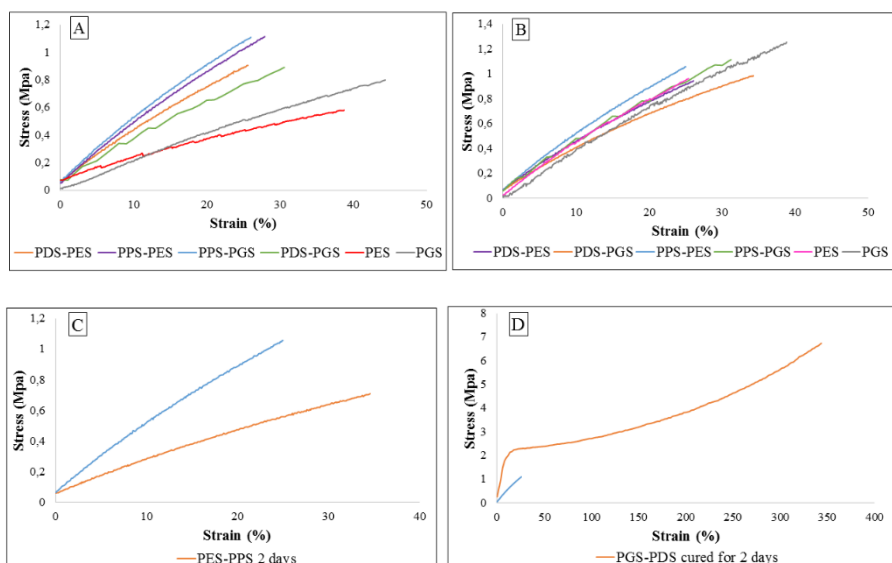
Figure 2.6: Stress vs. strain curve of the obtained elastomers: A) non-hydrated materials; B) materials hydrated in PBS pH 7.4 for 24 hours, at 37°C; C) PES-PS cured for 2d vs 4 d; D) curve of a semi-crystalline PGS-DS network.

Semi-crystalline thermosets were also reported for poly(erythritol dicarboxylates) such as PES, although in the present study only the decanediol-derived poly(erythritol sebacate) (i.e. PES-DS) presented semi-crystalline zones noticed by DSC measurements [18]. As for PES-DS, the decanediol-derived PGS material also presented several transitions (see

Table 2.2). The plain PGS, PES and propanediol-derived PES material did not present any noticeable crystallinity as the DSC curves reveal only glass transition temperatures within the investigated temperature interval. All findings are in accordance with previous studies that state that although some materials from this class of polymers are semi-crystalline, they are completely amorphous above 37° [56, 190, 191]. This was confirmed in the present work, as none of the herein obtained polymers presented any transition above this temperature. Thermal analyses were also performed in order to see whether the curing process renders homogeneous films. TGA and DSC measurements were executed on three different spots from an area of 12 cm^2 of the same cured polymer film. PES (Figure 2.7, B) and PGS (Figure 2.7C, D) were chosen as proof-of-concept materials. As can be noticed in Figure 2.7, all analyzed spots from the same sample (polymer cured at 135°C) revealed identical thermal profiles, making these films homogeneous throughout their surface.
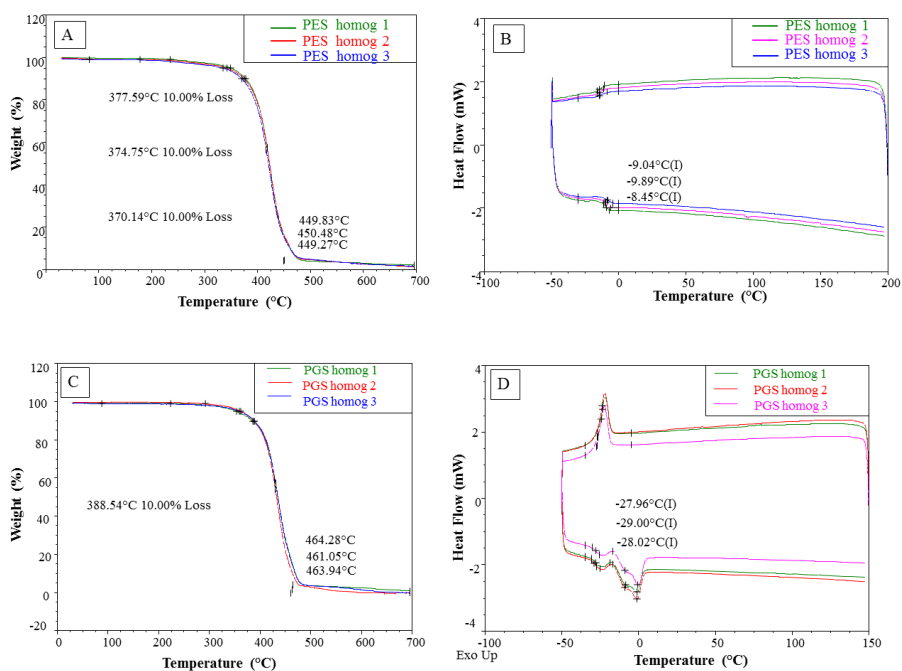

Figure 2.7: Determination of film homogeneity on PES (A,B) and PGS materials (C,D) as studied by thermal analyses (TGA and DSC).
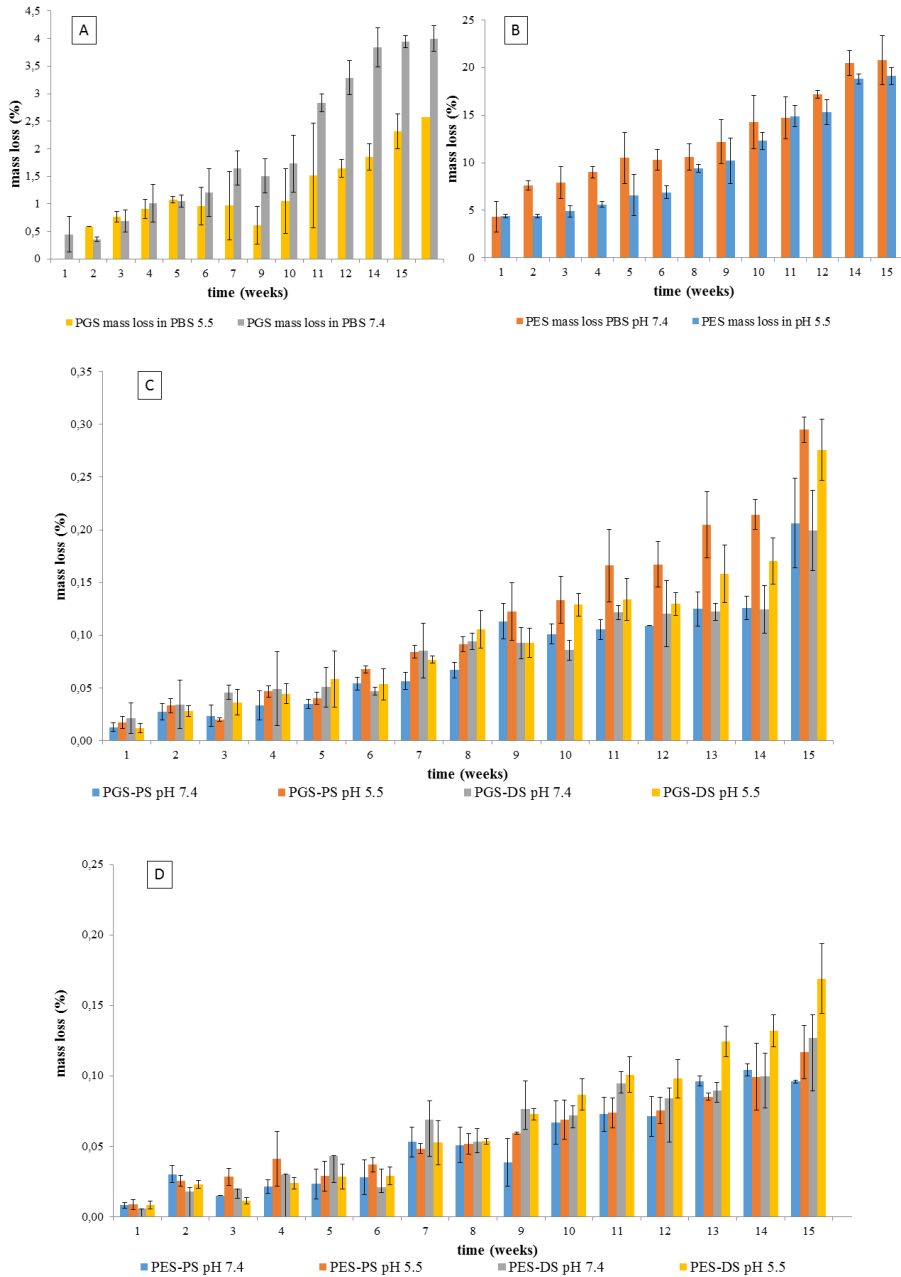
Figure 2.8: Degradation study for the newly synthesized poly(polyol sebacate) elastomers.

As there is a continuous and stringent need for biodegradable biomaterials for a variety of biomedical applications, we have studied the *in vitro* degradation of the synthesized poly (polyol sebacate) polymers. The *in vitro* degradation of the newly developed polymers was monitored over a period of 16 weeks. Previous studies reported that the PGS polymer degrades *in vitro* 15% over a period of 4 weeks, whereas *in vivo* studies observed a complete resorption of the material after 60 days [17].

The *in vivo* characteristics of PGS materials with different crosslinking densities [63] also revealed no significant correlation between the polymer mass loss and the crosslinking density (i.e. curing time). Therefore, we hypothesized that introducing new chemical functionalities in the PGS structure might provide a key to slower degradation rates [40].

In the present study, a significant difference ($p < 0.05$) was noticed between the mass loss of the initial polymers and the mass loss of the PGS- and PES-derived ones (Figure 2.8). The maximum mass loss of PGS-derived polymers was 0.29 ±0.02%, while PES-derived polymers lose less than 0.18 ±0.02% of their mass after 16 weeks of medium (i.e. PBS) incubation (Figure 2.8). No conclusive difference was noticed between the samples that were degraded at pH 5.5 and the ones at pH 7.4. Relative to the above described studies of the plain PGS (4.0±0.2%) and PES material (22.0 ±0.7%), the derived polymers show indeed a slower degradation *in vitro*. As it was reported that the *in vivo* degradation mechanism of these class of elastomers is probably controlled by an enzymatic surface erosion process, further degradation studies should be conducted in the future [64].

2.3.4. Surface Modification of Poly(polyol sebacate) Films

Like other synthetic biomaterials, PGS and PES-derived polymers are desired to create a biomimetic environment *in vitro*. For this purpose, they require modifications with extracellular matrix proteins [76]. Surface modification of the PGS native material is also required due to its high hydrophobicity, similar to that of polydimethylsiloxane, a known silicone [110, 192]. In the present

work, a surface modification strategy with gelatin, previously developed by Desmet et al., was chosen to be investigated [109].

Gelatin has been intensively reported in literature as a coating for various implantable biomaterials, such as PU [193, 194], PLLA [195], PCL [109, 196], PI [193], titanium [197], etc. As it is non-toxic, biodegradable, and non-immunogenic, it enhances cytocompatibility and cell proliferation [198]. Until now, only physical adsorption of the bioactive molecules such as gelatin [161], laminin, fibronectin, collagen and elastin [199] has been performed onto the surface of polymers like PGS. Therefore, gelatin type B (GelB) was chosen to be chemically immobilized on the surface of PGS films, via a graft polymerization procedure. PGS was chosen as a model system for the herein developed polymers. Figure 2.9 depicts the general scheme for this modification strategy.
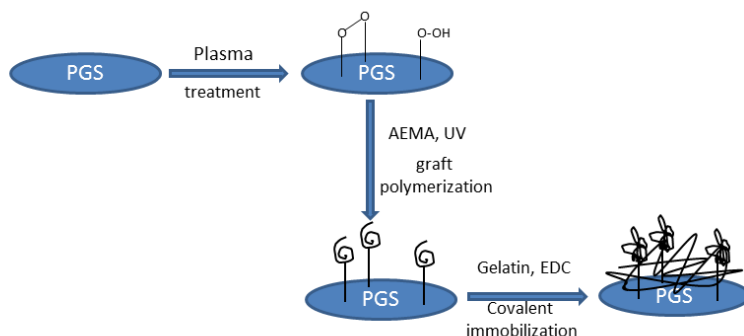
Figure 2.9: General scheme for the GelB immobilization strategy.

This modification strategy can be easily transferred to all the poly(polyol sebacates) developed in the present thesis, as the surface chemistry of these elastomers is similar to each other (i.e. only carbon and oxygen is present on the elastomer surface).

2.3.4.1. Optimization of the modification protocol

Firstly, the polymer surfaces were plasma treated in order to create reactive groups that would act as initiators for the subsequent graft polymerization step. The plasma discharge step was performed using Argon to induce free radicals on the PGS surface, which react with the atmospheric oxygen to form

(hydro)peroxide groups [77, 200]. These groups result from recombination or cross-linking reactions and serve as initiator sites for the subsequent covalent immobilization of AEMA on the elastomer surface. In order to optimize the plasma exposure time that is necessary for this initial step, the PGS polymer surfaces were exposed to argon plasma for 30, 60 and 90 seconds, respectively. Figure 2.10 presents the ageing of the elastomer surfaces after plasma exposure. In all cases it was noticed that the PGS surface did not recover to its initial SCA (i.e. 93°) even after 6 hours. As no significant difference (p= 0.07 > 0.05) was noticed in the contact angles of the samples treated at different plasma times, the optimal choice was to further use 30 seconds of argon plasma exposure.
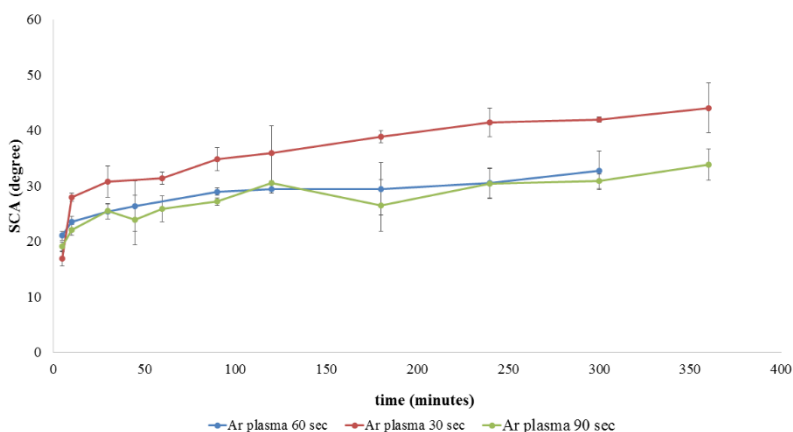
Figure 2.10: Ageing of PGS surfaces after plasma treatment

Secondly, a known methacrylate, 2-aminoethyl methacrylate (AEMA), was UV graft polymerized on the plasma treated PGS surfaces in order to enable GelB attachment. The optimization of the amount of AEMA to be applied on the polymer surface was monitored by XPS and SCA analyses, as presented in Figure 2.11. PGS samples were incubated in different concentrations of an aqueous AEMA solution (i.e. 0.5M, 1M and 1.5M) and exposed to UV light for 10, 30, 45 and 60 minutes, respectively. Although after AEMA grafting the static contact angles decreased significantly compared to the plain, unmodified material (i.e. 93°), there were no significant difference (p=0.5)

between the different AEMA concentrations at irradiation times between 10 and 45 minutes. The data showed that at 60 min UV irradiation time the lowest static contact angle was obtained for the 1M AEMA solution (Figure 2.11A). At this concentration, the PGS-AEMA samples also presented the highest nitrogen content (i.e. 3.18±1.24%), and therefore the highest content of amine groups (Figure 2.11B). Therefore, the optimized AEMA solution concentration used for the final surface modification step was 1M.
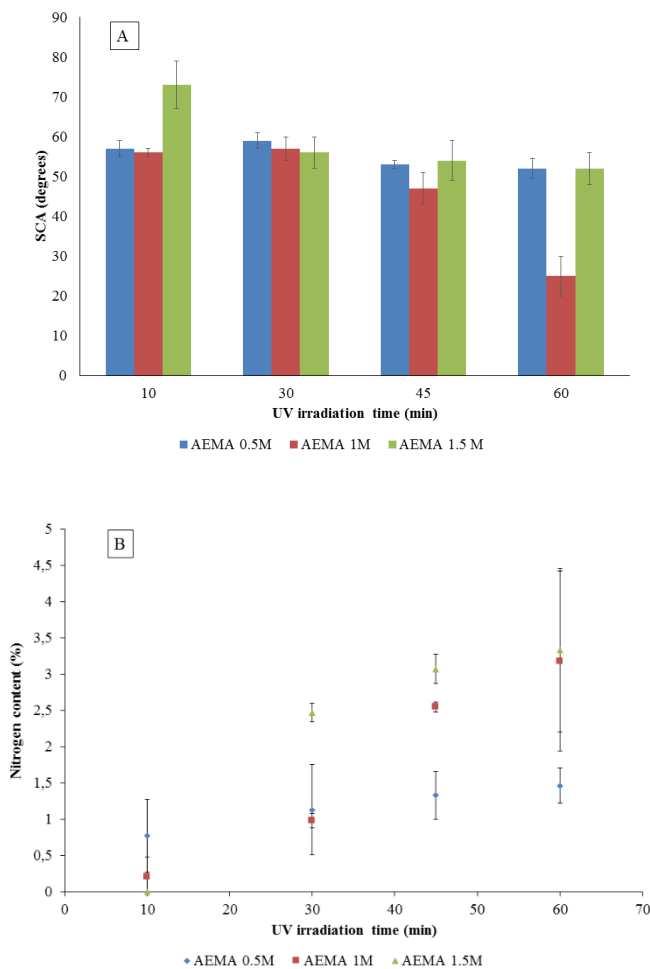
Figure 2.11: AEMA grafting optimization: (A) SCA vs. UV irradiation time; (B) XPS analyses - Nitrogen content vs. UV irradiation time.

Finally, the selected protein (i.e. GelB) was chemically immobilized onto the PGS-AEMA samples. The addition of EDC is important, as it generates a random crosslinking between the free amines on the polymer surface and the carboxyl groups of the adsorbed protein, as well as cross-linking of the free amines and carboxyl groups within the protein itself.

Different concentrations of GelB were also used in order to assess the optimum for its immobilization on the PGS films (Table 2.3). According to the XPS data, 1 mg/ml GelB concentration rendered a similar N/C ratio to that of the pure GelB. The atomic surface composition for gelatin, PGS, PGS-AEMA, and PGS-GelB films are presented in Table 2.3. A clear difference was observed as PGS spectra showed no N 1s peak. An increase in the nitrogen content was noticed from 3.2±1.3% for the PGS-AEMA samples to 10.2±1.7% for PGS-GelB samples. This attests to the fact that GelB is attached to the polymer surface, as more nitrogen containing groups are present. Furthermore, the compositions of the N/C x 100 ratio for the PGS-protein films was 16.5, similar to that of the pure protein we used (i.e. 17.9). Small percentages of Si peaks were also observed on the surface of the modified and non-modified polymer samples. This is probably due to either manipulation of the sample during the measurements or due to the glassware used in synthesis.

Table 2.3: The atomic compositions and ratios for the non-modified and GelB modified PGS films determined by XPS measurements.

	Gelatin B concentration	C (%)	O (%)	N (%)	Si (%)	N/C
PGS	n/a	67.0±1.3	26.7±0.8	n/a	6.3±0.5	n/a
PGS-AEMA	n/a	63.3±0.9	25.4±2.3	3.2±1.3	8.1±0.7	5.1
PGS-GelB	0.5 mg/ml	67.1±1.1	26.7±0.9	3.7±1.6	2.4±0.6	5.5
	1 mg/ml	62.0±0.2	24.6±1.1	10.2±1.7	3.3±0.4	16.5
GelB	powder	65.2±3.1	21.9±0.1	11.7±1.8	n/a	17.9

2.3.4.2. Characterization of the Optimized Film Surfaces

A preliminary qualitative staining test was performed in order to assess the presence of the amine groups on the surface of PGS-GelB samples. Commassie dye (Brilliant BlueR-250) was used as it binds to proteins through Van der Waals attractions and ionic interactions between the dye sulfonic acid groups and the positively charged protein amine groups. As it can be noticed in Figure 2.12, the modified samples presented a dark blue coloration that indicated the presence of amine groups. In contrast, the dye did not bind to the blank PGS samples that maintained their slightly yellowish, but clear color.
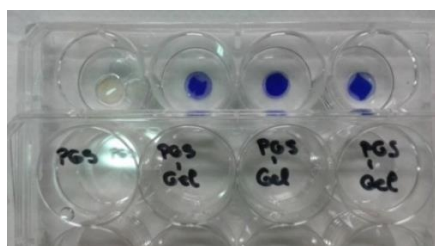
Figure 2.12: Commassie staining tests performed on PGS and PGS-GelB samples.

The presence of gelatin was also confirmed by ATR-IR mapping. The characteristic spectrum of gelatin contains specific bands at 1627 cm^{-1} that represents the C=O stretching of the of the peptide groups, at 1530 cm^{-1} representing the bending vibration of N-H groups and stretching vibrations of C-N groups, and at 1237 cm^{-1} that is related to the vibrations in plane of C-N and N-H groups [201]. The representative FT-IR spectra of GelB, PGS, and PGS-GelB samples are shown in Figure 2.13. The IR maps recorded in between 744 and 4000 cm^{-1} (Figure 2.13. (c)) indicate the complete protein coverage of the PGS film.

Static contact angle measurements using distilled water were performed in order to assess the wettability of the surface layer of the polymers (i.e. 0.5-1 nm). Although other research groups reported water-in-air-contact angles for PGS in the range of 17-32º [17, 58, 67], our measurements suggested a value of 93º for the non-modified PGS films.
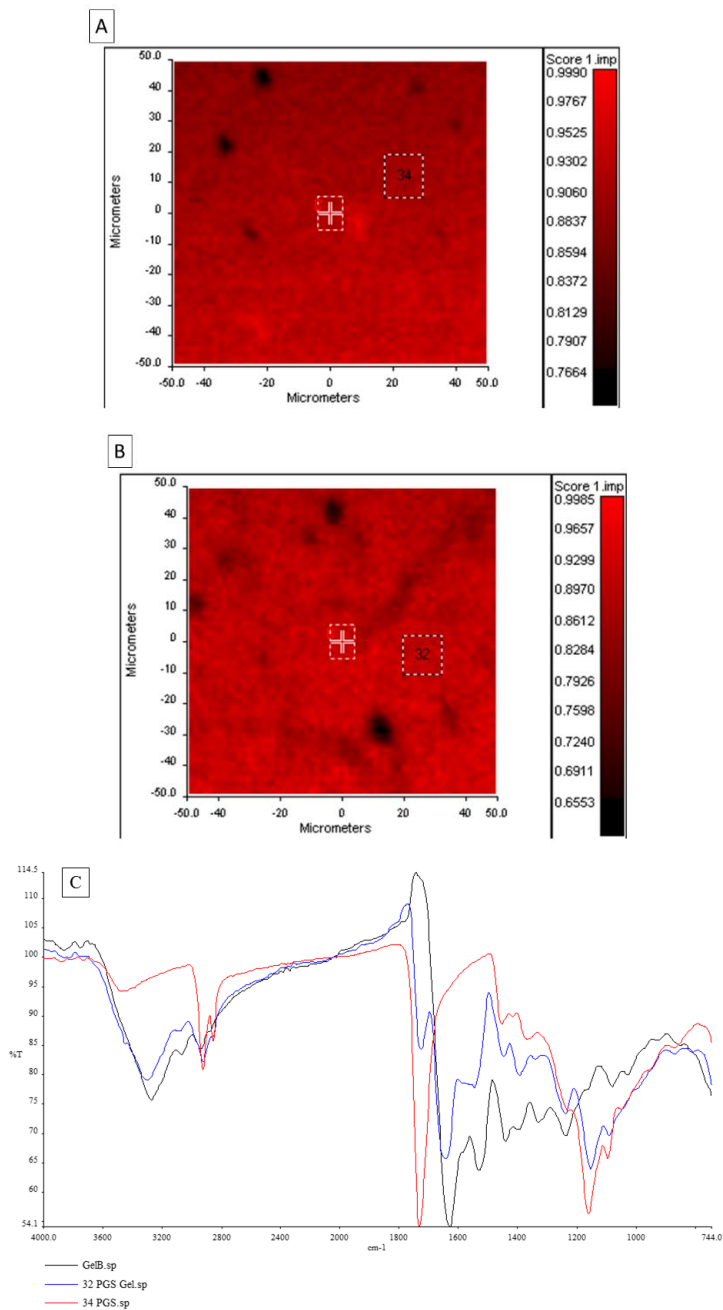
Figure 2.13: Attenuated Total Reflection Infrared (ATR-IR) maps showing the IR absorbance map of the (A) PGS-GelB and (B) GelB; (C) spectra of GelB (black), PGS-GelB (blue)and PGS (red).

This difference might be explained by the amount of OH groups left on the PGS surface after the curing step, and therefore also by the curing conditions. However, the hydrophilicity of the PGS-GelB films was significantly ($p<0.05$) higher than that of the plain PGS films. As anticipated, the contact angle decreased after the attachment of the gelatin coating from 93° to 34°.

AFM measurements were performed to determine the surface roughness at a resolution of 10 and 50 µm. As shown in Figure 2.14, the topographical analyses indicated that the chemical modification has an effect on the PGS surface morphology. The nano-depressions of PGS films were masked by GelB, rendering a smoother surface. While at 50 µm scale (50 x 50 µm^2) the blank PGS film had a root-mean-square roughness value (R_q) of 28.2 nm, the PGS-GelB film had an R_q of 14 nm (Figure 2.14 (c) and (d)). Taking a more detailed scan, at 10 µm scale (10 x 10 µm^2), the R_q value for the modified PGS samples is 0.6 nm, while the non-modified PGS has a value of 1.9 nm. The 10 µm scale measurements also showed that certain areas on the surface of the PGS-GelB film had a higher localized roughness (i.e. 42 nm) due to excess of the protein (Figure 2.14 (b)). However, the trend is similar for both 10 µm and 50 µm measurements; the general roughness decreased by approximately 2 fold. Furthermore, the surface of the gelatin-coated PGS (Figure 2.14(b) and 2.14(d)) indicates the absence of globular domains, which is atypical for globular proteins such as gelatin [193].

This might among others be related to surface wettability behavior of the AEMA modified PGS films. In order to quantify the amount of protein attached to the PGS film, a ^{125}I radiolabelled GelB analogue was used according to previous developed protocols [109, 172], following the procedure presented in this chapter's materials and methods section.

The effect of the AEMA grafting on the amount of the Gelatin B immobilized on the PGS surfaces was analyzed. Table 2.4 presents the significant difference ($p=<0.05$) between the AEMA coated PGS samples and the plain uncoated ones. The presence of AEMA on PGS surfaces led to higher amounts of immobilized GelB. More reproducible surfaces were also generated when AEMA was grafted on the polymer films prior to gelatin immobilization.
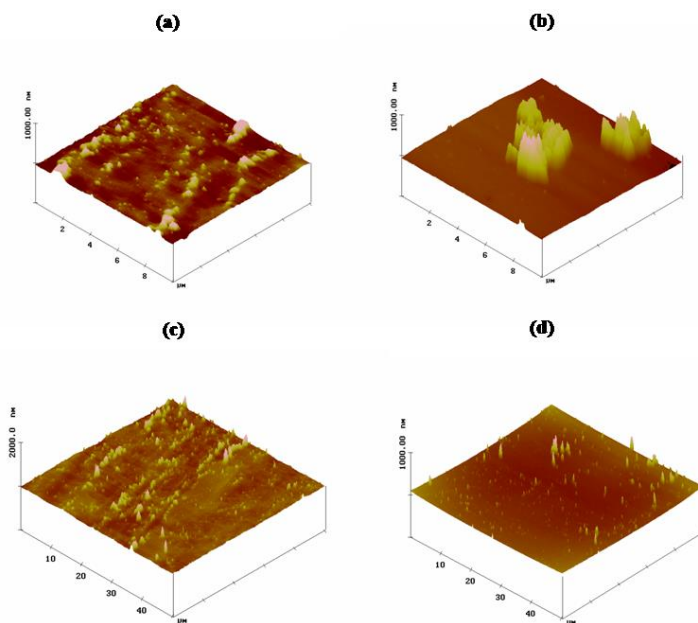
Figure 2.14: AFM images of (a) PGS 100 μm² ; (b) PGS-GelB 100 μm² ; (c) PGS 2500 μm² ; (d) PGS-GelB 2500 μm².

These findings are also in agreement with the studies performed by Desmet et al. and Kersemans et al. who developed protocols for AEMA grafting on PCL films and scaffolds prior to gelatin bonding [109, 172]. After the immobilization of GelB, the release profile, for a period of five days, of the unbound GelB from the PGS and PGS-AEMA samples was analyzed and presented in Table 2.4.

Table 2.4: The amounts of immobilized Gelatin on both AEMA treated and untreated PGS surfaces as determined using radiolabelling. The data is expressed as average ± standard deviation (n=3).

Incubation time of the PGS-GelB samples in medium, at 37°C (hours)	Immobilized ^{125}I radiolabelled GelB (μg/mm²)		
	Blank	AEMA	Released GelB (Δ)
0	4.5 ± 0.5	6.1 ± 0.5	1.6
24	4.2 ± 0.6	5.3 ± 0.1	1.1
48	4.0 ± 0.6	4.9 ± 0.1	0.9
120	3.6 ± 0.6	4.2 ± 0.1	0.6

A loss in activity over time was noticed for both AEMA treated and untreated PGS surfaces, probably due to the release of non-covalently bound gelatin. Nevertheless, the quantification of the Gelatin immobilized on the polymer showed that the protein coating is present on the PGS surface for at least five days.

2.5. Other Enabling Applications of the Developed Materials

According to the World Health Organization, cardiovascular diseases are the main cause of death globally, representing 31% of all deaths [202]. Percutaneous transluminal coronary angioplasty (PTCA) followed by stent implantation has gained a lot of interest since it was first introduced in 1986. Despite the significant improvement of stenting procedure over regular PTCA, it presents some serious clinical limitations that include intra stent restenosis and thrombosis. In order to prevent the overgrowth of tissue, drug eluting stents (DES) were introduced as a strategy to minimize the requirement for re-intervention [203-206]. Despite all efforts, long-term safety concerns emerged as incomplete endothelialization that gave rise to a life-threatening complication: late and very late stent thrombosis [207-209]. Late stent thrombosis is defined by the time interval between one month and one year after stent implantation, while very late stent thrombosis includes any thrombotic event beyond one year [210].

An incomplete endothelialization will maintain the implant in constant contact with human blood, which is a very hostile environment. As most coronary stents are made of metallic alloys, corrosion plays an important role on the implant outcome [211-213]. The corrosion process releases toxic ions into the surrounding tissue and into the blood flow that change the chemistry at the implant zone by promoting an overgrowth of endothelial cells as well as adhesion and activation of immune cells, giving rise to an inflammatory response and restenosis[214]. Corrosion also has an impact on mechanical properties affecting the integrity of the implant. Stent fracture due to corrosion attack has been detected in 1-3 % of coronary cases and this figure increases to 37 % in femoropopliteal stenting [215].

One approach to face this issue is to apply a coating on the stent surface with a biocompatible polymer in order to promote natural endothelialization and to prevent the material of being in contact with the aggressive content of the blood, specially the high levels of chloride that have been proven to promote localized corrosion including pitting and crevice corrosion (i.e. localized attack on a metal surface by which cavities are produced) in various metals and alloys [216, 217]. The most common bio-degradable polymers used for stent coating application include poly(glycolic acid) (PGA) or poly(lactic acid) (PLA) or their copolymers (PLGA), poly-ε-caprolactone (PCL) and copolymers using poly(ethylene glycol) (PEG) [218-221]. However, coatings made out of these polymers are often very brittle and tend to crack during stent implantation and expansion, requiring the need of a plasticizer to improve the tensile behavior [222]. Moreover, some lactide-glycolide and lactide-caprolactone copolymers were reported to swell up to 300% and to deform during degradation [223]. This alters the mechanical properties of the material and the physiology of the surrounding tissue [223].

Elastomeric materials have proven to offer mechanical integrity without influence on the tissue at the implantation site. Among the many elastomeric polymers, poly(glycerol-co-sebacate) (PGS) has gained special attention because it is a tough biodegradable material that undergoes surface erosion degradation with linear mass and strength loss during the resorption period with little deformation [60, 61, 183, 223]. PGS has been investigated with successful results for potential uses in soft tissue engineering including artificial microvasculature development [224]. It has been proven to be hemocompatible and its mechanical properties match the properties of the veins, especially in a dynamic environment [225].

In this context, the novel poly(polyol sebacate)-derived polymers synthesized herein were also applied for stent coating applications. As a proof of concept for the use of the herein developed materials, PES-PS was used to coat plain stainless steel stents via dip coating and electrospraying (Figure 2.15). This pre-polymer was chosen due to the fact that it had the highest molecular weight from all the synthesized materials. Higher molecular weight polymers imply higher viscosities, that always are advantageous for methods like

electrospinning and electrospraying. The pre-polymer solution was prepared in HFIP and the coating was further cured on the stent.

The dip coating technique is a conventional coating procedure that is normally used in coronary stents for drug eluting applications and to create a biocompatible surface in order to improve hemocompatibility [226-230]. It is well known to be a simple and fast one-step method with minimal requirements. In the present study, three concentrations were tried for the dip-coating procedure, namely 10 %, 15 % and 20 %. When using pre-polymer concentrations of 20 % and 15 %, pre-polymer accumulation was macroscopically visible in between stents struts. This finding led to the elimination of these two concentrations from further testing. The 10% pre-polymer solution was considered more optimal also due to the fact that it proved to remain on the metallic stent during the curing process, avoiding therefore pre-polymer removal from the metallic stent.
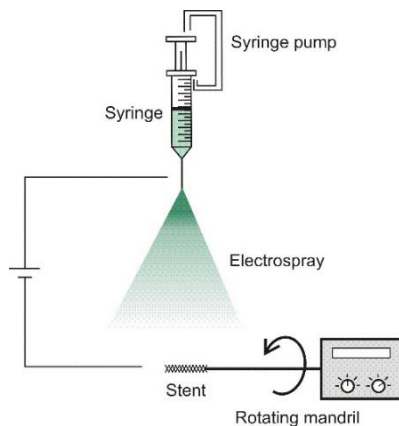
Figure 2.15: Electrospraying on metallic stents.

On the other hand, the electrospray technique had gained interest over the last decade for the ability to create films with nano or micro-thickness. This could potentially be used for fabrication of single or multi layered polymer structures on implants surface with complex topologies, including stents [231-234].

EDX (i.e. energy dispersive x-ray analysis) spot analysis was used to identify the elements present on the dip-coated and electrosprayed samples. Three

spots were chosen and analyzed for each stent. Figure 2.16 depicts the composition analyses of all the stents. An increase of carbon and oxygen was noticed for the coated stents when compared to the bare stent. This is an indication that a thin polymer coating was present on the metallic stent, as the surface and chemical structure of the material coating only contains the aforementioned elements.
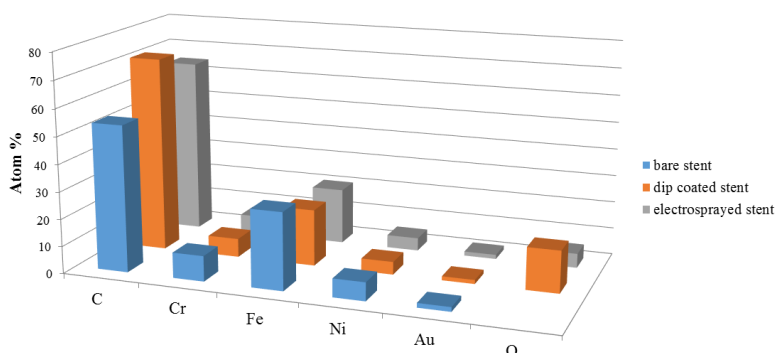
Figure 2.16: Elemental composition of bare vs. coated stents as determined using EDX spot analysis.

SEM micrographs of the plain stent, the dip coated stent and the electrosprayed stent are presented in Figure 2.17. BEC (Backscattered electron composition image) mode was also employed to attest to this fact and the coatings could be noticed in a darker shade, in contrast with the stent which is lighter. SEM micrographs for the dip coated stent are shown in Figure 2.17B. Polymer deposition mainly occurred as bridge formation at the curvatures of the metallic stent (Figure 2.17B). This is an undesired feature because it can interfere with the mechanical performance of the stent during the implantation and expansion. Also, bridges tend to delaminate and rupture the film during deployment and provide active sites for platelet and protein adhesion [235]. In addition, delaminated portions of the polymer film can migrate through the blood flow and block smaller and distant arteries leading to other complications [236].

In contrast to those results, electrosprayed stents revealed no polymer accumulation at the curvatures (Figure 2.17C) but leads to the production of

a non-uniform film with different thickness across the implant surface. Further investigations on these methods will therefore be the subject of future work.
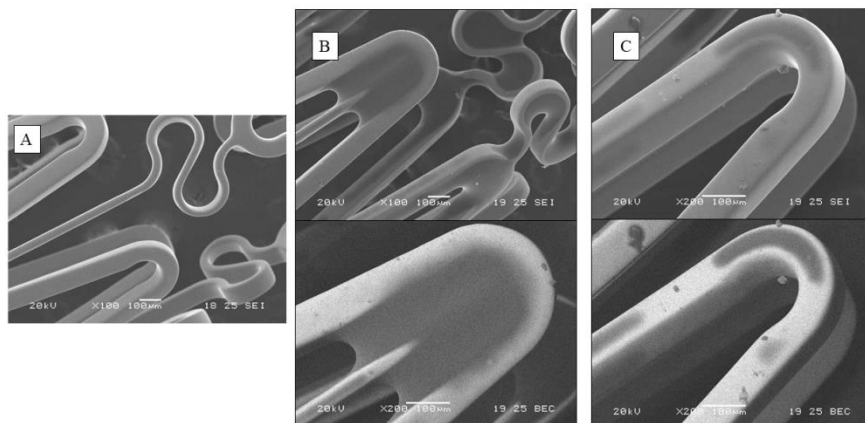
Figure 2.17: SEM images of (A) bare stent; (B) dip coated stent: top picture - SEI mode ; bottom picure - BEC mode; (C) electrosprayed stent: top picture - SEI mode vs bottom picture - BEC mode.

2.6. Conclusions

Biodegradable poly(polyol sebacate) elastomers with tunable properties have been synthesized and investigated for soft TE applications such as liver TE. The synthesis was performed via bulk polymerization and microwave irradiation. Although the latter polymerization type gained much interest due to its better reaction kinetics, and therefore advantageous synthesis time frames, in the present study only limited molecular weights were obtained via this synthesis path. This was due to the presence of the by-product, water, which can break some of the oligomer chains during the synthesis process. Bulk polymerization was concluded to be the better option for this type of synthesis, not only due to the fact that the PGS- and PES-derived polymer molecular weights were higher than for the microwave polymerization, but also because of the higher amount of pre-polymer that

can be synthesized in one batch (i.e. >30 g pre-polymer for bulk polymerization vs. maximum 3 g pre-polymer for microwave irradiation).

All synthesized pre-polymers were further thermally crosslinked and thoroughly characterized. The obtained polymers ranged from higher to lower elasticity (0.6 MPa to 3.8 MPa), from hydrophobic (PGS and PGS-derived polymers) to hydrophilic (PES and PES-derived polymers), and had low swelling degrees (up to 3%). A significant difference was noticed between the degradation rates of the plain PGS and PES materials (4 % and 22 % mass loss) and the derived ones (0.29 % and 0.18 % mass loss), proving the reported hypothesis that the degradation rate of the plain materials can be fine-tuned by adding different functionalities to their synthesis.

As synthetic biomaterials that mimic the ECM have a wide range of biomedical applications, PGS polymer films were also functionalized with gelatin via a chemical immobilization technique that has never been applied up to now for poly (polyol sebacate)s. This comes as an improvement to the already existing physio-sorbtion methods that lead to protein removal from the material.

In the context of the present thesis, the herein developed materials meet the requirements for the fabrication of microfluidic devices, as they are flexible, biodegradable and optically transparent (i.e. the latter being a much needed feature for the bioreactor assembly). As a proof of the versatility of the obtained materials to other soft tissue engineering applications than the main one stated in the introduction part of the present thesis, dip-coating and electrospraying were employed to process one of the materials for cardiovascular TE applications. The PES-PS material was therefore tested as a potential coating for stent applications. The tests showed that the dip-coated stents contained unwanted polymer accumulation at the curvatures, while electrosprayed stents had revealed a non-uniform polymer film with different thickness across the implant surface. As both methods suffer from limitations, further investigations on these methods should be the subject of future work.

In conclusion, the herein developed poly(polyol sebacate) pre-polymers have the advantages that their synthesis is fast (i.e. 28 hrs), straightforward (i.e. without the use of solvents and no purification needed) and can be transferred cheaply to industrial production (relatively simple infrastructure with low cost raw materials). Also, they can be easily processed through different scaffolding methods and microfabrication techniques, as presented in Chapter 3 and 4. The assessment of the biocompatibility of the herein developed polymer films will be assessed by culturing a hepatocellular line and human adipose-derived stem cells and presented in Chapter 5.

Chapter 3: Biodegradable Membrane Fabrication

3.1. Introduction

The primary goal of the present work was to develop biodegradable and biocompatible platforms/scaffolds for liver regeneration and tissue engineering. In this context, both the polymeric material and the scaffolding techniques play an important role in obtaining a functional tissue replacement or aid. As polymeric materials, synthetic polyesters have shown great potential for tissue engineering applications due to their shelf stability, property tunability and biocompatibility. Novel poly sebacate polymers were herein developed and presented in Chapter 2 of the current dissertation. Typical examples of scaffold fabrication techniques were described in more detail in the first chapter of the present thesis. Out of these, the electrospinning technique has become a versatile method that provides materials with high porosity and high surface area-to-volume ratios [123]. These characteristics enable a 3D environment which plays an important role in cell survival, morphogenesis, and function [14, 16]. During the last decade, another electrospinning procedure has emerged as a popular technique for scaffold fabrication, namely co-axial electrospinning. Its popularity derives from the fact that it creates micro- or nano-fibrous environments, enhances the quality of single spinneret obtained fibers and improves their mechanical performance.

In the context of the present thesis, electrospinning was used in order to obtain membranes that would further be integrated within microfluidic systems. Thus obtained membranes were the preferred choice as their structure also resembles the extracellular matrix, a non-cellular component present in all tissues and organs that provides structural and biochemical support to the surrounding cells. The uniqueness of the present project is given by the aforementioned design as the embedding of a porous membrane in between microfluidic channels would come as a solution to the

two-dimensionality characteristic of most microfluidic devices and has never been attempted before.

The porous membrane is required to have a thickness of a few tens of microns (i.e. 20 µm) and to be transparent enough to allow alignment when placed in between the microfluidic patterned layers. Its thickness should also not impart any structural damage to the final microfluidic bioreactor, that will have dimensions in the range of 100-200µm (i.e. 100 µm width, 100-200 µm height). Ideally, the pore size should have dimensions in between 2-5 µm such that cells do not pass through the membrane into the other side of the microfluidic channel. Biocompatibility and biodegradability are other aspects of the porous membrane, as the final bioreactor will also be assembled from biocompatible and biodegradable materials. Therefore, similar biodegradation rates would also be preferred for the two main components of the microfluidic bioreactor.

As a proof of concept, one of the biodegradable polyesters synthesized and presented in the previous chapter, namely poly(erythritol sebacate) (PES), was used in combination with poly (L-lactic acid) (PLLA) to obtain core/shell fibers. The motivation behind choosing PES was of practical nature, as the final bioreactors would also be developed using this material and a good uniformity of the materials within the final system would be preferred. As the molecular weight of a polymer is one of the most important parameters when using the electrospinning technique, PLLA was chosen to complement the PES material. PLLA is among the most frequently studied electrospinnable polymers and its use is justified also by the fact that it is approved by FDA for biomedical implants and drug delivery systems [237]. In addition, PLLA has been used in electrospun scaffolds for different tissue engineering applications such as bone, cartilage, vascular and neural tissue engineering [238, 239].

The reason for choosing to develop core/shell fibers is that none of the herein synthesized poly(polyol sebacate)s cannot be spun alone due to their very low molecular weights. Moreover, the shell part consisting of an electrospinnable material such as PLLA would retain the elastomeric core

from not leaching out of the membrane's structure during the assembly into the final bioreactor.

Thus developed PES/PLLA core/shell fibers were thoroughly characterized and their potential role as part of the microfluidic bioreactor was investigated.

3.1.1. Conventional Electrospinning

Electrospinning has become a versatile method of creating a three-dimensional space that allows cell proliferation and extracellular matrix deposition. The conventional single-spinneret electrospinning involves drawing micro or nano-fibers from a polymer solution. An electric field is applied to the liquid drop until it stretches enough to take the form of a fiber (Figure 3.1). The mechanism behind it consists in electrostatically charging the droplet at the spinneret tip. This implies that the drop comes under the action of two types of electrostatic forces: mutual electrostatic repulsion between the surface charges and the Coulombic force applied by the external electric field [240]. The liquid droplet elongates, taking a conical shape known as the Taylor cone. Once the electric field is high enough (i.e. reaches a critical value), the electrostatic forces overcome the surface tension of the polymer solution and force the ejection of the liquid jet from the tip of the Taylor cone. The solvent evaporates before reaching the grounded collector, leading to the formation of randomly oriented fibers.
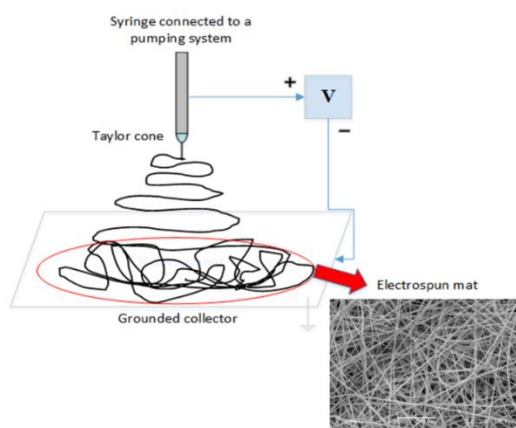
Figure 3.1: Schematic representation of the electrospinning process.

A multitude of factors affect the electrospinning process. Table 3.1 groups these parameters into main categories, namely polymer solution, process and ambient parameters.

Table 3.1: Parameters influencing the electrospinning process

Polymer solution parameters	Process parameters	Ambient parameters
Nature of the polymer	Feeding rate	Temperature
Polymer solubility	Needle diameter	Humidity
Viscosity	Collecting distance	Atmospheric composition
Polymer molecular weight	Collector shape	Pressure
Solution concentration	Electrical field	Surrounding materials
Dielectric constant of the solvent		
Volatility of the solvents		
Conductivity		

In the following paragraphs some of these effects will be illustrated with electrospinning experiments performed on widely used commonly available polyesters.

Solution Parameters

The solvent used for the preparation of the polymer solution has to have suitable vapour pressure, viscosity, and surface tension to promote fiber integrity [241]. Either single or mixed solvent systems are used to obtain consistent fibers in a reproducible manner. Figure 3.2 summarizes some of the solvent effects on PLLA fibers. In DCM/MeOH and HFIP (Figure 3.2A-B)

the fiber diameter is 2.5 μm, whereas when chloroform is used the diameter increases up to 6.5 μm. Also, the morphology of the PLLA fiber changes, as the fiber itself presents pores (Figure 3.2C). The importance of homogeneity of the polymer solution is highlighted in Figure 3.2D, where insufficient mixing of polyethylene glycol with PLLA results in uneven fibers and a distorted mat. PEG (M_w 1,000,000 g/mol) is usually used in electrospinning for increasing the spinnability of a polymer solution due to its high molecular weight.
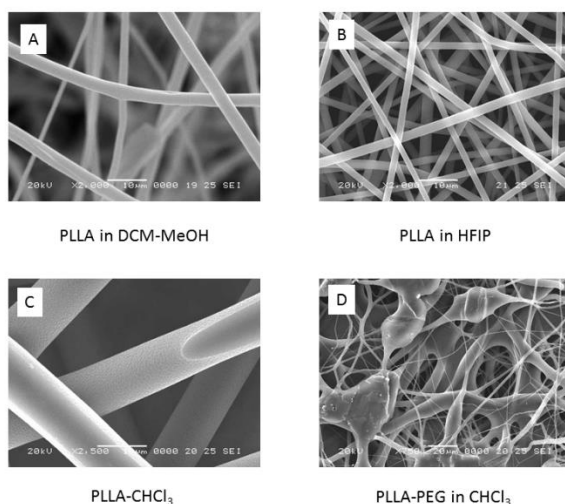
Figure 3.2: SEM micrographs presenting the solvent effect on electrospun PLLA fibers

The polymer molecular weight, as stated above, has a great influence on the morphology of the resulting fibers. As one can notice also from Figure 3.3A, if an insufficiently high enough molecular weight is used, beads are more likely to be obtained. An increased molecular weight renders smooth fibers (Figure 3.3B).

Process Parameters

Although a high enough voltage (i.e. higher than the threshold voltage) is important for the ejection of fibers from the Taylor cone, the influence of the voltage on the fiber diameter is a more controversial topic. This is due to the contradictory results obtained by different research groups.
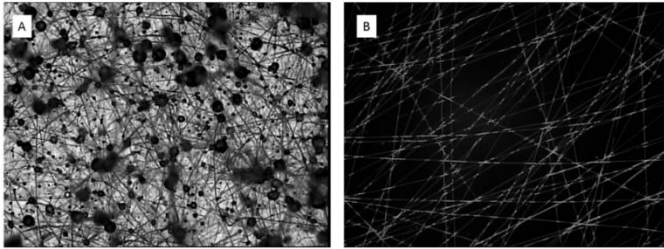
Figure 3.3: Optical microscope pictures of PCL fibers obtained from electrospinning a PCL solution 20% (w/v) with different molecular weights (A) 45 kDa and (B) 90 kDa; electrospinning conditions: chloroform/acetone 2/1, flow rate of 10 ml/h, 20 cm distance from the needle to the collector plate, and a voltage of 15 kV.

For example, some studies reported that there is no direct effect of the voltage on the diameter of electrospun polyethylene oxide nanofibers [242], while other stated that higher voltages can favour the formation of smaller diameter fiber [243, 244]. Figure 3.4 depicts the influence of some process parameters of PCL electrospinning on the fiber formation performed during the current dissertation. In the present work, the influence of altering the electric field on the fiber diameter was not extensively studied, as it was not essential for the planned goal. As can be observed from Figure 3.4A vs 3.4D and Figure 3.4B vs. 3.4E, due to the scale of the pictures taken with an optical microscope (i.e. low accuracy), no conclusion can be drawn on the voltage effect on the fiber dimension. A more in-depth study about this parameter variation and in-depth measurements, such as scanning electron microscopy, is needed in order to conclude on the effect of the voltage on the fiber diameter.

The distance from the needle to the collector is another parameter to be considered and optimized (Figure 3.4A, F). Whereas a too short distance will not allow appropriate solvent evaporation, the opposite will lead to beads formation. An optimum is therefore recommended. Within a certain recommended distance range, if no other parameter is changed, it has been shown that the fibers tend to stretch more and this leads to the development of thinner fibers [245].

The flow rate at which the polymer solution is pushed through the syringe is a factor that might contribute to the fiber diameter. Thicker fibers are more

readily obtained if the flow rate is increased. An excessive flow rate can sometimes lead to drop formation as an excessive volume is drawn away from the needle. Some defects can be thus formed as a result of electrospinning at high feeding rates [246].

Ambient Parameters

Environmental temperature and humidity can interfere with the electrospinning process and the morphology of the fibers. Temperature can have a direct effect on the process if it is higher than the room temperature. Some of the most common effects include a more quick solvent evaporation, increased diameters of the fibers, and even needle clogging.
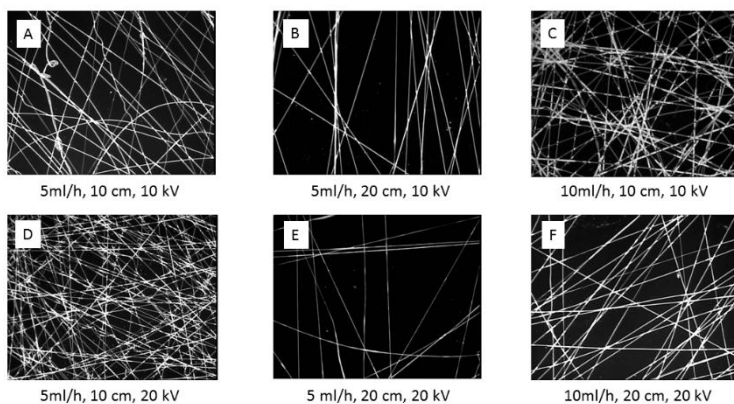
Figure 3.4: Optical microscope pictures illustrating the process parameters (flow rate, distance from the needle to the collector plate, voltage) that influence on PCL fibers: (A,B) and (C,D) change in the distance from the needle to the collector plate; (A, C) and (E,F) flow rate change; (A, D) and (B, E) voltage change;

Humidity is an important aspect, as low humidity may increase solvent evaporation while high humidity can lead to higher porosity of the fibres [247, 248]. In order to avoid the influence of these types of parameters, a room with constant humidity and temperature can be used for the electrospinning process.

3.1.2. Co-axial Electrospinning

In the last decade, co-axial electrospinning has emerged as a popular technique for scaffold fabrication as it creates micro- or nano-fibrous environments, enhances the quality of single spinneret obtained fibers and improves their functionality. In this process, core/shell fibers are obtained by simultaneously feeding different polymer solutions through the inner and outer capillaries or needles (Figure 3.5). The co-axial process is subjected to the same parameters as presented above. One requirement is that the viscosity of the shell solution has to overcome the interfacial tension between the two solutions [244]. The shell polymer is critical to the entire process as it has to be easily electrospinnable by itself. To these, the miscibility of the core-shell solutions is also to be considered as immiscible solutions separate in two phases once the solvent is evaporated [249]. The solvent choice can influence the formation of core/shell fibers and the solvent from one polymer solution should not precipitate the polymer in the other solution.
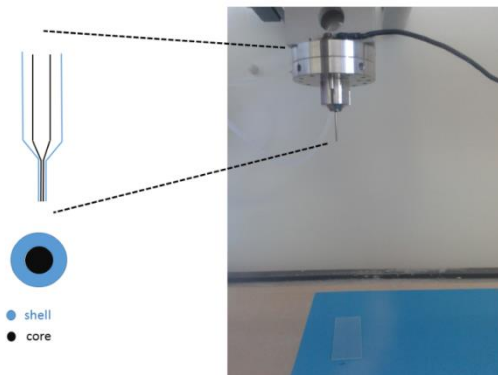
Figure 3.5: Image of the applied co-axial electrospinning head.

Up to now, there is contradictory data about whether the core and the shell solutions should be miscible or if the same solvent should be used to prepare both solutions. Some studies report that miscible solutions lead to a decreased surface tension between the two solutions and therefore favour the development of uniform core/shell fibers [242]. On the other hand, other

studies indicate that when using miscible solutions mixing can occur between them, resulting either in porous fibers or mixed fibers rather than core/shell [250]. Although the use of different solvents or immiscible solutions for co-axial electrospinning is considered an essential requirement [251], a clearer understanding of this parameter is necessary.

Products and Applications

The result of the co-axial electrospinning process can be hollow fibers, core/shell bi-component structures, fibers from non-electrospinnable materials, or fibers containing encapsulated microparticles. The potential uses of these type of fibers cover diverse fields, as they can be used as scaffolds for tissue engineering, carriers of drugs or biological objects, products for filtration or protective clothing, fiber reinforced composites products and even sensors and electrodes for use in electronics and optics [252].

The main idea behind core/shell bi-component fibers is to modify or coat a material. This strategy can result in increased hydrophilicity [253], higher tensile strengths [243] or tunable mechanical properties and improved surface compatibility [254, 255]. Natural polymers such as collagen [256] and gelatin can be therefore complemented with synthetic polyesters like PCL [257], PLLA [258], PLGA [259, 260]. The resulting fiber mats or membranes combine the best of the two worlds: good biocompatibility and advantageous mechanical properties. Soft and hard tissue engineering are some of the main beneficiary fields from this type of bi-component fibers.

The so-called "host/guest" electrospinning approach implies the use of non-spinnable materials which can be further chemically transformed or polymerized for the core, while the shell consists of an easily electrospinnable polymer [253]. This approach can render pure fibers of the core material, by removing the shell material.

Fibers encapsulating drugs, nanoparticles or biological compounds are most useful in applications such as gene therapy and drug delivery [252]. Enhancing performance of lithium ion batteries is another field where the use of coaxial electrospinning renders hollow carbon nanofibers as anode

materials [261]. Different loadings of Si in the carbon core matrix as the anode were also used for this purpose [262]; polyacrylonitrile was the shell material, while poly(methyl methacrylate) and silicon nanoparticles served as core materials.

Co-axial fibers used for electrodes of solar cells [263], luminescence materials [264] and supercapacitors [265] prove the flexibility of this technique and its future potential.

3.2. Materials and Methods

Methanol (MeOH), dicholomethane (DCM) and hexafluoroisopropanol (HFIP) were purchased from Sigma-Aldrich. All chemicals were used as received unless otherwise mentioned. Poly L-Lactic acid (PLLA) with a molecular weight of 81,000 g/mol was purchased from Nature Works LLC. Poly (lactic-co-glycolic) acid (80/20 lactic/glycolic ratio) with a viscosity of 1.7-2.6 dl/g was purchased from RESOMER®.

3.2.1. Core/shell fiber spinning of PES/PLLA

PES 20% (w/v) was dissolved in HFIP to form the core solution, while PLLA 20% (w/v) was dissolved in DCM/MeOH 8/2 (v/v) to form the shell solution. A two-fluid co-axial spinneret, with a 1 mm diameter inner tube and 2 mm diameter outer tube, was set up in the electrospinning device. Both polymer solutions were poured in plastic syringes and connected to the co-axial spinneret via Teflon tubings. The polymer solutions were injected through the co-axial spinneret with a constant flow rate of 5 ml/hour, using a New era Pump Systems LLC pump. A voltage of 18 kV was applied at the G21 tip of the spinneret and the fibers were collected on a grounded collector (DC high-voltage supply from Glassman High Voltage LLC). The distance between the tip of the spinneret and the collector was 15 cm. The obtained fibers were vacuum dried overnight to remove any residual solvents. For comparative reasons, the conventional electrospinning technique was applied for PLLA. Therefore, PLLA 20% (w/v) was dissolved in dichloromethane/methanol 8/2 (v/v) and electrospun similarly to the co-axial method. The PLLA solution was

pumped into the single spinneret with a flow rate of 5 ml/hour, at 18 kV. The distance between the G21 needle tip and the collector plate was 15 cm.

3.2.2. Characterization Techniques for Electrospun Fibers

FT-IR Spectroscopy

The chemical structure of the electrospun mats was investigated via fourier-transform infrared spectroscopy with a Bio-Rad FTS 575C spectrometer.

Static Contact Angle Measurements (SCA)

Mats (4 cm x 4 cm) were cut and the static contact angles were measured with a goniometric OCA 20 device (Dataphysics). SCA values were determined using the sessile drop method and distilled water as the dispensing liquid. The Young-Laplace procedure was used as processing method. The device was equipped with a video camera able to record a 10 s video (25 frames/s) of each drop. Aliquots of 0.5 µl of double distilled water were dropped on the mats. An average value of at least three drops (0.5 µL) per mat was considered.

Mechanical tests were performed to study the deformation, the rupture and fatigue profiles of the electrospun mats. The rupture profiles were evaluated in a Texture Analyser (TA500, Lloyd Instruments). The resistance to the deformation induced by a 0.4 cm diameter cylindrical probe was studied. The mats were clamped in a CellCrown ™ (Scaffdex) of 3 cm diameter, 1 cm high. A rupture was considered when the strain dropped rapidly to 20% of the maximum strain. Fatigue tests were also performed in this instrument. The maximum strain generated for each consecutive deformation (induced by the probe) was measured. The tests were performed for 5 or 10 cycles at a deformation of 1 mm, 3 mm and 5 mm.

Scanning Electron Microscopy (SEM)

The surface morphology of the electrospun fibers was evaluated using a scanning electron (SEM) JEOL JSM 5600 instrument, equipped with a secondary electron detector, in the high vacuum mode. Prior to analysis, all samples were coated with a thin (ca. 20 nm) gold layer through plasma

magnetron sputter coating. For measuring the fiber diameter, 9 fibers were chosen per analyzed sample and a total of 3 samples per type were investigated from the electrospun mats.

Transmission Electron Microscopy (TEM)

TEM analyses were also performed in order to visualize the structure of the core/shell fibers. TEM imaging was conducted using a Tecnai G2 (FEI) microscope, operated at an acceleration voltage of 200 kV. The optimum method to obtain contrast between shells and cores was to use a scanning transmission mode. As shown in Figure 3.6, the beam is focused onto and scanned across the sample. So the image is created sequentially. Different detectors can be used, such as bright-field (BF) or annular dark-field (ADF) detectors. Contrast is created because the electrons are scattered by interaction with the sample. For each scan position transmitted electrons are detected. If there is a density difference between shell and core of the fibers, we expect that more electrons are scattered to higher angles, so that for higher density more signal is generated in the ADF detector and less in the BF and vice versa.
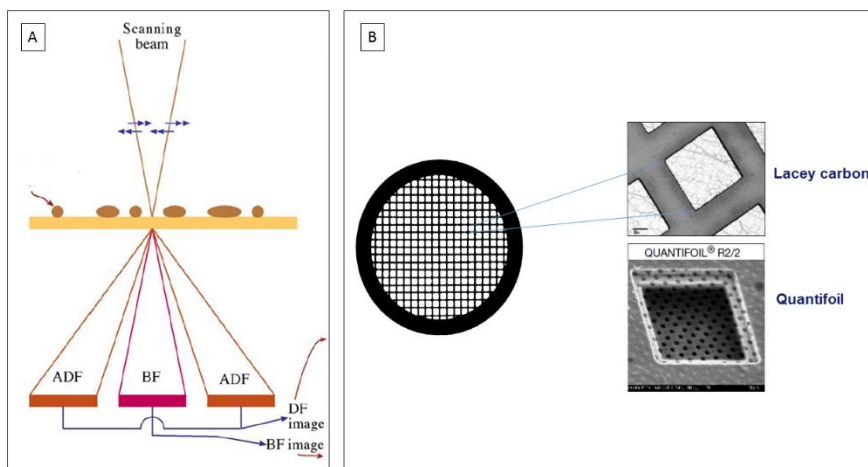
Figure 3.6: (A) Principle of Transmission electron microscopy; (B) Conventional grid for electron microscopy; it's size is 3 mm in diameter and contains bars of copper that separate squares, which are free of any material; grids with the same arrangement of copper bars but coated with holey carbon films, containing either random holes (Lacey) or regular holes (Quantifoil).

For TEM sample preparation, small pieces of PLLA or PES/PLLA fiber mats were transferred onto a holey carbon support film (Quantifoil®) (Figure 3.6B) as they are much more stable and can be investigated without movement. To obtain cross-sectional views, parts of a PES/PLLA sample were embedded in Epofix epoxy resin, as depicted in Figure 3.7. The procedure of embedding was initialized by impregnation of the sample with Epofix, followed by hardening at atmospheric pressure and room temperature.
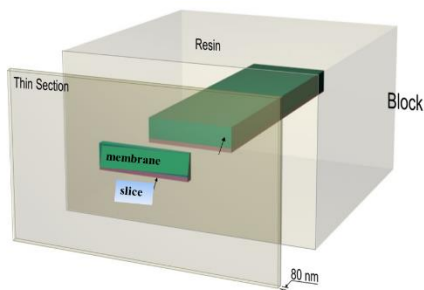
Figure 3.7: : Sample preparation for cross-section imaging via TEM.

The hardened block could be cut into ultrathin sections of 50 nm using a Leica UC7 microtome. Sections were collected on copper mesh grids and 5 nm of carbon was deposited using a Leica ACE600 carbon evaporator. While imaging of cross-sections was performed using conventional bright-field TEM, the non-embedded fibers were imaged using the scanning TEM mode in combination with a bright-field detector.

3.3. Results and Discussion

3.3.1. Production of PES/PLLA Core/Shell Fibers

In the current thesis, none of the elastomers synthesized and presented in Chapter 2 was electrospinnable as such due to the limitation of their molecular weight (i.e. 18,000 g/mol maximum molecular weight obtained). Nevertheless, combining them with well-established electrospinnable polymers provides an advantage as the result can offer fibrous scaffolds with tunable mechanical properties (from stiff to elastic), tunable degradation

rates and higher hydrophilicity than the initial easily electrospinnable polymers.

Therefore, the motivation for using co-electrospinning of PES pre-polymer with PLLA was based on the observation that the synthesized PES pre-polymer cannot be spun alone due to its low molecular weight, and therefore low solution viscosity. Furthermore, by combining these two polymers into an electrospun scaffold the properties of the fibrous mats can be broadened and in some aspects controlled (e.g. control over stiffness).

PES was electrospun as the core material in a concentration of 20% (w/v) in HFIP and PLLA as a shell material in the same concentration in DCM/MeOH (8/2). As reference material, PLLA was also spun into fibers using the same electrospinning conditions, polymer concentration and choice of solvents. The choice for using two different solvents for the core and the shell materials was made as to avoid blending of the two solutions during the spinning procedure. Different solvents would ensure that the solutions are not easily miscible and that the fibers obtained have a core/shell structure and not a blended one [250, 266].

3.3.2. Morphology and Topography of PES/PLLA Fibers via Scanning Electron Microscopy

The fiber morphology for the PLLA and PES/PLLA core/shell mats was studied with SEM (Figure 3.8). The fiber diameter and morphology is a result of multiple varying parameters such as polymer solution concentration, flow rate, applied voltage, distance between needle and collector plate, needle gauge, atmospheric humidity and choice of solvent. In the current work a significant ($p < 0.05$) difference was noticed between the fiber diameters of the as spun PLLA fibers and the core/shell ones. The PLLA fibers had an average diameter of 4.1 ± 1.3 µm, while the core/shell fibers presented a diameter of 2.3 ± 0.5 µm. On the other hand, there is no significant statistical difference between the various samples of PLLA mats ($p > 0.05$) and PES/PLLA core/shell mats ($p > 0.05$) investigated. This suggests that the reported

process and electrospinning parameters provide reproducible PLLA and PES/PLLA fibers.

Interestingly, the core/shell fibers are thinner than the PLLA single fibers although a higher diameter of the needle was used to extrude the core/shell fibers. This phenomenon can also be explained by the presence of some split jets when larger needles are used [240, 267]. The formation of branches within the electrospun jets occurs in more concentrated and viscous solutions that require larger diameter needle for their expulsion [240]. For lager diameter needles, the interface between the air and the solution is larger and therefore some solidification of the polymer may occur. This leads to smaller multiple jets that render thinner fibers. The fibers become uniform in diameters as they are produced from the same unique Taylor cone. Another factor contributing to the smaller fiber diameter can be the solvent choice for PES, namely HFIP, that can have an influence on the interfacial tension between the core and shell solution and thus on the Taylor cone formation [268]. Furthermore, from literature it is well known that the solvent choice influences parameters such as fiber morphology and fiber diameter [269, 270].
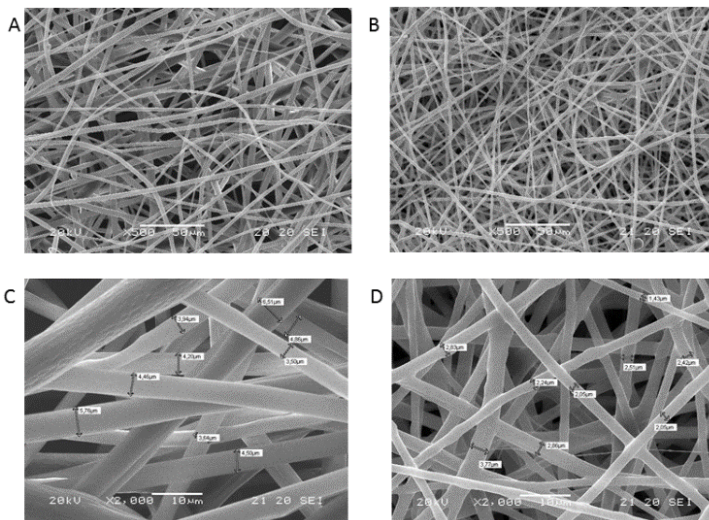
Figure 3.8: SEM micrographs of (A, C) - PLLA fibers and (B, D) - PES/PLLA core/shell fibers.

Although, ideally, the pore size (i.e. distance between fibers) should have dimensions in between 2 and 5 μm such that cells do not pass through the membrane into the other side of the microfluidic channel, the herein obtained membranes presented pore sizes of 2-50 μm. The pore size could not be controlled due to the random orientation of the fibers. Future work should consider the development of oriented fibers under different angles for a better control over the membrane porosity.

3.3.3. Chemical Composition of PES/PLLA Fibers

As FT-IR can determine the chemical composition of a sample, infrared spectra of PLLA and PES/PLLA core/shell fibers were recorded. This was performed to indicate whether a uniform mat was obtained (Figure 3.9). The bands corresponding to bending vibrations of CH_3 (asymmetric and symmetric) were found at 1451 and 1519 cm^{-1} in the polymer spectrum, while the peaks at 2992, 2947 and 1741 cm^{-1} of PLLA were assigned to the CH stretching vibration and C=O vibration, respectively. The band around 3300 cm^{-1} is related to the stretching of OH group and its intensity is decreased when compared to the spectrum of the PES polymer (Figure 3.9), denoting that the fibers are indeed comprised out of the PLLA and PES material.
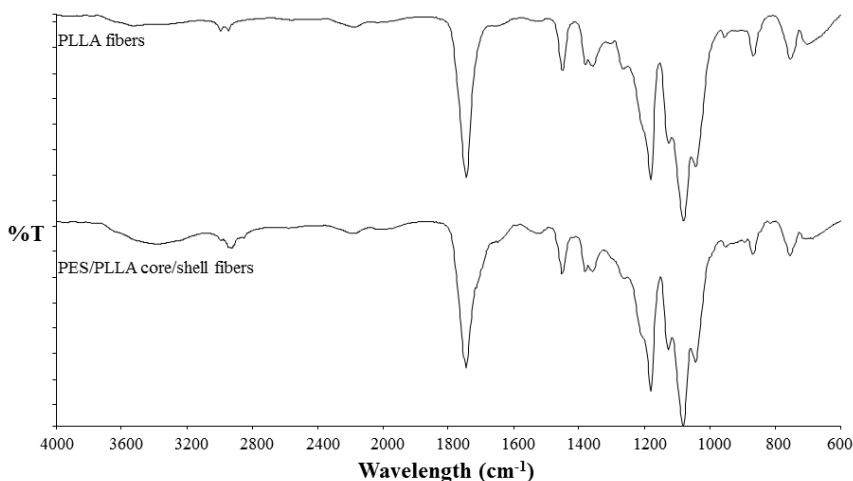
Figure 3.9: FT-IR spectra of PLLA and PES/PLLA core/shell fibers.

3.3.4. Thermal analyses of PES/PLLA fibers

The presence of the PES material within the core/shell fibers was also demonstrated by DSC analyses (Figure 3.10). PES/PLLA fibers contained glass transitions belonging for both polymers: for PES at -9°C and for PLLA at 58°C, respectively. While on the heating cycle a distinct melting peak was also noticed at 150°C for the PLLA polymer, during cooling only the glass transitions for the two constituents of the core/shell fibers were observed.
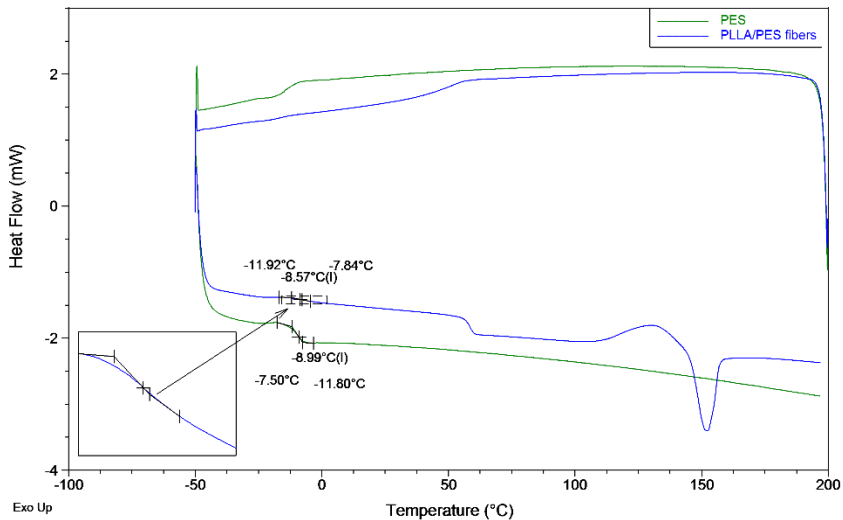
Figure 3.10: DSC curves for PES vs. PES/PLLA core/shell fibers

3.3.5. Hydrophilicity of PES/PLLA Fibers

Contact angle measurements were performed in order to study the wettability of the fibers. PLLA fibers had a water-in-air contact angle of 96° ± 3°, indicating a very hydrophobic material. For the PES/PLLA core/shell fibers, the water drop was not stable enough for the contact angle measurement to be registered over 10 seconds. The water drop was absorbed by the mat in ca. 2 seconds, demonstrating that the addition of the PES pre-polymer to the fibrous scaffold increased its hydrophilicity.

This result is in agreement with the data obtained when electrospinning the well-known polyester from the same family as PES, namely PGS [271]. In the

study of Ravichandran et al., PGS also increased the hydrophilicity of gelatin during a co-electrospinning process where the above elastomer constituted the core of the developed fibers [255, 271]. Such PES/PLLA system actually acts like a sponge, absorbing the water also probably due to possible fiber imperfections that expose the core (i.e. the very hydrophilic PES material - SCA 24°) of the fiber to the surface.

3.3.6. Mechanical properties of PES/PLLA fibers

The mats response to the deformation induced by a cylindrical intron probe (diameter = 0.4 cm) was measured by a texturometer. As the probe penetrates the mat and deforms it, an additional vertical force will be present. The rupture plot in Figure 3.11 demonstrates that the mats' disruption is less abrupt for slower probe speeds (i.e. 0.5 mm/min), than for higher ones (i.e. 5 mm/min).
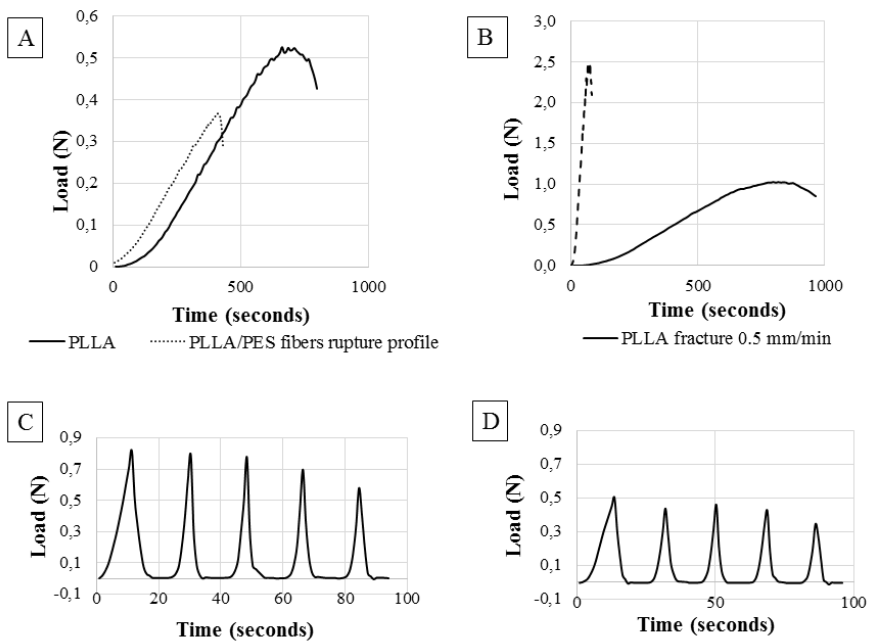
Figure 3.11 : Mechanical analyses of electrospun fibers: A - Rupture profiles of the electrospun fibers; B - Plot of the difference in rupture speed of a PLLA mat with a thickness of 40±7μm at different probe velocities; C - Fatigue profiles at 3 mm probe deformation for a PLLA mat; D - Fatigue profiles at 3 mm probe deformation for a PES/PLLA mat.

The extent to which the fiber mats resist deformation in response to the applied force, denominated as stiffness, was calculated. The parameters shown in Table 3.2 indicate that by introducing poly (erythritol sebacate) into the core of the PLLA fibers, the overall stiffness increases from 0.19 N/mm for the plain PLLA fibers to 1.19 N/mm for the core/shell fibers. This increase can be attributed to the introduction of the PES filling inside the PLLA fibers, which makes the fibers more rigid as it disrupts the consistency of the PLLA fiber structure. In addition to the chemical composition parameter of the fibers (i.e. core/shell vs. plain PLLA), the mechanical strength difference could also come from the fact that the plain PLLA fibers have a higher average diameter than that of the PES/PLLA fibers (i.e. 4.1 µm vs. 2.3 µm; Figure 3.8).

The maximal load and deflection is a measure of the maximum force and deformation that the electrospun mats can undergo. Rupture of the fibers was considered to occur when the force drops fast to 20% of the maximum load. A decrease in the maximum deflection is observed for the core/shell fibers, as the overall stiffness is higher than the plain PLLA fibers.

Table 3.2: Mechanical properties of electrospun fibers.

Fiber mats 40±7µm thick	Maximum Load (N)	Deflection at Maximum Load (mm)	Stiffness (N/mm)	Load at Rupture (N)	Deflection at rupture (mm)
PLLA	0.67 ± 0.27	5.51 ± 0.47	0.19 ± 0.06	0.54 ± 0.21	6.50 ± 0.73
PES/PLLA	0.20 ± 0.12	2.24 ± 0.90	1.19 ± 0.55	0.15 ± 0.09	2.60 ± 1.04

Depending on the fiber type, the probe can therefore deform the mat to some extent, but a fraction of the fibers can still provide resistance due to fiber rearrangement on the edges of the circular section of the probe. Fatigue tests have been performed in order to evaluate the structural damage that occurs when the electrospun mats are subjected to cyclic loading. The fatigue profiles (Figure 3.11 C,D) showed a decrease of the strain at maximum deformation which implied that some irreversible structural changes did

occur. For all deformation frequencies, this decrease was more evident during the first cycles. Fatigue tests where the mats were deformed for more than 5 cycles (i.e. 10 cycles, data not shown), indicated that, after the initial cycles, no other significant changes occur over time.

The thickness of the tested electrospun mats was 40±7 μm. As it is generally difficult to obtain a uniform thickness of the mat during the electrospinning process, the accuracy of the fatigue tests was evaluated by dividing the maximum loads of the last and first peaks. The ratio obtained (Table 3.3) can attest to the fact that all mats, indifferent of the thickness, have the same fatigue profile behaviour. The fatigue tests with the probe deformation of 5 mm were not applicable for the core/shell fibers as these fibres' maximum deflection at rupture was 2.60 ± 1.04 mm.

Nevertheless, the observations about the rigidity of the fibers deducted from the mechanical tests will not impart any problems for the final purpose of the present thesis, as the electrospun mat will be inserted in between microfluidic channels of 100 μm height.

Table 3.3: Last peak maximum/First peak maximum ratio of fatigue profiles of electrospun mats.

Ratio Fibers	1 mm* 5 cycles	1 mm* 10 cycles	3 mm* 5 cycles	3 mm* 10 cycles	5 mm* 5 cycles	5 mm* 10 cycles
PLLA	0.97	1.02	0.77	0.77	0.76	0.69
PES/PLLA	0.85	0.88	0.84	0.77	n/a	n/a

* 1, 3 and 5 mm deformation into the electrospun mat, respectively

It can be concluded from the mechanical tests that the produced structures are tension resistant, especially for lower deformations than 1 mm, and that the herein developed electrospun membranes are, therefore, suitable for the final microfluidic application.

3.3.7. Evaluation of the PES/PLLA Fibers via Transmission Electron Microscopy

To assess the structures of PES/PLLA fibers TEM was applied in scanning mode, i.e. a focused electron beam was raster-scanned across the sample as in SEM. However, since a primary energy of 200 keV was used, the transmitted electrons can be analyzed, so that a core/shell structure of the two different materials PES and PLLA could be visualized.
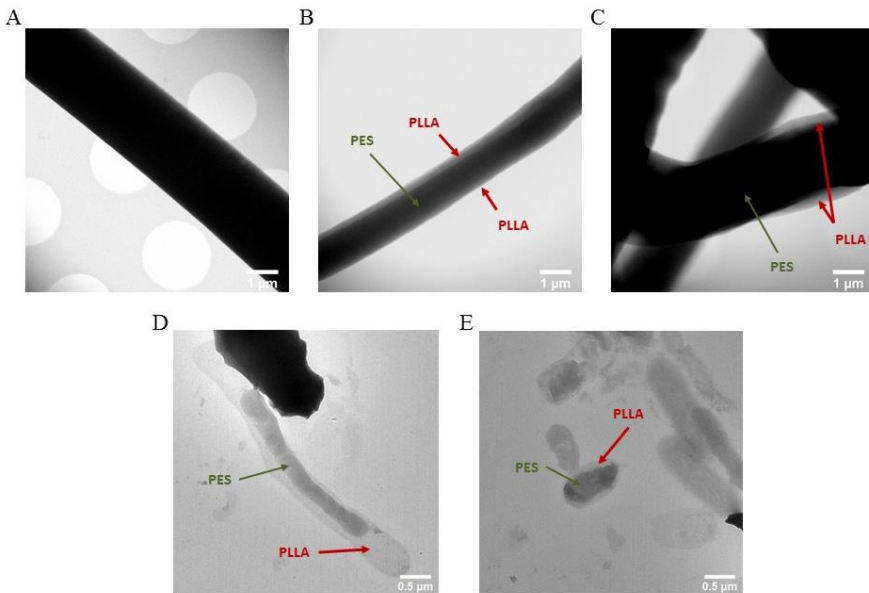
Figure 3.12: TEM analyses of the electrospun fibers: A - PLLA fiber (represented by the black color); B, C - PES/PLLA core/shell fiber, where PES is represented by the black color and PLLA by the lighter grey color; D, E - cross-sectional view of the PES/PLLA fibers, where PES is represented by the dark grey color and PLLA by the light grey color.

For transfer to a TEM sample holder, small pieces of the fiber mats were transferred onto a holey carbon support film. It was observed that the holes in the support did not add in improving imaging quality but the carbon film supports and stabilizes the deposition of the fibers. Figure 3.12 shows scanning TEM micrographs of a PLLA fiber and PES/PLLA fibers. A homogeneous distribution is found for PLLA in the single material fiber as

seen in Figure 3.12 A. Figure 3.12 B-C indeed reveals core-shell structures for PES/PLLA fibers. Many more of such fibers could be observed, which implies that the majority of the fibers consists of core/shell morphology. These images represent plane views of the samples. Since such a projection cannot prove that the PLLA forms a continuous shell, we also embedded PES/PLLA fibers into an epoxy resin, followed by ultramicrotomy to obtain ultrathin cross-sections for TEM analysis. Figure 3.12 D-E shows TEM micrographs of embedded parts of core-shell fibers. As pointed out in Figure 3.12E, the visible shell in the cross-sectional view is continuously covering the core.

Another interesting observation was that some fibers fused together (Figure 3.13A, B), after the curing process. This was due to the fact that some PES/PLLA fibers presented disruptions, with the PES core reaching the shell of the fiber (Figure 3.13C).
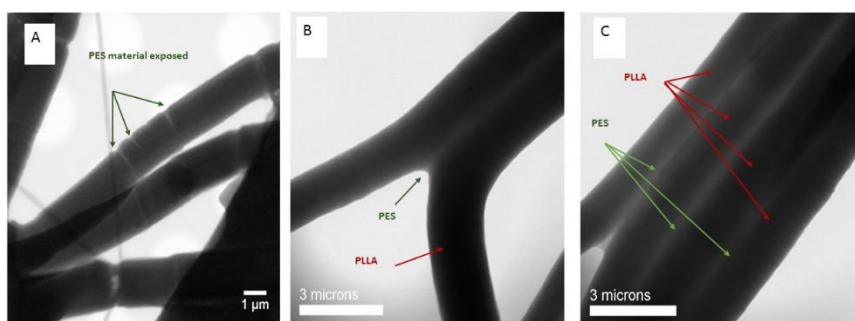
Figure 3.13: TEM micrographs: (A) cracks within the uncured PES/PLLA fiber reveal the PES material (arrows) that allows fusion of the fibers during curing; (B, C) 2 and 4 fused PES/PLLA fibers, respectively;

This disruptions can lead to the loss of fiber integrity and can be the cause of the increased rigidity of the core/shell fibers vs. the plain PLLA fibers (Table 3.2). Although the cause of these fiber disruptions can be the electrospinning process itself, another aspect should also be considered, namely the mat deposition on the TEM grids. It is highly likely that the disruptions are a result of the fiber stretching during the deposition of fibers on the grid.

In report to the present project's application, these fiber inconsistencies would not impart any disruptions to the bioreactor assembly and its final

usage. Although some parts of the fibers might have the core PES material exposed, this material is biocompatible and biodegradable and is therefore suitable for the final tissue engineering application.

3.3.8. Degradation Rates of PES/PLLA Fibers

One other important property for biomedical applications that can be changed using the co-axial electrospinning is the polymer degradation rate. As expected, an increase in the degradation rate was noticed in the case of the core/shell fibers (Figure 3.14). While the plain PLLA fibers showed a mass loss of 0.05 ± 0.02% after 16 weeks, the PES/PLLA core/shell fibers lost 0.39 ± 0.01% of the mass in the same time interval. The results for the PLLA fibers are in agreement with previous studies that also showed almost no weight loss during degradation studies of 6 and 35 weeks in phosphate buffer [272, 273]. The degradation was approximatively 8 times higher for the PES/PLLA fibers. This higher degradation rate can also be attributed to the smaller diameter of the core/shell fibers (in comparison with the plain PLLA fibers) that implies a higher surface area per unit mass exposed to the degradation medium.

In the context of inserting the electrospun membranes inside a microfluidic bioreactor, the obtained degradation test results are satisfying. As the final bioreactors are intended to be prepared from the elastomeric materials prepared in Chapter 2, the degradation rates of all materials and fibers involved in the microfluidic system assembly should have similar trends. The PES/PLLA core/shell fibers degradation properties could, therefore, match the degradation properties of the PGS- and PES-derived elastomers which had a maximum mass loss of 0.29 and 0.18% respectively.

The major advantage of the core-shell fibers is therefore the potential to obtain a combination of properties of various types of materials. Coaxial electrospinning can comply to specific required properties, a fact that makes this technique one of the most popular scaffolding methods.
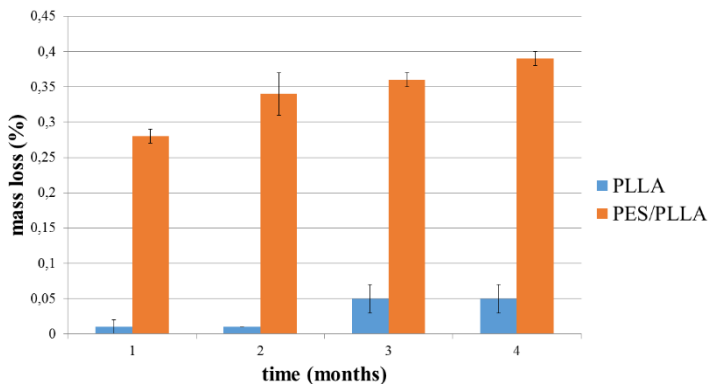
Figure 3.14: Degradation of electrospun fibers over a period of 4 months.

3.4. Conclusions

In the present study PES/PLLA core/shell porous membranes have been successfully developed for liver tissue engineering applications. The herein developed core/shell membranes had a smaller fiber diameter (i.e. 2 vs. 4 μm), a higher wettability, and higher degradation rate (0.39% vs. 0.05% mass loss) than the plain PLLA fibers. In addition, all the developed fibrous scaffolds offered high porosity and high surface area-to-volume ratio, that are key-factors in creating good 3D environments for cell culturing and tissue engineering. All these results are in agreement with the targeted values for fiber size and biodegradability: 1-2μm fiber diameter, and 0.18-22% mass loss representing the mass loss of the developed materials for the final bioreactor. Although the pore size could not be controlled and varied in between 2 and 50μm due to the random orientation of the fibers, a future perspective would be the investigation of obtaining oriented fibers via the electrospinning. Nevertheless, thin membranes with a thickness within the desired range (i.e. maximum 20 μm) were obtained for the final application.

From all characterization techniques it can be concluded that both plain PLLA and PES/PLLA core/shell fibers provide good candidates for integration within microfluidic bioreactors or systems. From the thermal point of view,

the aforementioned membranes are stable up to temperatures as high as 150°C; mechanically, the mats have suitable fatigue resistance for deformations lower than 1 mm and therefore could withstand small flow rates within microfluidic systems. Furthermore, all materials are biodegradable which is in agreement with the aim of the present thesis, namely to design fully biodegradable bioreactors.

The integration of thus obtained fibers in microfluidic devices will be evaluated and presented in the next chapter. The biocompatibility of the herein developed scaffolds will be evaluated with a hepatocellular cell line, which is a known *in vitro* study model for liver tissue engineering applications. These results are presented in Chapter 5 of the current thesis.

Chapter 4: Microfluidic Bioreactor development

The development of biodegradable and biocompatible microfluidic bioreactors for liver tissue engineering is presented in this chapter. The work presented in this chapter was previously published in Materials & Design [274].

4.1. Introduction

Nowadays there is a growing interest from the scientific and industrial world for drug screening using *in vitro* cultured cells, for cell culturing and tissue engineering. A stringent need of producing and using more complex tissues with different types of cells and with a more complex 3D structure drives researchers to study biomaterials and imprint novel designs using different tools [28-31]. In the last decade, synthetic elastomeric materials such as poly (glycerol sebacate), and poly (polyol sebacate)s [55] in general, have attracted a lot of attention for soft tissue engineering applications due to their biocompatibility. The tunability of the materials' mechanical properties, that can resemble those of the native tissue [56] constitute another important aspect. Moreover, these thermoset materials can be designed to be amorphous and their degradation mechanism allows the retention of the 3-dimensional structure during the mass loss or resorption process [64].

Microfabrication and microelectromechanical system technology are micro-engineering methods designed to shape these materials such that a good spatial resolution is obtained. Up to now, most of the developed microfluidic bioreactors were created by essentially two ways: either bonding a patterned layer on top of a flat one [20], or by stacking and bonding single-layer microfluidic networks [21]. Nonetheless, microfabrication technology is basically a 2-dimensional technique that generates patterns on 2D surfaces, and therefore it limits their use in the study of surface morphology effects on cell growth [22]. Another limitation consists in the hypoxic oxygen concentrations that arise from the use of polymer thicknesses over 200 μm and that further restricts the maximum thickness of the engineered tissue

[20]. In order to counteract these limitations, we propose the integration of porous membrane (with a maximum thickness of 20µm) in between two micro-patterned microfluidic layers. From the best of our knowledge, this unique strategy has not been reported for biodegradable microfluidics by other research groups.

The microfluidic devices developed in the present work were fabricated out of biodegradable and biocompatible elastomers, such as poly (glycerol-sebacate) and poly (erythritol-sebacate). The two biomaterials were synthesized and micro-patterned by previously mentioned methods [17, 18]. The above mentioned polymers serve as a proof of concept that the herein presented technology can be transferred to all poly(polyol sebacates) developed in this thesis. An alternative method for the curing step that leads to the film formation and pattern generation is also reported. The effect of a nitrogen flushed oven on the curing of the pre-polymers was studied and led to the observation that it enhances the crosslinking rate in comparison with the conventionally used vacuum oven.

The porous membrane that was placed in between the patterned microfluidic layers was obtained by electrospinning, a traditional scaffold fabrication technique. As a proof of concept for this idea we have chosen PLLA as a material for the electrospinning fabrication process. Its purpose is similar to that of the extracellular matrix, namely to provide cell support, cell-to-cell interaction, and also to solve the oxygen diffusion limitations imparted by microfluidic membranes with thicknesses exceeding 200 µm [20]. Electrospun membranes have been introduced before in microfluidic systems, biosensors and lab-on-a-chip devices [23]. Most of the applications involve point-of-care diagnostics or tissue engineering and regenerative medicine. Up to now, the membranes consisted of polyvinylidene difluoride [24], track-etched polycarbonate [25], polystyrene [26], polyurethane [27], polyvinylpyrrolidone and were mainly incorporated in PDMS or PMMA. In the context of tissue engineering and regenerative medicine, the ability to manipulate the cell microenvironment is important in achieving an *in vitro* organ model.

Therefore, it is preferable that the system comprises materials that are easily biodegradable in order to minimize the foreign body response. In the present thesis a biocompatible system was developed, for which both the membrane and the microfluidic material are biodegradable. The combination of traditional scaffold fabrication (i.e. electrospinning) and microfabrication techniques might provide the needed platform to create complex *in vitro* environments that allow the culture of multiple cell types, and oxygenation and nutrients diffusion to the cells.

4.2. Microfabrication of Master Molds

Microfabrication implies the generation of micro- and nano-scale features in modern engineering materials and has its foundations in microelectronics. Although initially created to satisfy the demands of the semiconductor industry, it is increasingly being applied in other fields such as biotechnology and tissue engineering. One of the most popular master mold fabrication techniques is SU8 photolithography which uses light to pattern a substrate (Figure 4.1). Photolithographic techniques were therefore used to introduce relief structures on the surface of wafers. The features, created by SU8 epoxy resists are deposited on substrates. SU8 is a viscous polymer that can be spin coated over clean substrates over a thickness in the range of tens to hundreds of microns. Briefly, clean 4-inch silicon wafers were spin coated with SU8 100 epoxy negative photoresist (Microchem Co.) to achieve a 100 µm thick layer and exposed to UV light in a mask aligner SET MG1410 through a mask. The mask was designed using AutoCAD 2008 and printed on a transparency.

Si wafers were chosen as substrates in the current thesis as they offer good adhesion of the SU8 features and a reproducible and easy delamination of the subsequent elastomer that is to be patterned. A key step in the development of the master molds is cleaning the substrate prior to SU8 spinning. The goal is to remove any organic residues by soaking it in acetone, acetone/isopropyl alcohol and deionized water, followed by a dehydration bake on a hotplate. This process ensures a good adhesion of the SU-8

features on the Si wafer. Herein, SU8-100 was used to create features of 100 μm height.

The SU8 is therefore poured in the center of the silicon wafer and spin coated in two steps: at 500 rpm for 10 seconds and then gradually increasing until the final spin speed of 2700 rpm is reached. At this high speed the SU8 is further spun for another 30 seconds. After spin coating, the edge bead is removed in order to decrease the distance between the mask and the wafer during UV exposure. In another step, a soft bake is performed in 2 stages (i.e. 20 min at 65°C with a gradual increase to 95°C and an additional baking of 50 min at this temperature) in order to evaporate solvents from the photoresist and reduce thermal stress.
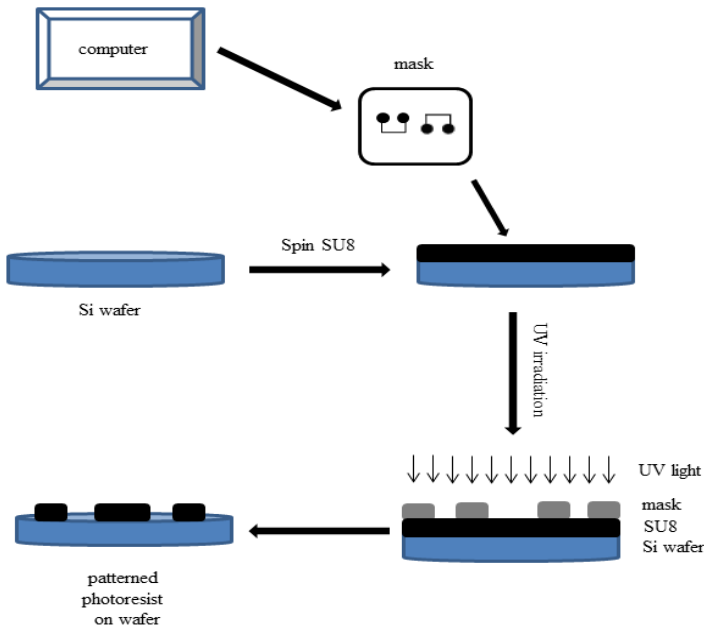
Figure 4.1: SU8 photolithography process

After a proper soft bake procedure, the SU-8 does not flow at room temperature and allows the placement of a mask for the subsequent UV irradiation step. During this step, a strong acid is generated and this opens the epoxide rings of the resist, amplifying the crosslinking reaction of the

exposed regions. Therefore, when exposed to UV light, solidification of the SU8 material occurs. During the UV exposure (i.e. 55 seconds), a mask (Figure 4.1) was used to create the desired patterned. As reports in literature [275] state that wavelengths shorter than 350nm are absorbed near the top surface causing lateral diffusion of the acid, a long pass filter PL-360-LP (Omega Optical) was used. Via this way, UV radiation below 350 nm was eliminated and vertical sidewalls were ensured. As for the soft bake, to avoid temperature shocks, the post-exposure bake occurs in two steps: at 65°C and 95°C. As SU8 is an epoxy based negative resist, the unexposed material can be removed with a developer solution. After allowing the wafer to cool to room temperature, the unexposed/un-crosslinked regions are removed with MicroChem's SU-8 developer and rinsed with isopropyl alcohol. Therefore, only the solidified features remain adhered on the wafer. A final (hard) bake is done to further crosslink the SU-8.

The thickness uniformity of the SU8 features was measured using an optical profiler WYKO NT3300 (Figure 4.2). The SU-8 features were investigated on 2 different molds, in three places on each mold, resulting in an average height of 104.8 ± 4.8 μm.
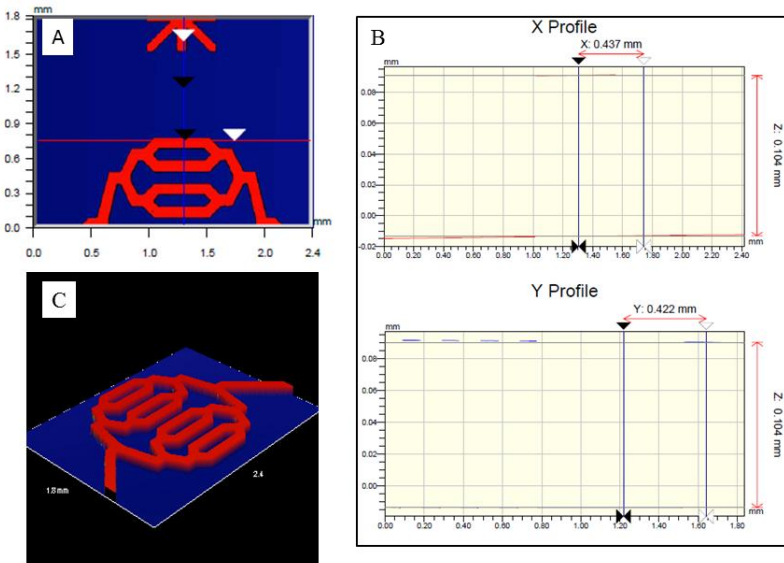
Figure 4.2: Wyko profilometry: measurement of the height of the SU8 features (red color) on a Si wafer (blue color): (A) 2D image of features on mold; (B) measurement profiles of the SU8 features; (C) 3D image of a channel with multiple arms.

4.3. Poly (polyol sebacates) Fabrication and Replica Molding

Poly(polyol sebacates) are thermoset materials and possess several characteristics that make them a good choice for developing microfluidic bioreactors. Amongst these properties, one of outmost importance is the fact that these polymers can be designed to be completely amorphous. This implies not only that they will have a consistent degradation rate, but also that they retain their structural integrity during degradation (i.e. linear loss of mechanical properties) [64]. From the technological point of view, these materials are pliant, easy to process into scaffolds with different geometries via different methods (e.g. replica molding, laser ablation, etc.).

Typically, the materials used in this chapter, PGS and PES, were synthesized and characterized as described in a previous chapter (Chapter 2). Typically, the monomers are reacted at high temperatures (120-150°C) in inert atmosphere and vacuum for times ranging from a few hours to a few days to yield pre-polymers of low molecular weight. At this point they can still be solubilized in different solvents or melted; if further subjected to high temperatures and vacuum, the pre-polymers can be crosslinked (or cured) into a network or an elastomer (Fig 4.3, Figure 4.8a-c). The curing is performed by melting the pre-polymer on a master mold and subjecting it to high temperatures (135-150°C) under vacuum conditions or inert gas. The master mold used was a Si wafer with SU8 relief structures introduced by the photolithographic techniques mentioned above.

In the present work, the curing step was performed via two methods: either via the classical vacuum oven (i.e. typically 2 days at 135°C) and via a nitrogen flushed oven (i.e for 17 hours), in the absence of any vacuum condition. An interesting observation during the curing step was that the nitrogen condition fastens the curing process. The PGS pre-polymer was cured in the nitrogen oven when subjected to 150°C for 8 hours, whereas the pre-polymer subjected to vacuum in the same conditions was still very low crosslinked, having a wax-like consistency and no film was formed. Consequently, the nitrogen oven was considered a more time-reducing

process and it was used also for the bonding of the two different patterned layers.
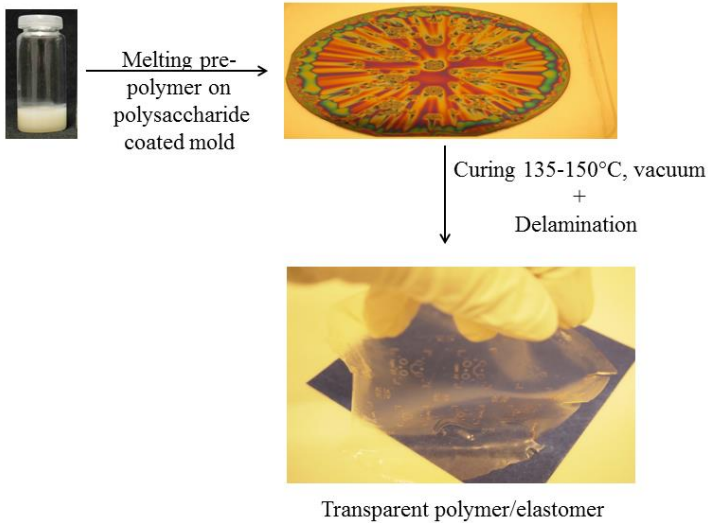
Figure 4.3: Replica molding of biodegradable elastomers.

Biodegradable and biocompatible materials used for fabrication of microsystems require a release layer during the replica molding process. In literature, sucrose was reported as a sacrificial layer for biodegradable elastomers such as PGS [21]. Briefly, the procedure is as follows: after fabrication of the master mold, a sucrose solution in water (90% w/v) is spin coated for 30sec, at 1000rpm, pre-baked on a hot plate at 95°C for 2 min and post-baked in an oven at 120°C for 24h. Although previously reported in other studies, herein it was noticed that sucrose crystallizes on the wafer, thus influencing the delamination and even the transparency of the final polymer film.

Figure 4.4 below shows a silicon wafer (with relief pattern) covered by sucrose, after the baking steps. After replica molding the PGS pre-polymer on the sucrose coated mold, the resulting polymer sheet does not easily delaminate.
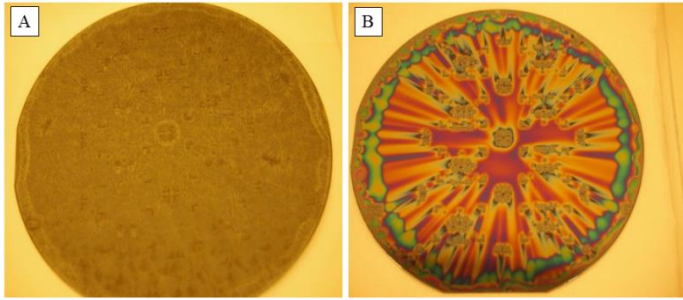
Figure 4.4: Two silicon wafers (with relief pattern) covered by (A) sucrose 90%; (B) dextran 12.5%.

Macroscopic traces of polymer can be observed on the master mold (Figure 4.5B), therefore the features imprinted on the polymer are not the ones expected. As a consequence, other polysaccharides such as chondroitin sulfate (CS), alginate or dextran were investigated as release layers for the biodegradable microfluidic layer fabrication presented in the present thesis. The advantages of using the above mentioned polysaccharides are that they require less baking steps after spin coating on the mold, they provide a better release of the polymeric material from the master mold and last but not least, they do not crystallize on the wafer.
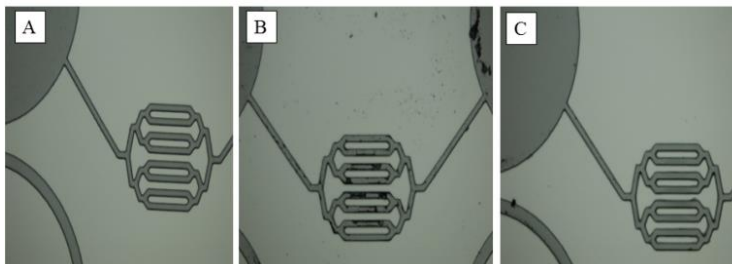
Figure 4.5: Master molds: (A) Multiple channel structures on a master mold; (B) master mold, sucrose coated, after delamination shows traces of polymer; (C) master mold, previously coated by dextran, after polymer delamination shows little to no polymer residues.

In the present study, the obtained patterned wafers were therefore spin coated with dextran at 1000 rpm for 30 seconds. The polysaccharide layer was dried by heating the wafer at 95°C for 2 minutes and then overnight at 120°C. In order to measure the thickness of the release layer, 100 µm holes

were drilled in the polysaccharide on the coated wafer with a CO_2 laser; all samples were then coated with a thin (ca. 20 nm) gold layer through plasma magnetron sputter coating and measured using the Wyko optical profilometer, as the holes thickness represents the thickness of the release layer. The thickness of the polysaccharide layer was measured considering 3 points randomly chosen on 3 coated molds. The results of the polysaccharide thickness measurements are presented in Table 4.1 and represent the average value and the standard deviation. The concentrations of the polysaccharide solutions were optimized as to obtain an easy delamination and accurate features in the polymeric materials. The best results were obtained with dextran 12.5% solution in water (w/v) where the molds did not present any polymer remains after delamination (Figure 4.5C) and could be reused.

Table 4.1: Polysaccharide thickness and static contact angle (SCA) measurements on master molds.

Polyssacharide	Thickness (nm)	SCA (°)
Dextran 12.5%	287 ± 2.5	19 ± 0.8
CS 4%	125 ± 2.9	11 ± 1.0
Alginate 1%	56 ± 8.4	17 ± 1.4

After replica molding of the elastomers, the patterned microfluidic layers were obtained and further aligned and bonded as presented in the subsequent sub-chapters. In Figure 4.6 the measurements performed on a single-arm channel imprinted in an elastomer is presented. The channels of the microfluidic layer had a depth of 102±2 µm.
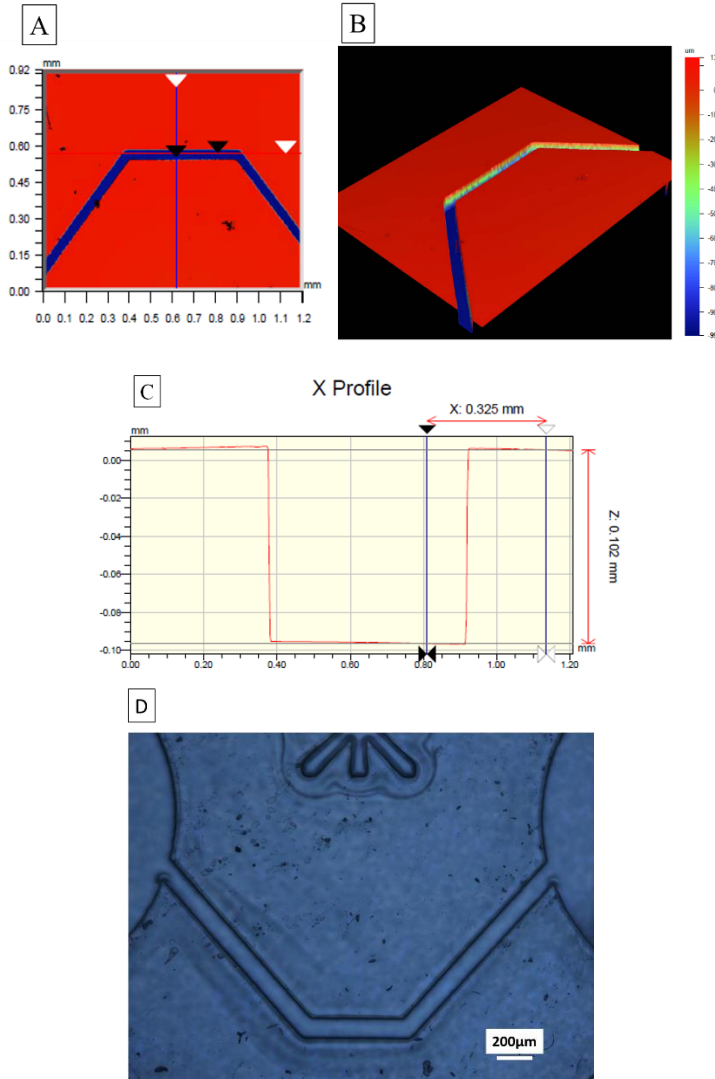
Figure 4.6: Profilometry measurements of the replica molded elastomer: (A) 2D image of a single channel imprinted on an elastomer; (B) 3D image of the patterned elastomer; (C) Profile graph measuring the height of the imprinted features in the elastomer; (D) microscope picture of the replica molded elastomer – air bubbles can be noticed as the elastomer layer was measured on a glass substrate. Picture adapted from [274].

4.4. Preparation of Electrospun Membrane for Bioreactor Integration

The electrospinning technique produces materials with high porosity and high surface area-to-volume ratio [40]. These characteristics of the electrospun materials influence the cellular growth in the scaffolds' 3D microenvironment. PLLA and PES/PLLA core/shell fibrous mats were produced for the integration in the microfluidic devices due to considerations described in previous chapters (Chapter 3). These fibrous mats were chosen as a proof of concept for the present design. Other electrospun mats could also be integrated, depending on the requirements of specific applications. Thicknesses of approximately 10-15 µm were obtained for the electrospun mats by adjusting the needle and the conveyor belt speed during the electrospinning process.

It was noticed that the PLLA fibers were electrostatic (Figure 4.7C) after the solvent removal process (i.e. drying in vacuum at room temperature) and easy manipulation of the mats was not possible in this context. Therefore, an adapted version of the "wet-pressed" method reported by Yang et al. [23] was implemented. Firstly, the electrospun mat was placed on a 4-inch glass plate. A few drops of water were placed on the mat; the membrane was sandwiched in between glass plates and introduced in an oven overnight at 100°C. Weights of about 40N were placed on the glass plates for 24 hours after which the membrane became compact and easy to manipulate (Figure 4.7D). No alteration of the mat's structure or fiber diameter was noticed after this process, as PLLA is a very hydrophobic material and does not react with water. For the PES/PLLA core/shell fibers this procedure was not required, as the PES core provided the entire mat with a more consistent density that led to easy manipulation.

For the integration between the microfluidic layers of the biodegradable system, the membranes were cut with a femtosecond laser in 2 x 2 mm^2 pieces. These dimensions were chosen as the design of the bioreactor involved either a single channel with a length of 2 mm, or multiple channels spread over an area of approximately 4 mm^2. The laser treatment resulted in

melted edges (Figure 4.7B). This proved not to influence the sealing process of the membrane in between the polymer slabs. The thickness of the fibrous mats was approximately 15 μm as determined using a MTG Benchtop Contact Thickness Gauge.
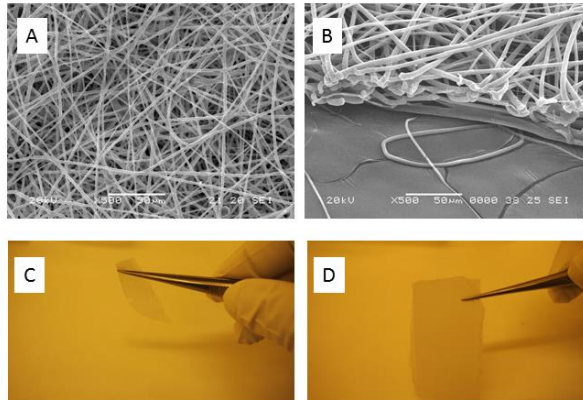
Figure 4.7: Electrospun membrane pictures: (A) SEM micrograph of a 15μm thick PLLA membrane; (B) SEM micrograph of the laser cut edges of the PLLA membrane; (C,D) photographs of PLLA membrane before and after the use of the adapted "wet-pressed" method.

4.5. Microfluidic Device Assembly and Characterization

In the current dissertation a fibrous membrane was embedded in between two aligned and bonded patterned microfluidic layers (containing channels with widths and heights in the order of 100 μm). The advantage of the technology is that it would enable not only cell co-culture on both sides of the membrane, but also distribution of nutrients and oxygen. The embedding of the porous electrospun membrane inside the microfluidic system would provide both 3-dimensionality and a controlled microenvironment for the cultured cells.

4.5.1. Device Assembly

The general scheme of the 3D bioreactor fabrication is presented in Figure 4.8. The mold was coated with a known polysaccharide (i.e. dextran) to facilitate the delamination of the patterned polymer, as indicated in the previous sub-chapter. After the pre-polymer is melted on a dextran coated mold (Figure 4.8a-b), it is further cured into an elastomer. A uniform polymer layer is obtained by melting and spreading the pre-polymer on the mold and ensuring that the curing process is done on a flat surface.

Delamination of the patterned elastomer form the mold was done by incubating the system in double-distilled water. The released patterned layer (Figure 4.8c) was dried prior to alignment and bonded to the other corresponding patterned layer. As static incubation of the polymer-mold system resulted in long delamination times (from hours to days depending on the polymer thickness), the system was introduced in an ultrasonic bath. This decreased the delamination time to minutes. The disadvantage of this approach is that for prolonged times the SU8 features also delaminate from the mold and the mold cannot be reused.
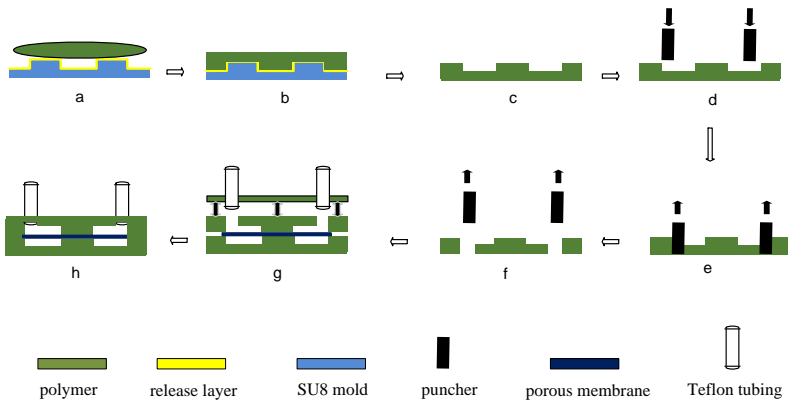
Figure 4.8: Fabrication scheme of the 3D bioreactor. Picture presented in [274].

For the static incubation approach, the mold could be reused up to at least 2 times after which polymer remnants are noticed around the SU8 features due to poor or incomplete delamination. These polymeric residues compromise the accuracy of molding the features in new polymer films. In a

next step, one of the patterned layers was punched with a sterile puncher (2 mm diameter) in order to insert, in a later step, the tubings (Figure 4.8d-f). Two microfluidic layers (Figure 4.8c and 4.8f) were aligned (under a mask aligner SET MG1410) with a porous membrane covering the channel area of the device and then put into contact. Alignment of the microfluidic layer is done using a SET Aligner that comprised a positioning table and a microscope. Both microfluidic layers are fixated with vacuum chucks on the positioning table and the microscope was then used to align both parts before bringing them into contact and bonding them.

Separately, Teflon tubings (0.75 mm diameter) were inserted in a 0.25 cm thick plain polymer film that was then manually placed over the already aligned layers (Figure 4.8g). Medical grade silicone glue (ACS Applied Silicone Corporation, USA) was used in order to seal the base of the connections and to stabilize the tubings. The entire system was finally bonded in a nitrogen flushed oven overnight (Figure 4.8h). The total thickness of the device was approximately 700 µm for 3.5g of pre-polymer cured on the mold.

Due to thermal expansion coefficient of the polymer or to the material shrinkage/expansion during the curing process (also see Table 4.2), displacement of features on the micro-patterned polymer films has been noticed. This led to reduced aligning accuracy when multiple micro-patterned polymer films were aligned relative to each other. A similar phenomenon has been noticed for another elastomer used in microfluidics systems, namely PDMS [276]. The solutions reported included modification of the material or the curing temperature, or even designing the features with an offset. In the present work we have adapted the "sandwich mold fabrication" process reported by Moraes *et al.* [277] where liquid PDMS was sandwiched between a mold and a plastic film. In their process, the sandwich was then placed in between rigid metal plates, clamped, and cured at elevated temperatures. The stack was then disassembled and the plastic film/patterned PDMS layer system was peeled from the mold. This way, lateral shrinkage of the PDMS was avoided. In the same context, to achieve better alignment of the patterned layers and to restrict polymer lateral shrinkage or expansion, a transparent temporary polypropylene (i.e. PP,

Goodfellow Cambridge Limited, 0.025 mm thickness) carrier was used for each microfluidic layer during the alignment process. The thin PP foil was placed over the polymer/mold system in the last stage of the polymer curing process. The polymer/carrier system was delaminated from the mold by incubation in water and dried overnight in a convection oven. The shrinkage/extension degree was calculated with the below formula (1), according to the method reported by Lee et al. [276].

$$Shrinkage\ (\%) = \frac{1}{4} \times (\frac{\Delta d_{AB}}{d_{AB-SU8}} + \frac{\Delta d_{BC}}{d_{BC-SU8}} + \frac{\Delta d_{CD}}{d_{CD-SU8}} + \frac{\Delta d_{DA}}{d_{DA-SU8}}) \quad (1)$$

After delamination of the polymer/PP system from the mold, the features located at the corners of the micropatterned polymer film were compared to the corresponding features on the SU-8 master mold (Figure 4.9). The distances between the points A, B, C and D were measured on the SU-8 master mold (dAB-SU8) and on the micropatterned polymer film (dAB), and subtracted from each other (e.g. ΔdAB = dAB-SU8 – d$_{AB}$). Table 4.2 presents the shrinkage of both polymers according to the curing time. The PP carriers were peeled off after the alignment of the 2 patterned microfluidic layers. Due to the small thickness of the carrier (i.e. 20 µm) and the negligible force applied during the carrier peeling, the microfluidic layers alignment was not disturbed.
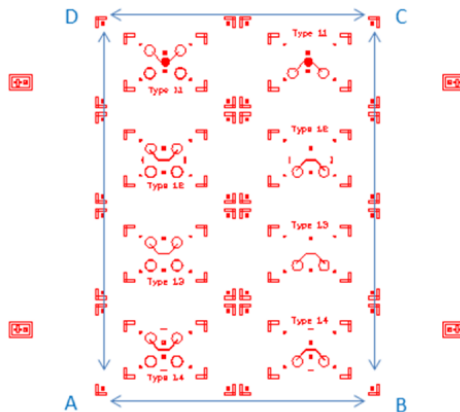
Figure 4.9: Mask design used to characterize the shrinkage of micropatterned polymer films. Picture presented in [274].

Although there was not an obvious correlation between the shrinkage of the polymers and the tested curing temperatures, the PES polymer had a very low crosslinking degree with features not very well defined when cured at 120°C for 2 days. Interestingly, PGS tends to shrink while PES tends to slightly expand during this process. This is probably due to the presence of one more hydroxyl group in the chemical structure of erythritol in comparison with glycerol, which makes PES polymer to bind water at a higher extent than PGS. The statement is also supported by a higher swelling degree of PES (i.e. 8.6%) in comparison with PGS polymer (i.e. 2.1%) [17, 18].

Table 4.2: Shrinkage/expansion behaviour of 350μm thick polymer films.

Curing temperature (°C)/time(days)	PGS shrinkage (%)	PES expansion (%)
120/2	0.42 ± 0.04	n/a
130/2	0.58 ± 0.01	0.13 ± 0.01
135/2	0.52 ± 0.02	0.32 ± 0.01

The bonding process implied further curing thus obtained system (Figure 4.8g) at high temperatures (i.e. 135-150°C) in a nitrogen flushed oven, in the absence of any pressure. The method of bonding microfluidic layers is a critical design consideration as some techniques can alter the chemistry within the channels [278] that can lead to either helpful or problematic results according to the specific application. Some bonding strategies used for microfluidic devices are: oxygen plasma treatment, adhesive bonding [279], physical entanglement among loosened polymer chains by solvent vapour absorption [280], thermal fusion bonding, localized welding [281], etc. The advantage of bonding PPS microfluidic layers is that there are no special or additional requirements needed such as applying pressure, plasma or using solvents. The PPS microfluidic layers will bond under heating provided that the individual films are not fully crosslinked. During the bonding process, the remaining hydroxyl groups (i.e. -OH from the polyol) from one layer react with the remaining carboxyl units (i.e. –COOH from the sebacic acid) of the other microfluidic layer and create ester bonds (i.e. –COO-). Therefore, it is actually a chemical esterification reaction that occurs during the bonding process. The result of this process is that the

interface/bond between the PPS microfluidic layers has the properties of the bulk polymer that constitutes the individual films that are bonded.

The bonding of the microfluidic layers was evaluated by SEM measurements (Figure 4.10). Cross-sections were made by cutting the devices with a CO_2 laser (100 Hz, 100 µm spot, 1 mm/sec, and two passes). As presented in Figure 4.10A, the interface between the microfluidic layers cannot be seen. This is an indication that the bond is strong and the channels are completely sealed. As the cross-sections were made with a CO_2 laser, some optimization of the parameters was necessary. In some cases (Figure 4.10B, C) the laser power was too high and melting of the PLLA membrane could not be avoided. It can easily be observed that the approximately 10 µm thick PLLA membrane (Figure 4.10C) is embedded in between the microfluidic layers and imparts no disruption to the device's channels or to the bonding (e.g. entrapped air, misalignment issues, etc.). When lowering the laser power, more passes of the laser beam are required in order to cut the device. In this case, some material debris was noticed (Figure 4.10E, F). Nevertheless, there was a better visualization of the PLLA membrane that did not melt during the cutting process (Figure 4.10F).
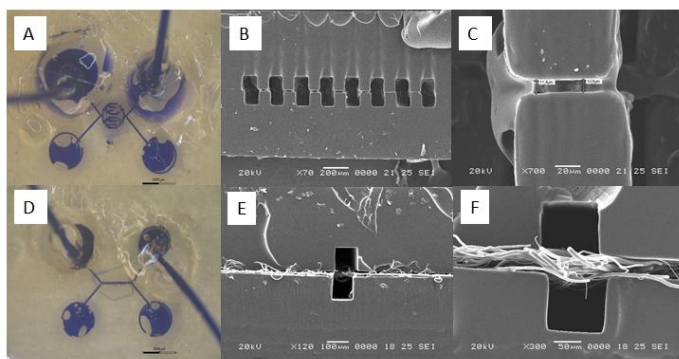
Figure 4.10: (A) – top view of a perfused multiple channels bioreactor; (B,C) - SEM micrographs of the cross-section of a multiple channel bioreactor; (D) - top view of a single channel bioreactor; (E,F) - SEM micrographs of the cross-section of a single channel bioreactor. Picture presented in [274].

4.5.2. Perfusion of the Microfluidic Devices

The macroscopic image of the bioreactor is presented in Figure 4.11. The patency of the microfluidic network was evaluated by injecting a solution of blue ink with water through the channels via a syringe connected to a syringe pump (TSE Systems), as presented in Figure 4.11A-C. Teflon tubes go through the inlet and outlet chambers. Medical grade silicone glue was used to seal the tubings and can be noticed in Figure 4.11B. The disadvantage of using Teflon tubings for the inlet and outlet chambers of the microfluidic system is that it is time consuming as it implies an extra step in the device assembly (Figure 4.8g). As an alternative to the Teflon tubings, a PMMA frame that is specially developed for the current microfluidic design can also be considered (Figure 4.11D, E). The frame used in this case consisted in two PMMA rectangular blocks with drilled holes corresponding to each chamber of the microfluidic design (i.e. the inlet and outlet chambers). The final microfluidic system was placed in between the PMMA blocks, with the punched inlet and outlet chambers aligned to the drilled holes of the PMMA. This alignment can be done macroscopically, as the punched chambers with a diameter of 2 mm can be easily visualized. In a next step, the screws of the PMMA frame are tightened so that the bioreactor is properly sealed. It is important to apply enough pressure on the microfluidic device (by tightening the screws) in order not to have any leaks during the perfusion process, but in the same time not to restrain the device too much as this may lead to increased pressure drop along the channels.

Thus perfused system presented no leaks and the bonding between the microfluidic layers was sufficiently strong to allow perfusion flow rates in the range 0.1-300 µl/min. This broad range was chosen as different cell types can withstand different forces induced by the friction of liquid against the distal cell membrane. The induced force is called shear stress and its value can vary depending on the cell type and application. For example, flow rates of 0.08-0.1 µl/min induce proliferation of osteoblasts [282] and of bone marrow–derived human mesenchymal stem cells [283] for bone tissue engineering, while the gradual increase of the flow rate from 75 to 200 µl/min leads to

higher glycosaminoglycan (GAG) concentrations required for cartilage tissue engineering [284].

The flow rates that were chosen in our study generated shear stress values between 0.002 Pa and 0.4 Pa. The values were calculated for a micro-channel with a rectangular cross-section (i.e. with a height of 100-200 μm, a width of 100 μm and a channel comprised of three arms of 2 mm length) [285]. The low flow rates were chosen considering the possible culturing of hepatocytes and endothelial cells inside the bioreactor. It is well known that relatively high shear stresses may be harmful for hepatocytes and that even the increase of medium flow rate that supplies nutrients and oxygen to the cells, can also damage them [286]. In the liver tissue, the hepatic cells are protected by the endothelial cells from the direct effects of shear stress of the environment. As a comparison, most segments of the circulatory system that contain microvascular endothelial cells maintain a uniform vessel wall shear stress of ~15 dyn/cm2 or 1.5 Pa [287].
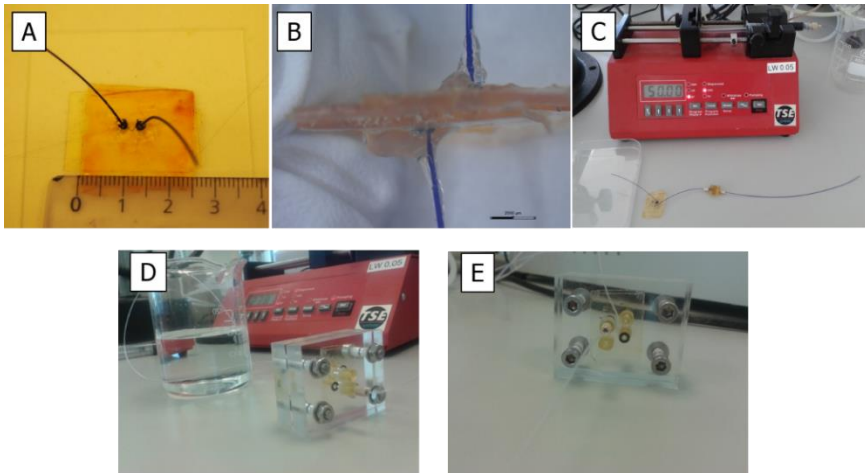
Figure 4.11: Perfusion tests of the 3D bioreactors: (A) image of a perfused bioreactor; (B) lateral view of a perfused bioreactor; (C) perfusion set-up; (D-E) perfused PES bioreactor clamped in between two PMMA frames.

4.5.3. Pressure Drop Experiments

A digital pressure transducer (Alicat Scientific) was used to determine the differential pressure drop in the above mentioned flow rate interval. The transducer was part of a pressure valve controller and it recorded the pressure drop along the channels of the microfluidic system. The final pressure drop also considered the pressure drop along the tubings (i.e. 300 μm diameter). A schematic representation of this experiment is depicted in Figure 4.12 below.
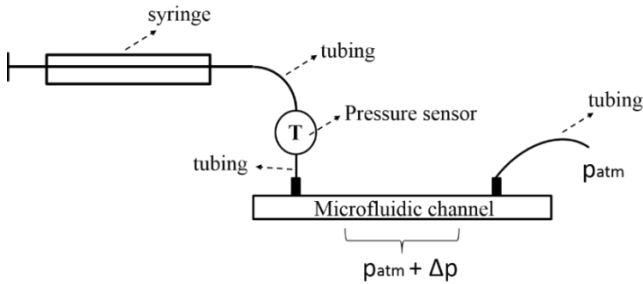
Figure 4.12: Schematic representation of the pressure drop experiment, where Δp – pressure drop; p_atm – atmospheric pressure

The theoretical pressure drop (Δp) for a rectangular channel cross-section with the aspect ratio width/height ~ 1 was calculated according to the formula (2) below [288]:

$$\Delta p = \frac{12Q\mu L}{h^3 w (1-0.63\frac{h}{w})} \qquad (2)$$

where Q is the flow rate, μ is the viscosity of the medium that passes through the channels, L is the length, w is the width and h is the height of the channel. This equation is also accurate to within 0.26% for any rectangular channel that has w/h < 1 and provided that Reynolds number (Re) is below 1000 (i.e. in the present study Re < 0.05) [289, 290].

Pressure drop experiments through the channel shown in Figure 4.13A, B and transversally across the integrated electrospun membrane (Figure 4.13C, D) were also conducted for a single channel bioreactor (Figure 4.10D, E, F) at different flow rates.
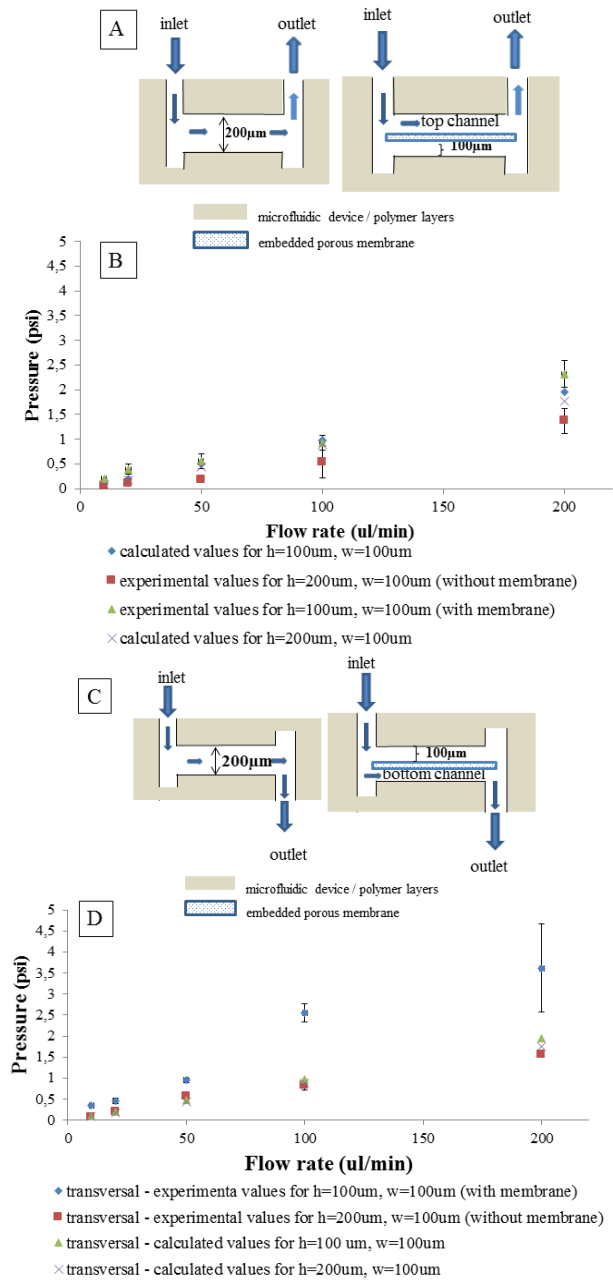
Figure 4.13: Pressure drop along a microfluidic channel (A) schematic representation of flow across the channel and PLLA membrane; (B) calculated vs. experimental pressure drop across the channel; (C) schematic representation of flow transversally through the membrane; (D) calculated vs. experimental pressure drop through the membrane.

The calculated and experimentally determined values are plotted in Figure 4.13. The error bars represent the standard deviation of 3 samples measured per flow rate. All experimental values (Figure 4.13A, C where h=200 µm, w=100 µm) are similar to the calculated ones, for both experiments namely through the channel and transversally across the channel. An increase is noticed in the pressure drop values for the transversal flow, when the PLLA membrane was present compared to the calculated theoretical values (Figure 4.13C, D where h=100 µm, w=100 µm). This should be considered when choosing the appropriate flow rate for introducing specific cell types in the microsystems.

4.6. Conclusions

Biodegradable 3-dimensional microfluidic devices were developed for the design of a tissue-engineered organ by combining a traditional scaffolding technique, electrospinning, and microfabrication. The three-dimensionality was given by the insertion of either a fibrous PLLA or PES/PLLA membrane in between 2 patterned microfluidic layers. The bonding of the final bioreactor was performed in a nitrogen flushed oven, which enhanced the curing rate in comparison with the traditional used vacuum oven. Good patency of the microfluidic channels was obtained as the system presented no leaks and the bonding between the microfluidic layers was sufficiently strong to allow perfusion. If up to now only single-layer microfluidic systems were stacked and bonded, the herein presented concept comes as solution to the 2-dimensionality issue that exists in most microfluidic devices. This unique design is intended to solve the known and previously reported problems of hypoxic oxygen concentrations that arise from the use of polymer thicknesses over 200 µm. In addition, it can also provide distribution of nutrients to the cells, as well as the 3-dimensional support that cells need to retain their morphology and proliferate. The present work is highly relevant for tissue engineering applications and point-of-care diagnostics. Future work should be done in order to visualize and analyze the behavior of different cell lines inside these microfluidic devices.

Chapter 5: Conclusions and future perspectives

5.1. General

The general aim of the proposed research project was the development and biological assessment of biodegradable microfluidic bioreactors for the controlled 3D culturing of liver cells and liver tissues. The idea behind this aim is that the 3D bioreactor initially offers the necessary mechanical/fluidic/chemical environment for the culturing of the desired final tissue, and gradually (synchronous with the tissue growth) degrades as the tissue approaches its final structure. Therefore, a platform is desired that could sustain cell culturing and tissue growth, with the final goal of obtaining a tissue-engineered organ. Based on the existing research and clinical literature, poly(polyol sebacate)s elastomers were chosen as starting materials due to their biodegradability and biocompatibility. Novel polymers of this class were synthesized, characterized and processed into films, fibers and patterned membranes. For the purpose of the present dissertation, the optimization of the elastomers' synthesis and processing led to the ability to assemble microfluidic systems made of biodegradable materials. The unique feature of the developed microfluidic devices is the insertion of a porous membrane that can impart the 3-dimensionality that cells need to grow, while the micro-channels will guide the cells and align them in a specific way as to better mimic the native tissue.

Up to now, no such complex design of a microfluidic device was attempted as cell and tissue culturing is currently done at best using flat uniform biodegradable layers, or 2-dimensional (planar), non-biodegradable microsystems. The combination of the electrospinning technique with microfluidics could be a key towards the development of 3D biodegradable microsystems that better mimic a complex tissue/organ.

5.2. Biodegradable Poly (polyol sebacate)s

In the present study, novel biodegradable elastomers with tunable properties have been synthesized and investigated. The initial work started from mainly two polymers, poly(glycerol sebacate) and poly(erythritol sebacate), and continued with the synthesis of novel poly(polyol sebacate)s via the addition of short and long chain diols. Microwave and bulk polymerization were studied and compared for the synthesis of the above stated materials.

Up to now, microwave irradiation has not been investigated for these materials. This polymerization process rendered lower molecular weights of product (pre-polymers) in comparison with bulk polymerization. After synthesis, all obtained pre-polymers have a molecular weight between 2000 g/mol and 18000 g/mol and, at this point they could still be melted and cured into a desired shape. After the curing process, the polymers ranged from flexible to more rigid elasticity which is verifiable through the Young's modulus that varies between 0.6 MPa and 3.8 MPa. Poly(polyol sebacates) are thermoset materials and possess several characteristics that make them a good choice for developing microfluidic bioreactors. Amongst these features, we mention optical transparency that is especially important during the alignment of two patterned microfluidic layers. The tunability of the mechanical properties, making these materials range from very elastic to rigid, together with their degradability are important characteristics that were considered when choosing these materials.

Other advantages of these materials include the fact that they are pliable, they can be easily processed through different scaffolding techniques, and the synthesis is fast, straightforward and can be transferred cheaply to industrial production. The potential of the herein presented elastomers in different branches of soft tissue engineering was also highlighted by their use as coating materials for metallic stents.

In conclusion, the herein newly synthesized polymers are good substrate materials for microsystem technology and important candidates for soft tissue engineering applications such as liver TE.

5.3. Fibrous membrane fabrication

In order to develop the key-feature of the final microfluidic channel, the porous membrane, electrospinning was used as scaffolding technique. This type of scaffolds provide the three-dimensionality cells need in order to proliferate as they can mimic the extracellular matrix, as they offer high porosity and high surface area-to-volume ratio. A variety of polyesters can be used to form fibers, the most known in literature being PCL, PLLA, and PLGA. As the final bioreactors would consist of the synthesized materials, obtaining elastomeric fibers was attempted in combination with the more easily electrospinnable polyesters mentioned above. Core/shell and blended fibers were therefore successfully developed. The fibrous PES/PLLA core/shell mats rendered scaffolds with tunable mechanical and biodegradability properties. The core/shell materials had a smaller fiber diameter, a higher hydrophilicity, and lower degradation rate than the PLLA fibers, as required by the final goal of this project.

This novel core/shell porous mats developed via electrospinning can be used as cell delivering porous membranes and can serve various applications, from soft to hard tissue engineering. The fibrous membranes were further integrated in microfluidic devices, for the purpose of providing a 3D environment for the final engineering of liver tissue.

5.4. Bioreactor development

Two elastomers, namely PGS and PES, were used as a proof of concept for the development of the microfluidic layers. After the obtaining of the patterned films, the assembly was performed with the inclusion of a porous membrane in between 2 fluidic layers. The bondage of the final device was performed in a nitrogen flushed oven, which enhanced the curing rate in comparison with the traditional used vacuum oven. The patency of the device network was evaluated and the bonding between the microfluidic layers was sufficiently strong to allow perfusion flow rates in the range 0.1-300 µl/min. For the flow rates studied, the pressure drop through the

channels was evaluated and a comparison was performed between microfluidic systems with and without the porous membrane.

From the best of our knowledge, up to now only single-layer microfluidic systems were stacked and bonded, making the herein presented strategy unique as it can provide both distribution of nutrients to the cells, as well as the 3-dimensional support that cells need to retain their morphology and proliferate. This concept can also solve the previously reported problems of hypoxic oxygen concentrations that arise from the use of polymer thicknesses over 200 µm. The present work and developed technology is highly relevant for tissue engineering applications and can be easily transferred to all poly(polyol sebacate)s developed in the present thesis as well as to the ones already present in literature.

5.5. Biocompatibility of developed materials – preliminary results

The biocompatibility of the herein newly developed material films and fibrous scaffolds was investigated with two cell lines, namely liver hepatocellular cells and human adipose-derived stem cells. The hepatocellular cell line, HepG2, was used as it is considered a good in vitro study model for liver tissue engineering applications. It was shown that HepG2 cells adhered and proliferated on the developed films and fibrous mats, making the herein obtained scaffolds suitable candidates for liver tissue engineering.

Human adipose-derived stem cells, hASCs, were also chosen for investigation as they are available in abundant quantities and have been shown to differentiate in various cell types, including endothelial cells which is another major constituent of liver tissue. The cells proliferated on all investigated materials, as evidenced by the increase in DNA amount and metabolic activity.

Although further testing is needed, these preliminary results of the ongoing *in vitro* screening tests are promising for the assessment of the herein biomaterials' non-cytotoxicity.

5.5.1. *In vitro* biocompatibility

Biocompatibility of a (bio)material is a key-aspect to be considered in applications such as implants and medical devices. The term "biocompatible" describes the quality of a material of not being harmful or toxic when in contact with human tissue or cells [291]. Biomaterials used for medical devices have to be tested before in order to prevent any negative effects on the body [292]. The initial biocompatibility tests performed on potential (bio)materials are *in vitro* tests for cell compatibility (i.e. cytotoxicity). These are essential before using the materials in any animal model and usually comprise direct or indirect cell contact methods [293]. The direct contact tests imply the culturing of cells on a material and can screen if there are any toxic substances in the material that do not leach out from it during the prior medium incubation step. In the indirect contact tests or extraction tests, the materials are usually incubated in the medium for a period of time, which is then extracted and added onto cells. If any harmful substances leached out of the material into the medium, their toxicity will be indicated through the cells' reaction. Cell adhesion, proliferation, function and differentiation can be therefore analyzed via qualitative and quantitative assays.

International Organization for Standardization (ISO) standards such ISO 10993 are established for the biological evaluation of medical devices, but not all systems require this testing, including the following: lab-on-a-chip (LOC) devices, micro total chemical analysis systems (µTAS) used in laboratory instrumentation, MEMS devices used in medical imaging machines. Nevertheless, testing the cytotoxicity of individual components is important to assess if there is any cell damage caused by the materials, either by direct contact or leachable substances (extracts). There are three types of cytotoxicity test stated in the International Organization for Standardization 109993-5: extract, direct contact and indirect contact tests. The choice of one or more of these categories depends upon the nature of the sample to be

evaluated, the potential site of use and the nature of the use. Therefore, the details of the preparation of the samples to be tested, the preparation of the cultured cells, and the way in which the cells are exposed to the samples or their extracts are determined accordingly. The numerous methods used in cytotoxicity determination can be grouped into the following categories of evaluation: assessments of cell damage by morphological means; measurements of cell damage; measurements of cell growth; measurements of specific aspects of cellular metabolism [294].

For hepatic tissue engineering, a good *in vitro* model of studying cell compatibility/cytotoxicity is hepatocellular carcinoma cells. Human adipose stem cells have also become of growing interest for tissue engineering applications as their source, adipose tissue, is abundant and easily accessible. In the context of the current tissue engineering application, these cells can also be representative due to their ability to differentiate into endothelial cells *in vitro* [295].

In the present work, the developed elastomeric films and porous electrospun scaffolds were screened using the cell types mentioned above. The materials synthesis and elastomeric films development were described in Chapter 2, while the fibrous membranes were presented in Chapter 3.

5.5.2. Effect of Sample Preparation on the Biocompatibility of Poly(polyol sebacate) Films

Sample preparation is of great importance when considering cell tests. The removal of any unreacted oligomers within the polymer film is needed in order to have no toxic effect on the cells and to sustain their adherence to the material and subsequent cell proliferation.

In the present study, the initial developed biomaterials (i.e. PGS and PES) were evaluated for biological compatibility at KU Leuven, by assessing the attachment of HUH-7, a human hepatoma cell line. Prior to the biocompatibility tests, 8 mm disks were punched from all materials (films) and subsequently sterilized with ethylene oxide gas. Figure 5.1A-B shows the

cells cultured for 7 days on PGS film and PGS coated with an ECM protein, gelatin (i.e. PGS-Gel). The cells do not attach well on to the materials, as observed from the fact that they become round. Compared to the control (i.e. tissue culture plate, Figure 5.1C), the morphology is completely different. Live-dead staining did not offer more information because the polymer materials absorb the dye and are therefore fluorescent [296].
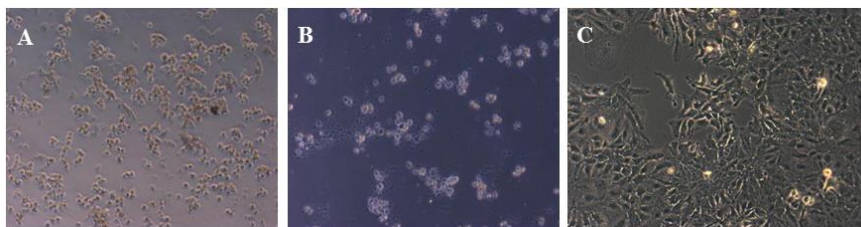
Figure 5.1: HUH-7 cell viability on PGS film (A), PGS-Gel (B) versus TCP control (C) after 7 days of culturing.

For the evaluation of poly (erythritol sebacate), HUH-7 cells were seeded in 12 well plates in which the PES film had been previously inserted. While cells were able to attach in the control wells without biomaterials, the PES material did not allow cell adherence. To investigate whether the incompatibility was due to poor attachment or remains of toxic components used to create the PES material, pre-coating the biomaterial with serum was tested. Interestingly, when the PES films were incubated overnight with 100% fetal bovine serum, HUH-7 cells could attach. However, as attachment was very poor, and cells proliferated at a significantly slower rate compared to the control wells (Figure 5.2). This behavior could be potentially attributed to the presence of toxic remnants.

As the tests presented in the below sub-chapters, performed with HepG2 and hASCs, will show no cytotoxicity, one can conclude that these initial tests were not successful probably due to a number of reasons, such as: oligomers that leach out of the material during the cell seeding, the difference in cell lines used for culturing, the culturing protocol as such (i.e. pre-incubation medium, culturing with human platelets, etc.). Nevertheless, the preparation of the sample before the cell seeding is important, as before the initial HUH-

7 cell tests the materials were washed in ethanol at room temperature, whereas the samples prepared for the HepG2 and hASCs compatibility tests material films were washed in ethanol at 60°C. The increased temperature could facilitate the swelling of the elastomer film and the better release of any entrapped residues.
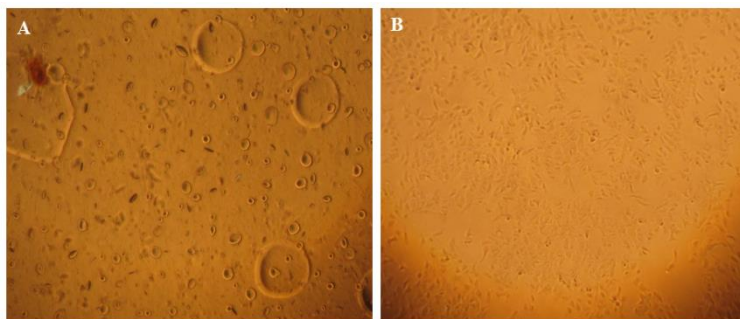
Figure 5.2: Evaluation of biocompatibility of PES material (A) versus TCP control (B). HUH-7 cells were seeded at a density of 100 000 cells per cm² on either PES with an overnight pre-coating of 100% fetal bovine serum (FBS) or on non-treated plastic as a control. Pictures were taken at 10x and 5x magnification respectively after 2 days of culture. At this point the TCP control cells were growing towards confluence whereas only a small amount of cells attached in the PES condition, having a non-conform morphology.

Therefore, although there was no or poor HUH-7 cell adhesion on the initially developed PGS and PES materials, cell attachment and proliferation can be stimulated by thorough washing steps, further surface coating the material films (i.e. Gelatin immobilization, Chapter 2) and/or pre-incubation in cell medium and/or FBS before cell seeding.

5.5.3. Liver Hepatocellular Cells (HepG2)

Hepatic tissue engineering comes as a potential solution for alleviating the need of liver donors. For this purpose, biocompatible and biodegradable polymer films and scaffolds are used to sustain the growth and proliferation of suitable cells that can replace the damaged tissue [155]. For a better assembly of the cells into a tissue similar to the native one, the scaffolds should mimic the Extracellular Matrix (ECM) [297]. This fact led to the

development of a wide range of different scaffolds with different characteristics (i.e. porosity, surface pattern, etc.), amongst which fibrous scaffolds are well-known for their more similar structure to that of the ECM.

5.5.3.1. Materials and Methods

To assess the cell attachment and proliferation, the biomaterial scaffolds were pre-incubated with cultivation medium (DMEM+10% FBS) overnight. Subsequently HepG2 cells were seeded at a density of 100 000/well (24 well plate) and evaluated at day 1, 3 and 7 after cell seeding; cells seeded on tissue culture plastic were considered as a positive control. To assess the cell number, a 5 mg/ml solution of 3-(4, 5-dimethylthiazol-2-yl)-2,5-diphenyltetrazolium bromide (MTT; Calbiochem) was prepared in PBS and 10 times diluted with the cultivation medium and filter sterilized. After washing with PBS, the cells were incubated with the MTT solution (4h) in a 5% CO_2 incubator at 37°C. The lysed cells and the formazan crystals were dissolved by incubation with 0.04 N HCl in 2-propanol and 1 v% Triton X100 (Sigma) for 30 minutes. The absorbance was measured at 580 nm with an EL800 Universal microplate reader (BioTek instruments Inc.). The relative cell number was calculated and compared to the control. For each condition, three independent samples were assessed at each time point.

5.5.3.2. HepG2 screening of the biomaterials

For the herein studied materials (i.e. fibrous scaffolds and films), the indirect contact tests (Fig 5.3A) revealed that the HepG2 metabolic activity was significantly reduced after incubation with 24 hours material extracts when compared to the control. Thus, after 24 hours of exposure to the extracts, the percentage of viable, metabolically active cells was reduced to 64.4%, 60.6% and 61.5 % for PLLA fibers, PES/PLLA core/shell fibers and the PES film respectively.

HepG2 cells were seeded on the materials (Fig 5.3B) after 24 hours medium pre-incubation. At day one, 81.9%, 82.9% and 8.56% of the cells was attached to the PLLA fibers, PES/PLLA fibers and the PES film respectively. The results

imply a sufficient cell attachment for the PLLA and PES/PLLA fibers while cell attachment to the PES film was considerably low. The cell proliferation assay (Fig 5.3C) shows that after initial adhesion to the materials, the HepG2 cells on the PLLA and PES/PLLA fibers show a comparable growth pattern as the TCP control. While the initial adhesion to the PES film was rather low, the proliferation graphs shows that the attached cells can proliferate and colonize the PES film, fact that was confirmed by microscopy on day 7 (Figure 5.3D).
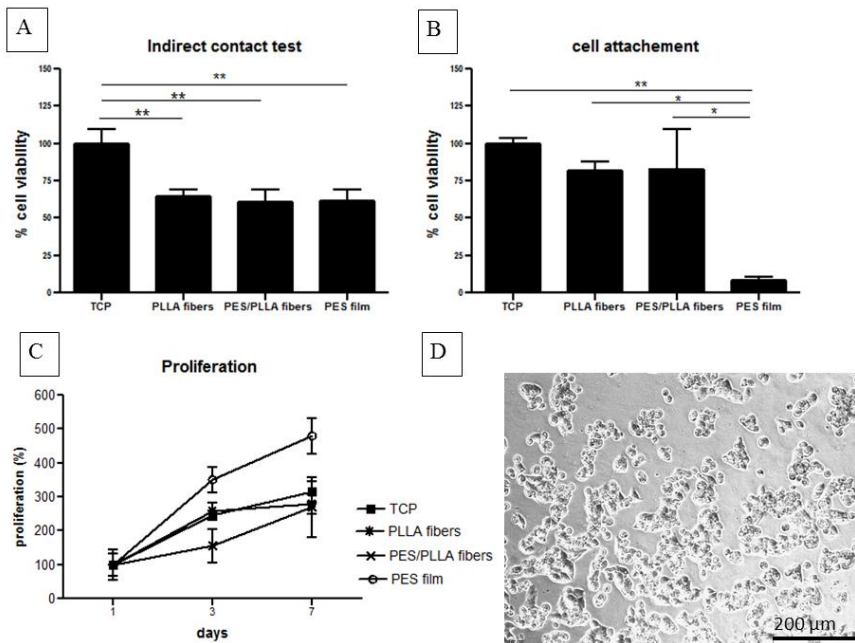
*Figure 5.3: Biocompatibility tests: (A) Indirect contact tests. HepG2 cells were exposed to material extracts and cell metabolic activity was determined after 24 hours. The data are mean % ± SD compared to the control (n=3) (B) cell attachment test. The cells were seeded on the materials. After washing, the viability of the cells was determined and compared to cells seeded on TCP. The data are mean % ± DS compared to the TCP control (C) Cell proliferation assay. After initial attachment, the percentage of viable, metabolically active cells was evaluated at day 3 and day 7. The data are mean % ± SD compared to the initial attachment at day 1 (n=3) (D) Brightfield microscopic image of PES film, 7 days after cell seeding. (for all experiments n=3, significant data are indicated by * (p<0.05) or **(p<0.01))*

The steeper proliferation curve of the PES film when compared to the others can be explained by the lower initial cell adhesion: while the cells in the

control, PLLA and PES/PLLA fibers almost reach confluence by day 7, the cells on the PES film are still in the exponential growth phase.

These results are in agreement with the state of the art, where porous scaffolds are preferred for tissue engineering as they can provide additional benefits in comparison with plain films, such as more attachment places, increased surface area, support for a larger cell mass, and the capability of shaping specific structures [298]. The poly(α-hydroxy acids) polymers is one of the most investigated group of polymers. Amongst this type of polymers, PLA, PGA, PLLA and PLGA were processed into 3D porous scaffolds and rendered suitable long-term culturing systems for hepatocytes [299]. As plain films cannot provide in itself a lot of attachment places and cells that are cultured on these surfaces can display flattened shaped, abnormal polarization or loss of differentiated phenotype [300], surface modification with biologically active proteins seems at least a minimum requirement for the growth and proliferation of cells on such 2D surfaces.

5.5.4. Human Adipose-Derived Stem Cells (hASCs)

5.5.4.1. Materials and Methods

Unless specified otherwise, materials were obtained from Life Technologies, Bleiswijk, the Netherlands, and the manufacturer's instructions were followed.

Cell Expansion Culture

Human adipose-derived stem cells of six female donors (age = 45.6±8.0 years; range 33-54 years) were obtained as described previously [301]. The cells were pooled and cultured until passage 4 in minimal essential medium alpha (αMEM) with 2% human platelet lysate (PL), 10 IU/ml heparin (Leo Pharma, Amsterdam, The Netherlands), 100 IU/ml penicillin (P), 100 IU/ml streptomycin (S) and 0.25 IU/ml fungizone (F) [302]. The PL was created from 5 transfusion bags (180-350 ml) containing clinical-grade random-donor-pooled platelets (Sanquin, Amsterdam, the Netherlands), and was constant for all experiments.
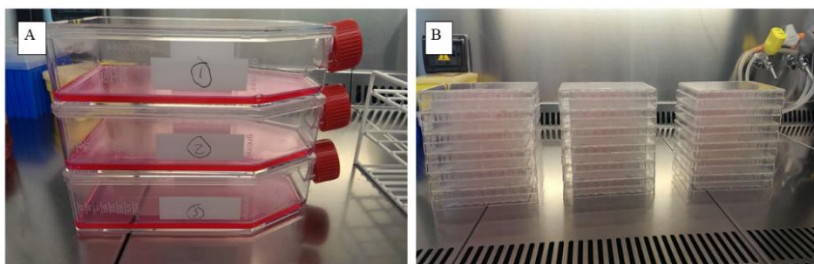
Figure 5.4: (A) Independent cell expansion, and (B) cell seeding on materials and TC-plastic.

Cell Culture on Materials

Tissue culture plastic (TC-plastic) served as positive controls, non-cell seeded materials and TC-plastic served as negative controls. The materials and TC-plastic were incubated for 24 hours in 400 µl culture medium: αMEM with 5% PL, 10 IU/ml heparin and 1% P/S/F. Thereafter, hASCs were detached with phosphate-buffered saline (PBS) containing 0.5 mM EDTA/0.05% trypsin and suspended at 25,000 cells/ml in culture medium. After washing the materials with 400 µl culture medium, 400 µl cell suspension was added to each material and TC-plastic, resulting in a cell seeding density of 10,000 cells per well. The cells were cultured for 7 days, culture medium was refreshed after 4 days.

Metabolic Activity Assay

After 1, 3 and 7 days of culture, the metabolic activity of the hASCs was determined by the Alamar Blue assay. Alamar Blue (40 µl) was added to the culture medium and incubated for 3 hours. After incubation, 75 µl of the reaction product from each well was transferred into a 96-well ELISA plate. Fluorescence was read at 530/25, 590/35 nm in the Synergy multi-plate reader (Biotek systems, Bad Friedrischshall, Germany). Readout values from negative control samples were deducted from values of experimental samples.

DNA Quantification

After 1, 3 and 7 days of culture, DNA was quantified by the CyQuant assay. After the Alamar blue assay, cells were washed with PBS, lysed with 250 µl

CyQuant lysis buffer and frozen over night at -20 ˚C. Per sample, 100 μl lysate was transferred into a 96-well ELISA plate and conjugated with CyQuant GR dye. After incubation, fluorescence was read at 480/520 nm in the Synergy multi-plate reader. DNA content was determined from a standard curve that was included in the assay.

Statistical Analysis

Prism 5 (GraphPad) was used for statistical analysis. Per time-point, ANOVA with Bonferonni multiple comparisons post-hoc tests were used to test if cells on materials differed from cells on TC-plastic. Each n represents an independent experiment, P-values <0.05 were considered significant.

5.5.4.2. hASCs screening of the biomaterials

Biocompatibility of the novel developed material films was tested with hASCs. There is a vast literature on PGS and PES polymers, and their compatibility has been proven for many applications such as cardiovascular [57, 58], neural [59], cartilage [60], and retinal tissue engineering [61]. For the current tests, hASCs formed a confluent monolayer on all novel materials, except PGS-PS. On all materials the cells retained an elongated star-shaped morphology, which is characteristic for adipose derived stem cells cultured on the golden standard TC-plastic (Figure 5.5).

<u>Biocompatibility of the Novel Developed Polymer Films</u>

The cells proliferated well on all materials, as evidenced by the increase in DNA amount (Figure 5.6A). At day 1, DNA amount was comparable between all materials and TC-plastic. At day 3 and 7, for cell cultures grown on all materials tested, the DNA amount had further increased compared to day 1. The DNA was slightly lower on the novel biomaterials compared to TC-plastic.
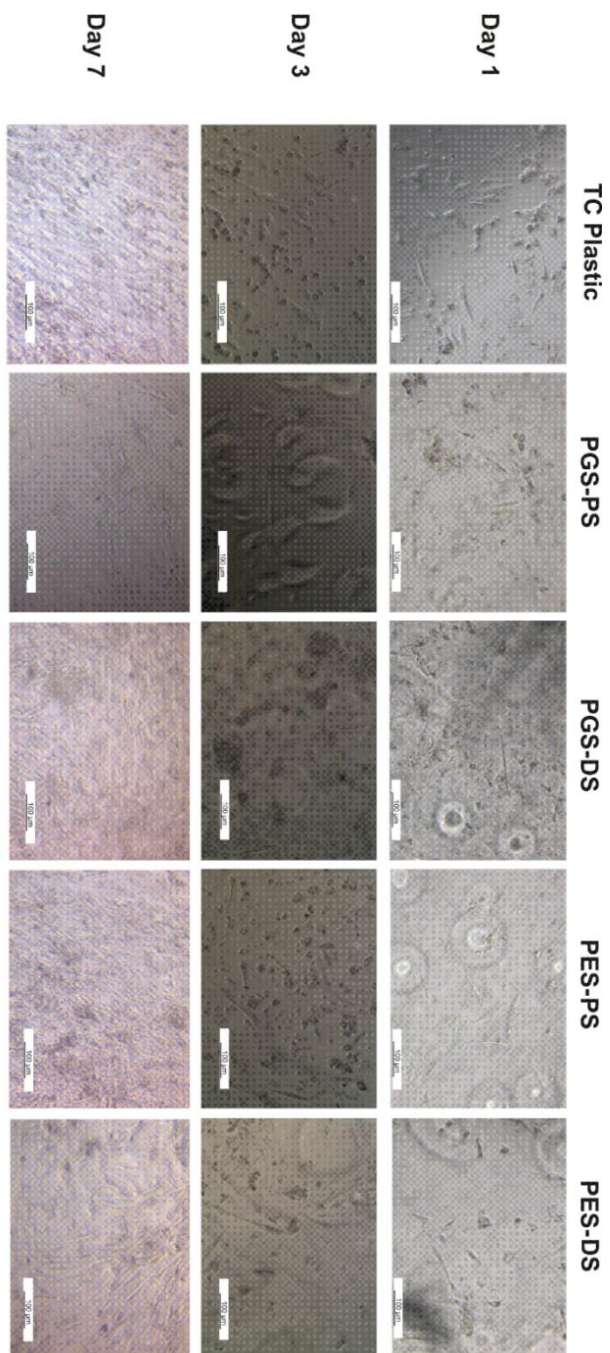
Figure 5.5: hASC morphology on newly synthesized poly(polyol sebacates).
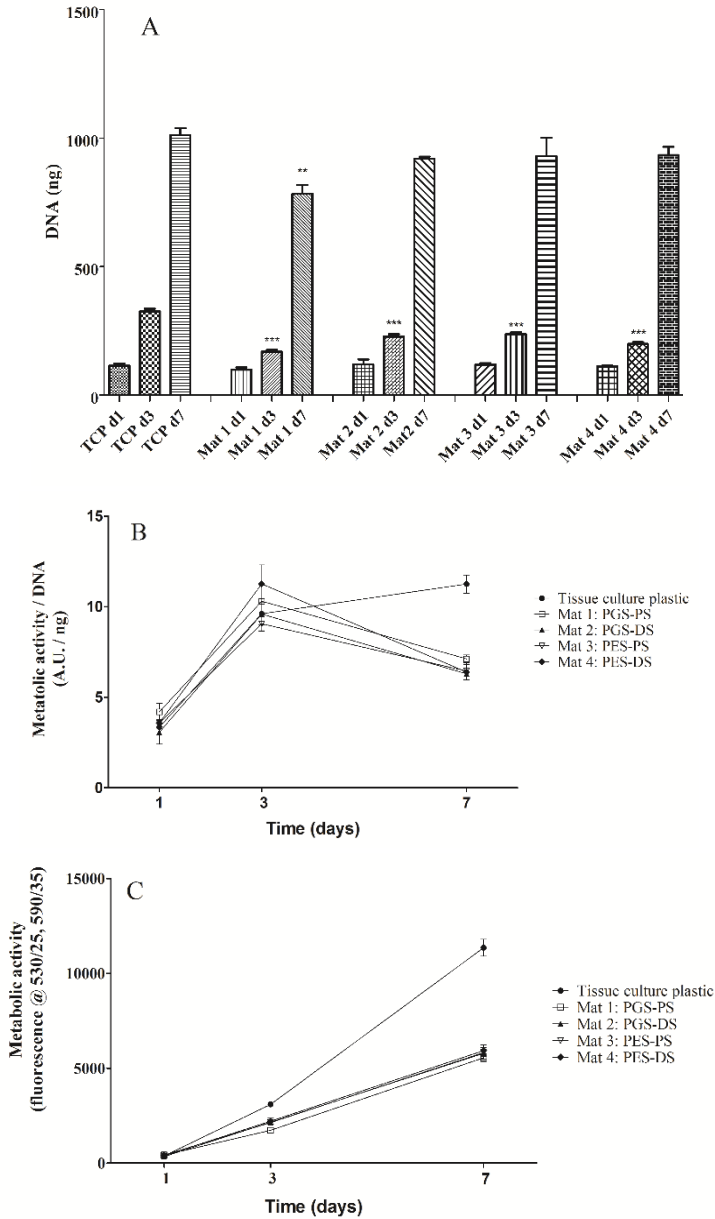
Figure 5.6: Biocompatibility tests. A) DNA content of hASC cultures grown for 7 days on the different materials. B) Metabolic activity per DNA content; C) Metabolic activity normalized at day 1; ANOVA and Bonferonni multiple comparisons post-hoc test were performed, to test if cells on materials differ from cells on TC-plastic *** p<0.001 and **p<0.01.

The total DNA amount on the PGS-PS was lower than that of other materials. Although the difference between DNA amount on the different materials is only small, this likely means that the proliferative capacity of the cells is reduced by PGS-PS. The photographs indicate that attachment to the material is weak. In terms of cell attachment and proliferation, this data combined makes PGS-PS the least biocompatible of all materials tested.

During culture, the cells remain metabolically active on all materials and TC-plastic, as shown in Figure 5.6B. For cells grown on all materials tested, the metabolic activity per cell is higher on day 3 and 7 compared to day 1. At day 7, the metabolic activity per cell was lower for cultures grown on PGS-PS, PGS-DS, PES-PS, and PES-DS than that of cells grown on TC-plastic. Compared to day 3, the metabolic activity per cell decreased on the novel biomaterials at day 7. This decrease, in combination with cells that remain firmly attached and proliferate, could possibly be attributed to differentiation of the cells, since metabolic changes can coincide with differentiation of stem cells as early as 7 days [303].

Although the observed reduction in metabolic activity on day 7 might be caused by differentiation of the cells, from the images taken at days 1, 3, and 7, it is not possible to draw conclusions in which specific direction the stem cells differentiate. This is because hASCs have multi-lineage differentiation potential and no chemical mediators of differentiation were added to the culture medium in the current experiments.

Biocompatibility of the Plain vs. Surface-Modified Polymer Films

In another experiment, the initial PGS material was compared to the gelatin-surface modified PGS (i.e. PGS-Gel; Figure 5.7). It was noticed that the cells adhered to the materials. The cells proliferated over a period of 7 days, and reached confluence on all materials (PGS, PES, derived biomaterials and surfaced modified ones). However, as they reached confluence they also started to contract and detach from all materials. These phenomenon occurred on all samples except on the PGS film that has a gelatin coating

immobilized on its surface (i.e. PGS-Gel, Figure 5.7). This may be an indication that the protein coating has a beneficial effect on the cells.
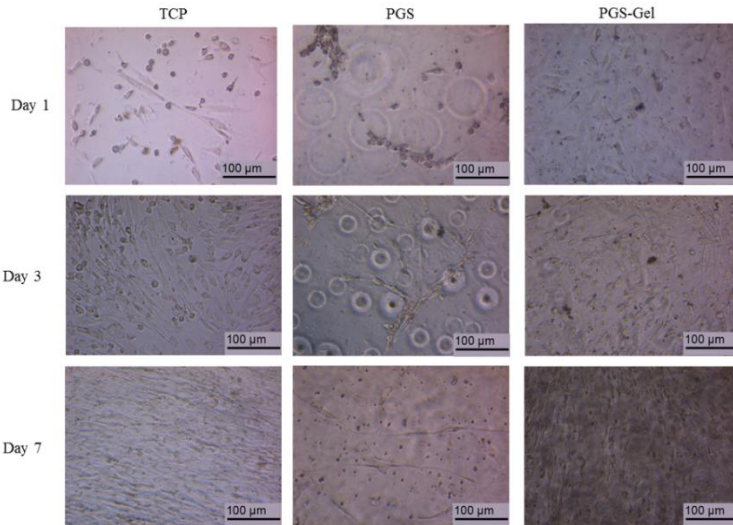
Figure 5.7: hASC morphology on PGS and PGS-GelB films.

The cells on tissue culture plastic (TCP) remain adherent. At day 7 photos there was a high concentration of cells on the TCP that borders the materials. On all materials, the cells remained metabolically active (Figure 5.8-5.9), and after 7 days there was no difference between the cells on TCP or on the materials (metabolic activity/cell).
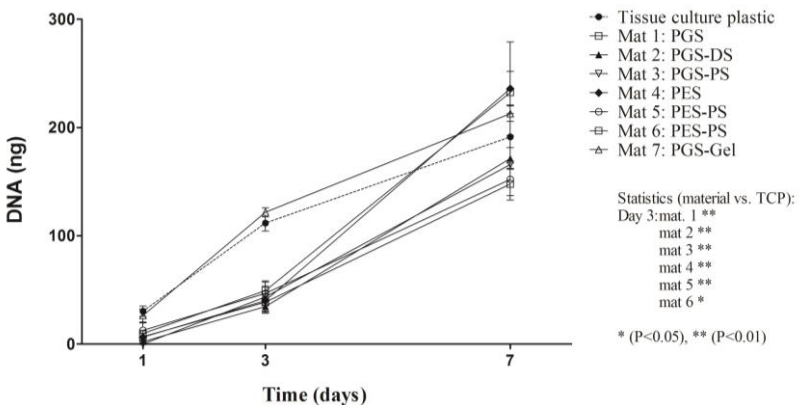
Figure 5.8: Biocompatibility tests. DNA content of hASC cultures grown for 7 days on the material films.
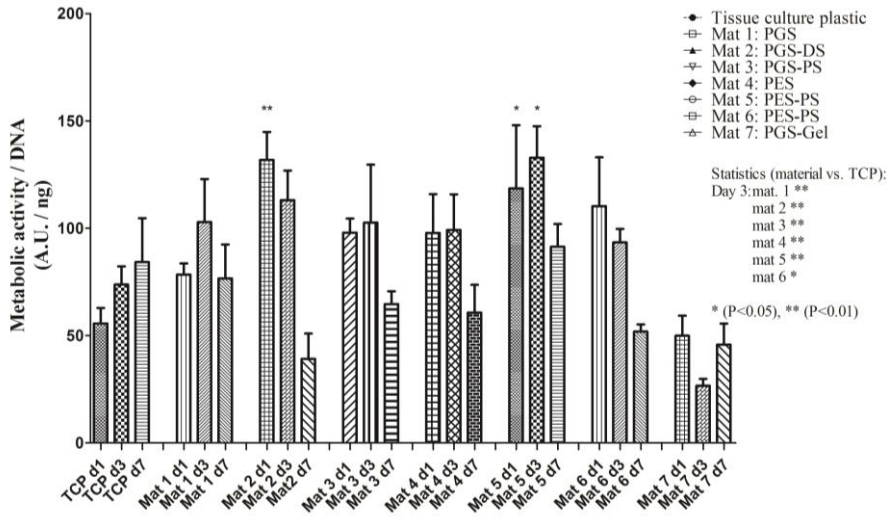
*Figure 5.9: Biocompatibility tests. Metabolic activity per DNA content for PGS, PGS-derived polymers, PES, PES-derived polymers and PGS-Gel;; ANOVA and Bonferonni multiple comparisons post-hoc test were performed, to test if cells on materials differ from cells on TC-plastic *p<0.05, **p<0.01.*

5.5.5. Preliminary Conclusions on Cell Screening of the Developed Biomaterials

The effect of sample preparation on the biocompatibility of the herein developed biomaterials was studied. The importance of the polymer film preparation was highlighted by evaluation of PES and PGS films with a human hepatoma cell line (HUH-7). The mentioned materials showed poor or no cell attachment that could be correlated with an insufficient removal of unreacted oligomers from the polymer films.

Further cytotoxicity investigations were performed after thoroughly washing the samples by incubation in ethanol at a higher temperature (60°C). The non-cytotoxicity or compatibility of the designed materials was demonstrated by investigating their interaction with two other cell lines, namely liver hepatocellular cells and human adipose-derived stem cells. Amongst the initial biocompatibility tests that should be performed, the *in*

vitro cytotoxicity of cells should be performed in order to avoid unnecessary animal tests.

HepG2 and hASCs were used to evaluate the *in vitro* compatibility of the materials and scaffolds developed in the present dissertation. It was shown that HepG2 cells adhered and proliferated on the developed films and fibrous mats. The hASCs also proliferated on the material films, as evidenced by the increase in DNA amount and metabolic activity.

In conclusion, all biomaterials developed in the current thesis can be considered biocompatible and, therefore suitable for cell culturing and tissue engineering.

5.6. Outlook and future directions

The development of biodegradable materials will remain an important aspect of tissue engineering and regenerative medicine. In this regard polymers play a crucial role, as they can be designed to possess different properties ranging from biodegradable to non-biodegradable, from soft to hard, from cell-interactive to cell-repelling, etc. This tunability of properties makes synthetic polymers an appealing class of materials to be used in a variety of tissue engineering applications, including liver tissue engineering. In comparison to natural polymers, not only that the properties of synthetic polymers can be tuned to suit a specific application, but they can also be fabricated in large quantities and have a longer shelf life. The latter are important considerations for mass fabrication and commercialization. A brief overview on some synthetic biomaterials used for soft TE was provided in Chapter 1 of the present thesis. Chapters 2 and 3 highlighted the development of novel poly(polyol sebacate) elastomers and scaffolds for liver TE. One important aspect in choosing the poly(polyol sebacate) class was their compatibility with the herein used microfabrication process. Their transparency is a key-feature for the assembly and alignment of different patterned layers. Another main considerations of synthesizing these new polymers was the need for elastomers of this class with longer degradation

times than the ones already present in the literature. Although, in the present work, the latter aspect was achieved and novel elastomers with lower *in vitro* degradation rates were obtained, more studies are required to see the translation in the human body.

Traditional and advanced scaffolding techniques provide the possibility of developing complex patient specific implant materials. Chapter 3 of the present dissertation presents a scaffolding technique (i.e. electrospinning) that used the earlier developed and novel polymers to produce application specific porous interconnected scaffolds. One of the most important advantages of electrospun fibrous scaffolds or membranes is its resemblance to the structure of extracellular matrix, which largely consists out fibrous proteins. The extracellular matrix is a substantial part of a tissue's volume, that is mostly filled by a network of macromolecules such as (but not limited to) the ones mentioned above. For the current application, the obtained fibrous membranes were intended to be inserted into a microfluidic device and to provide a space on which cells can proliferate and differentiate into the desired liver tissue. The required thickness of the fibrous membrane was achieved, but design limitations still exist as the pore size (i.e. the space between two neighboring fibers) of the randomly oriented fibers could not be controlled to a homogeneous size of maximum 5 μm. This size is important as one future goal is to culture liver cells (i.e. 5 μm typical hepatocyte size, 8-12 μm endothelial cells size) in such a way that they don't fall through the fibrous membrane. A future perspective for this problem would be the investigation of aligned electrospun fibers instead of random ones. It is assumed that by aligning the electrospun fibers under different angles, such a pore size can be obtained. Nevertheless, more studies are required in this direction.

An intensive work has also been done on the development of biocompatible microsystems. In the current work, a combination of a traditional scaffolding technique, electrospinning, and microfabrication rendered a three-dimensional fluidic environment in which cells could potentially proliferate (Chapter 4). This biological inspired engineering approach is essential for reproducing the cellular and extracellular components of a tissue or organ.

For this approach to succeed, mimicking a tissue on a microscale is of outmost importance as it can give a better understanding of the microenvironment. The current project was aiming to insert a 3D environment to a rather planar microfluidic system. The innovation consists of introducing a porous membrane inside a microfluidic bioreactor. This membrane is hypothesized to provide the liver cells with a more familiar in vivo environment that will support their proliferation and differentiation into a new liver tissue. The porous membrane was successfully integrated inside the microfluidic system as the bioreactor presented no leakages and a good bonding of the patterned microfluidic layers was obtained. One of the unknowns that still remain to be studied and analyzed is how such a system will actually behave during culturing of cells. Although all materials and scaffolds designed herein proved non-cytotoxic in the preliminary biological testing, future work should be done in order to visualize and analyze the behavior of different cell lines inside this type of microfluidic devices. Will the passage from rigid tubing and frames at a macro scale to soft materials at a micro scale have an influence on the cells? Will the cells behave in the hypothesized way when cultured in the final bioreactor? Such questions are still to be answered, as research is a continuous process and sometimes the more in–depth one goes the more unknown or unexpected aspects can arise. A continuous interaction between different disciplines is required considering that the aim of tissue engineering and regenerative medicine is to restore, maintain, or improve tissue function. The interaction of cell biologists, engineers, clinicians and regulatory authorities is crucial in bringing such engineered platforms from the lab bench to commercialization.

References

1. Mathers, C.D. and D. Loncar, *Projections of global mortality and burden of disease from 2002 to 2030. .* PLoS Med, 2006(3): p. 442.

2. Ellis, A.J., et al., *Pilot-controlled trial of the extracorporeal liver assist device in acute liver failure.* Hepatology, 1996. **24**(6): p. 1446-1451.

3. Kahraman, A., et al., *Comparison of extracorporeal liver assist devices - albumin dialysis versus plasma exchange - in acute-on-chronic liver failure.* Deutsche Medizinische Wochenschrift, 2014. **139**(33): p. 1653-1658.

4. Hassanein, T.I., R.R. Schade, and I.S. Hepburn, *Acute-on-chronic liver failure: extracorporeal liver assist devices.* Current Opinion in Critical Care, 2011. **17**(2): p. 195-203.

5. Murphy, S.V. and A. Atala, *Organ engineering combining stem cells, biomaterials, and bioreactors to produce bioengineered organs for transplantation.* Bioessays, 2013. **35**(3): p. 163-172.

6. Korbling, M. and Z. Estrov, *Adult stem cells for tissue repair - a new therapeutic concept?* N Engl J Med, 2003. **349**(6): p. 570-82.

7. Carpentier, B., A. Gautier, and C. Legallais, *Artificial and bioartificial liver devices: present and future.* Gut, 2009. **58**(12): p. 1690-1702.

8. Lee, P.J., P.J. Hung, and L.P. Lee, *An artificial liver sinusoid with a microfluidic endothelial-like barrier for primary hepatocyte culture.* Biotechnology and Bioengineering, 2007. **97**(5): p. 1340-1346.

9. Chapekar, M.S., *Tissue engineering: Challenges and opportunities.* Journal of Biomedical Materials Research, 2000. **53**(6): p. 617-620.

10. Dvir-Ginzberg, M., et al., *Liver tissue engineering within alginate scaffolds: Effects of cell-seeding density on hepatocyte viability, morphology, and function.* Tissue Engineering, 2003. **9**(4): p. 757-766.

11. Davis, M.W. and J.P. Vacanti, *Toward development of an implantable tissue engineered liver.* Biomaterials, 1996. **17**(3): p. 365-372.

12. Domansky, K., et al., *Perfused multiwell plate for 3D liver tissue engineering.* Lab on a Chip, 2010. **10**(1): p. 51-58.

13. Nomi, M., et al., *Role of growth factors and endothelial cells in therapeutic angiogenesis and tissue engineering.* Curr Stem Cell Res Ther, 2006. **1**(3): p. 333-43.

14. Kulig, K.M. and J.R. Vacanti, *Hepatic tissue engineering.* Transplant Immunology, 2004. **12**(3-4): p. 303-310.

15. Palakkan, A.A., et al., *Liver tissue engineering and cell sources: issues and challenges.* Liver International, 2013. **33**(5): p. 666-676.

16. Allen, J.W. and S.N. Bhatia, *Engineering liver therapies for the future.* Tissue Eng, 2002. **8**(5): p. 725-37.

17. Wang, Y.D., et al., *A tough biodegradable elastomer.* Nature Biotechnology, 2002. **20**(6): p. 602-606.

18. Barrett, D.G., W. Luo, and M.N. Yousaf, *Aliphatic polyester elastomers derived from erythritol and alpha,omega-diacids.* Polymer Chemistry, 2010. **1**(3): p. 296-302.

19. Sackmann, E.K., A.L. Fulton, and D.J. Beebe, *The present and future role of microfluidics in biomedical research.* Nature, 2014. **507**(7491): p. 181-189.

20. Fidkowski, C., et al., *Endothelialized microvasculature based on a biodegradable elastomer.* Tissue Engineering, 2005. **11**(1-2): p. 302-309.

21. Bettinger, C.J., et al., *Three-dimensional microfluidic tissue-engineering scaffolds using a flexible biodegradable polymer.* Advanced Materials, 2006. **18**(2): p. 165-+.

22. Ryu, W., et al., *Microfabrication technology of biodegradable polymers for interconnecting microstructures.* Journal of Microelectromechanical Systems, 2006. **15**(6): p. 1457-1465.

23. Yang, D.Y., et al., *Electrospun Nanofibrous Membranes: A Novel Solid Substrate for Microfluidic Immunoassays for HIV.* Advanced Materials, 2008. **20**(24): p. 4770-+.

24. Liu, Y.Y., et al., *Incorporation of electrospun nanofibrous PVDF membranes into a microfluidic chip assembled by PDMS and scotch tape for immunoassays.* Electrophoresis, 2009. **30**(18): p. 3269-3275.

25. Neeves, K.B. and S.L. Diamond, *A membrane-based microfluidic device for controlling the flux of platelet agonists into flowing blood.* Lab on a Chip, 2008. **8**(5): p. 701-709.

26. Jo, E., et al., *Microfluidic channels fabricated on mesoporous electrospun fiber mats: A facile route to microfluidic chips.* Journal of Polymer Science Part B: Polymer Physics, 2011. **49**(2): p. 89-95.

27. Wallin, P., et al., *A method to integrate patterned electrospun fibers with microfluidic systems to generate complex microenvironments for cell culture applications.* Biomicrofluidics, 2012. **6**(2).

28. Moradi, A., et al., *Fabrication and characterization of elastomeric scaffolds comprised of a citric acid-based polyester/hydroxyapatite microcomposite.* Materials & Design, 2013. **50**: p. 446-450.

29. Bahraminasab, M., et al., *Multi-objective design optimization of functionally graded material for the femoral component of a total knee replacement.* Materials & Design, 2014. **53**: p. 159-173.

30. Campoli, G., et al., *Mechanical properties of open-cell metallic biomaterials manufactured using additive manufacturing.* Materials & Design, 2013. **49**: p. 957-965.

31. Shin, K.H., et al., *A method for the design and fabrication of heterogeneous objects.* Materials & Design, 2003. **24**(5): p. 339-353.

32. Ma, P.X., *Scaffolds for tissue fabrication.* Materials Today, 2004. **7**(5): p. 30-40.

33. O'Brien, F.J., *Biomaterials & scaffolds for tissue engineering.* Materials Today, 2011. **14**(3): p. 88-95.

34. Keane, T.J. and S.F. Badylak, *Biomaterials for tissue engineering applications.* Semin Pediatr Surg, 2014. **23**(3): p. 112-8.

35. Scott, J.E., *Extracellular matrix, supramolecular organisation and shape.* J Anat, 1995. **187 (Pt 2)**: p. 259-69.

36. Nelson, C.M. and M.J. Bissell, *Of extracellular matrix, scaffolds, and signaling: tissue architecture regulates development, homeostasis, and cancer.* Annu Rev Cell Dev Biol, 2006. **22**: p. 287-309.

37. Tran Le Bao, H., et al., *Naturally Derived Biomaterials: Preparation and Application*, 2013.

38.   Dubruel, P., et al., *Porous gelatin hydrogels: 2. In vitro cell interaction study.* Biomacromolecules, 2007. **8**(2): p. 338-44.

39.   Van Vlierberghe, S., S.K. Samal, and P. Dubruel, *Development of Mechanically Tailored Gelatin-Chondroitin Sulphate Hydrogel Films.* Advanced Polymers in Medicine, 2011. **309-310**: p. 173-181.

40.   Mogosanu, D.E., et al., *Polyester Biomaterials for Regenerative Medicine*, 2014, Bentham Science: Frontiers in Biomaterials: The Design, Synthetic Strategies and Biocompatibility of Polymer Scaffolds for Biomedical Application. p. 155-197 (43).

41.   Kazemnejad, S., *Hepatic tissue engineering using scaffolds: state of the art.* Avicenna J Med Biotechnol, 2009. **1**(3): p. 135-45.

42.   Lee, J.W., et al., *Development of a 3D cell printed construct considering angiogenesis for liver tissue engineering.* Biofabrication, 2016. **8**(1): p. 015007.

43.   Cama, G., et al., *Synthetic biodegradable medical polyesters: Poly-ε-caprolactone*, in *Science and Principles of Biodegradable and Bioresorbable Medical Polymers*, Z. Xiang, Editor 2016, Woodhead Publishing. p. 476.

44.   Van Natta, F.J., J.W. Hill, and W.H. Carruthers, *Polymerization and ring formation, ε- caprolactone and its polymers.* J Am Chem Soc, 1934(56): p. 455-9.

45.   Chandra, R. and R. Rustgi, *Biodegradable polymers.* Progress in Polymer Science, 1998. **23**(7): p. 1273-1335.

46.   Hedrick, J.L., et al., *Application of complex macromolecular architectures for advanced microelectronic materials.* Chemistry-a European Journal, 2002. **8**(15): p. 3308-3319.

47.   Sinha, V.R., et al., *Poly-epsilon-caprolactone microspheres and nanospheres: an overview.* International Journal of Pharmaceutics, 2004. **278**(1): p. 1-23.

48.   Woodruff, M.A. and D.W. Hutmacher, *The return of a forgotten polymer-Polycaprolactone in the 21st century.* Progress in Polymer Science, 2010. **35**(10): p. 1217-1256.

49.   Makadia, H.K. and S.J. Siegel, *Poly Lactic-co-Glycolic Acid (PLGA) as Biodegradable Controlled Drug Delivery Carrier.* Polymers, 2011. **3**(3): p. 1377-1397.

50.   Nair, L.S. and C.T. Laurencin, *Biodegradable polymers as biomaterials.* Progress in Polymer Science, 2007. **32**(8-9): p. 762-798.

51.   Chen, Q.Z., S.L. Liang, and G.A. Thouas, *Elastomeric biomaterials for tissue engineering.* Progress in Polymer Science, 2013. **38**(3-4): p. 584-671.

52.   Mizumoto, H. and K. Funatsu, *Liver regeneration using a hybrid artificial liver support system.* Artificial Organs, 2004. **28**(1): p. 53-57.

53.   Ijima, H., et al., *Hepatocyte spheroids in polyurethane foams: Functional analysis and application for a hybrid artificial liver.* Tissue Engineering, 1998. **4**(2): p. 213-226.

54.   Anderson, J.M., et al., *Recent advances in biomedical polyurethane biostability and biodegradation.* Polymer International, 1998. **46**(3): p. 163-171.

55.   Bruggeman, J.P., et al., *Biodegradable poly(polyol sebacate) polymers.* Biomaterials, 2008. **29**(36): p. 4726-4735.

56.   Rai, R., et al., *Synthesis, properties and biomedical applications of poly(glycerol sebacate) (PGS): A review.* Progress in Polymer Science, 2012. **37**(8): p. 1051-1078.

57.   Park, H., et al., *The significance of pore microarchitecture in a multi-layered elastomeric scaffold for contractile cardiac muscle constructs.* Biomaterials, 2011. **32**(7): p. 1856-1864.

58.   Ravichandran, R., et al., *Minimally invasive injectable short nanofibers of poly(glycerol sebacate) for cardiac tissue engineering.* Nanotechnology, 2012. **23**(38): p. 385102.

59.   Stabenfeldt, S.E., A.J. Garcia, and M.C. LaPlaca, *Thermoreversible laminin-functionalized hydrogel for neural tissue engineering.* Journal of Biomedical Materials Research Part A, 2006(77): p. 718-725.

60.   Kemppainen, J.M. and S.J. Hollister, *Tailoring the mechanical properties of 3D-designed poly(glycerol sebacate) scaffolds for*

cartilage applications. Journal of Biomedical Materials Research Part A, 2010. **94**(1): p. 9-18.

61. Pritchard, C.D., et al., *The use of surface modified poly(glycerol-co-sebacic acid) in retinal transplantation.* Biomaterials, 2010. **31**(8): p. 2153-2162.

62. Barrett, D.G. and M.N. Yousaf, *Design and Applications of Biodegradable Polyester Tissue Scaffolds Based on Endogenous Monomers Found in Human Metabolism.* Molecules, 2009. **14**(10): p. 4022-4050.

63. Pomerantseva, I., et al., *Degradation behavior of poly(glycerol sebacate).* Journal of Biomedical Materials Research Part A, 2009. **91A**(4): p. 1038-1047.

64. Barrett, D.G. and M.N. Yousaf, *Thermosets synthesized by thermal polyesterification for tissue engineering applications.* Soft Matter, 2010. **6**(20): p. 5026-5036.

65. Liu, Q.Y., et al., *Study on the control of the compositions and properties of a biodegradable polyester elastomer.* Biomedical Materials, 2009. **4**(2).

66. Wu, Y., et al., *Nanosilica Filled Poly(glycerol-sebacate-citrate) Elastomers with Improved Mechanical Properties, Adjustable Degradability, and Better Biocompatibility.* Journal of Applied Polymer Science, 2012. **123**(3): p. 1612-1620.

67. Sant, S., et al., *Hybrid PGS-PCL microfibrous scaffolds with improved mechanical and biological properties.* Journal of Tissue Engineering and Regenerative Medicine, 2011. **5**(4): p. 283-291.

68. Cheng, S.J., L.J. Yang, and F.R. Gong, *Novel branched poly(l-lactide) with poly(glycerol-co-sebacate) core.* Polymer Bulletin, 2010. **65**(7): p. 643-655.

69. Barbosa, J.N., M.A. Barbosa, and A.P. Aguas, *Adhesion of human leukocytes to biomaterials: An in vitro study using alkanethiolate monolayers with different chemically functionalized surfaces.* Journal of Biomedical Materials Research Part A, 2003. **65A**(4): p. 429-434.

70.   Barbosa, J.N., M.A. Barbosa, and A.P. Aguas, *Inflammatory responses and cell adhesion to self-assembled monolayers of alkanethiolates on gold.* Biomaterials, 2004. **25**(13): p. 2557-2563.

71.   Marois, Y., M.F. Sigot-Luizard, and R. Guidoin, *Endothelial cell behavior on vascular prosthetic grafts: Effect of polymer chemistry, surface structure, and surface treatment.* Asaio Journal, 1999. **45**(4): p. 272-280.

72.   Wilhelm, L., et al., *Immune response against polyester implants is influenced by the coating substances.* Journal of Biomedical Materials Research Part A, 2007. **83A**(1): p. 104-113.

73.   Cunha, A.G., et al., *Immobilization of Yarrowia lipolytica lipase-a comparison of stability of physical adsorption and covalent attachment techniques.* Applied Biochemistry and Biotechnology, 2008. **146**(1-3): p. 49-56.

74.   Thommes, M. and K.A. Cychosz, *Physical adsorption characterization of nanoporous materials: progress and challenges.* Adsorption-Journal of the International Adsorption Society, 2014. **20**(2-3): p. 233-250.

75.   Giol, E.D., et al., *Bio-inspired surface modification of PET for cardiovascular applications: case study of gelatin.* Colloids and Surfaces B: Biointerfaces, (0).

76.   Kim, H., M.J. Cooke, and M.S. Shoichet, *Creating permissive microenvironments for stem cell transplantation into the central nervous system.* Trends in Biotechnology, 2012. **30**(1): p. 55-63.

77.   Goddard, J.M. and J.H. Hotchkiss, *Polymer surface modification for the attachment of bioactive compounds.* Progress in Polymer Science, 2007. **32**(7): p. 698-725.

78.   Pachence, J.M., *Biodegradable polymers*. Principles of Tissue Engineering2000: Academic Press: Burlington.

79.   Nair, L.S. and C.T. Laurencin, *Polymers as biomaterials for tissue engineering and controlled drug delivery*. Tissue Engineering I: Scaffold Systems for Tissue Engineering, 2006. **102**: p. 47-90.

80.   Yang, J., et al., *Synthesis and evaluation of poly(diol citrate) biodegradable elastomers.* Biomaterials, 2006. **27**(9): p. 1889-1898.

81. Ji, Y.L., et al., *Mussel-inspired soft-tissue adhesive based on poly(diol citrate) with catechol functionality.* Journal of Materials Science-Materials in Medicine, 2016. **27**(2).

82. Arpornwichanop, T., N. Kanjanathaworn, and P. Tangboriboonrat, *Surface Modification of Natural Rubber Film with PMMA Nanoparticles Stabilized by Chitosan or Its Derivative.* Materials Research and Applications, Pts 1-3, 2014. **875-877**: p. 59-62.

83. Yoshimura, S., et al., *Sputtering yields and surface modification of poly(methyl methacrylate) (PMMA) by low-energy Ar+/CF3+ ion bombardment with vacuum ultraviolet (VUV) photon irradiation.* Journal of Physics D-Applied Physics, 2012. **45**(50).

84. Grassini, S., et al., *Surface modification plasma treatments of PMMA optical fibres for sensing applications.* Surface and Interface Analysis, 2012. **44**(8): p. 1068-1071.

85. Nam, C.H.L., et al., *Ultrathin and smooth poly(methyl methacrylate) (PMMA) films for label-free biomolecule detection with total internal reflection ellipsometry (TIRE).* Biosensors & Bioelectronics, 2012. **36**(1): p. 250-256.

86. Bae, W.J., et al., *Comparison of Biocompatibility between Pdms and Pmma as Packaging Materials for the Intravesical Implantable Device: Changes of Macrophage and Macrophage Migratory Inhibitory Factor.* International Journal of Urology, 2014. **21**: p. A284-A284.

87. Ferreira, L.M.C., et al., *Miniaturized flow system based on enzyme modified PMMA microreactor for amperometric determination of glucose.* Biosensors & Bioelectronics, 2013. **47**: p. 539-544.

88. Szaloki, M., et al., *Binding of leachable components of polymethyl methacrylate (PMMA) and peptide on modified SPR chip.* 2nd International Conference on Competitive Materials and Technological Processes (Ic-Cmtp2), 2013. **47**.

89. Prasad, G., et al., *Facile preparation of Chaetomorpha antennina based porous polysaccharide-PMMA hybrid material by radical polymerization under microwave irradiation.* Journal of Materials Science, 2009. **44**(15): p. 4062-4068.

90.   Wang, H.X., et al., *Microfluidic immunosensor based on stable antibody-patterned surface in PMMA microchip.* Electrochemistry Communications, 2008. **10**(3): p. 447-450.

91.   Boulares-Pender, A., et al., *Surface-Functionalization of Plasma-Treated Polystyrene by Hyperbranched Polymers and Use in Biological Applications.* Journal of Applied Polymer Science, 2009. **112**(5): p. 2701-2709.

92.   Nahar, P., A. Naqvi, and S.F. Basir, *Sunlight-mediated activation of an inert polymer surface for covalent immobilization of a protein.* Analytical Biochemistry, 2004. **327**(2): p. 162-164.

93.   Chen, Y., et al., *Biocidal polystyrene beads. IV. Functionalized methylated polystyrene.* Journal of Applied Polymer Science, 2004. **92**(1): p. 368-372.

94.   Holmberg, K., et al., *Effects on Protein Adsorption, Bacterial Adhesion and Contact-Angle of Grafting Peg Chains to Polystyrene.* Journal of Adhesion Science and Technology, 1993. **7**(6): p. 503-517.

95.   Glodek, J., et al., *Derivatization of fluorinated polymers and their potential use for the construction of biosensors.* Sensors and Actuators B-Chemical, 2002. **83**(1-3): p. 82-89.

96.   Prissanaroon, W., et al., *Fabrication of patterned polypyrrole on fluoropolymers for pH sensing applications.* Synthetic Metals, 2005. **154**(1-3): p. 105-108.

97.   Kang, E.T., et al., *Surface modification and functionalization of polytetrafluoroethylene films via graft copolymerization.* Polymers for Advanced Technologies, 1997. **8**(11): p. 683-692.

98.   Li, J.M., et al., *Immobilization of human thrombomodulin to expanded polytetrafluoroethylene.* J Surg Res, 2002. **105**(2): p. 200-8.

99.   Kang, E.T., et al., *Surface modification and functionalization of polytetrafluoroethylene films.* Macromolecules, 1996. **29**(21): p. 6872-6879.

100.   http://www.goodfellow.com.

101. Ravindranath, K. and R.A. Mashelkar, *Polyethylene Terephthalate .1. Chemistry, Thermodynamics and Transport-Properties.* Chemical Engineering Science, 1986. **41**(9): p. 2197-2214.

102. Khodakov, D.A., et al., *Surface modification of poly(dimethylsiloxane) (PDMS) microchannels with DNA capture-probes for potential use in microfluidic DNA analysis systems.* Smart Nano-Micro Materials and Devices, 2011. **8204**.

103. Makamba, H., et al., *Surface modification of poly(dimethylsiloxane) microchannels.* Electrophoresis, 2003. **24**(21): p. 3607-3619.

104. Tan, F., et al., *A PDMS microfluidic impedance immunosensor for E. coli O157:H7 and Staphylococcus aureus detection via antibody-immobilized nanoporous membrane.* Sensors and Actuators B-Chemical, 2011. **159**(1): p. 328-335.

105. Ishimoto, T., et al., *Efficient immobilization of the enzyme and substrate for a single-step caspase-3 inhibitor assay using a combinable PDMS capillary sensor array.* Rsc Advances, 2014. **4**(15): p. 7682-7687.

106. Duan, Y., et al., *Preparation of collagen-coated electrospun nanofibers by remote plasma treatment and their biological properties.* Journal of Biomaterials Science-Polymer Edition, 2007. **18**(9): p. 1153-1164.

107. Morent, R., et al., *Plasma Surface Modification of Biodegradable Polymers: A Review.* Plasma Processes and Polymers, 2011. **8**(3): p. 171-190.

108. Klomp, A.J.A., et al., *Adsorption of proteins from plasma at polyester non-wovens.* Biomaterials, 1999. **20**(13): p. 1203-1211.

109. Desmet, T., et al., *Post-Plasma Grafting of AEMA as a Versatile Tool to Biofunctionalise Polyesters for Tissue Engineering.* Macromolecular Bioscience, 2010. **10**(12): p. 1484-1494.

110. Haubert, K., T. Drier, and D. Beebe, *PDMS bonding by means of a portable, low-cost corona system.* Lab on a Chip, 2006. **6**(12): p. 1548-1549.

111.   Xu, L., et al., *Surface-initiated graft polymerization on multiwalled carbon nanotubes pretreated by corona discharge at atmospheric pressure.* Nanoscale, 2010. **2**(3): p. 389-93.

112.   Elahi, A. and D.J. Caruana, *Plasma electrochemistry: voltammetry in a flame plasma electrolyte.* Physical Chemistry Chemical Physics, 2013. **15**(4): p. 1108-14.

113.   Tuominen, M., et al., *The Effect of Flame Treatment on Surface Properties and Heat Sealability of Low-Density Polyethylene Coating.* Packaging Technology and Science, 2013. **26**(4): p. 201-214.

114.   De Cooman, H., et al., *Role of Radicals in UV-Initiated Postplasma Grafting of Poly-epsilon-caprolactone: An Electron Paramagnetic Resonance Study.* Journal of Polymer Science Part a-Polymer Chemistry, 2012. **50**(11): p. 2142-2149.

115.   Delplanque, A., et al., *UV/ozone surface treatment increases hydrophilicity and enhances functionality of SU-8 photoresist polymer.* Applied Surface Science, 2014. **314**: p. 280-285.

116.   Yan, L., W.T.S. Huck, and G.M. Whitesides, *Self-assembled monolayers (SAMS) and synthesis of planar micro- and nanostructures.* Journal of Macromolecular Science-Polymer Reviews, 2004. **C44**(2): p. 175-206.

117.   Whitesides, G.M. and P.E. Laibinis, *Wet Chemical Approaches to the Characterization of Organic-Surfaces - Self-Assembled Monolayers, Wetting, and the Physical Organic-Chemistry of the Solid Liquid Interface.* Langmuir, 1990. **6**(1): p. 87-96.

118.   Saha, K., et al., *Designing synthetic materials to control stem cell phenotype.* Current Opinion in Chemical Biology, 2007. **11**(4): p. 381-387.

119.   Hollister, S.J., *Porous scaffold design for tissue engineering.* Nature Materials, 2005. **4**(7): p. 518-524.

120.   Billiet, T., et al., *A review of trends and limitations in hydrogel-rapid prototyping for tissue engineering.* Biomaterials, 2012. **33**(26): p. 6020-6041.

121.   Desmet, T., E. Schacht, and P. Dubruel, eds. *Rapid Prototyping as an elegant Production Tool for Polymeric Tissue Engineering Scaffolds: a*

review. Tissue Engineering: Roles, Materials and applications2008, Nova Science Publishers, Inc. Chapter 7-> 141-189.

122.   Woodruff, M.A. and D.W. Hutmacher, *The return of a forgotten polymer—Polycaprolactone in the 21st century.* Progress in polymer science, 2010. **35**(10): p. 1217-1256.

123.   Cipitria, A., et al., *Design, fabrication and characterization of PCL electrospun scaffolds—a review.* Journal of Materials Chemistry, 2011. **21**(26): p. 9419-9453.

124.   Sachlos, E. and J. Czernuszka, *Making tissue engineering scaffolds work. Review: the application of solid freeform fabrication technology to the production of tissue engineering scaffolds.* Eur Cell Mater, 2003. **5**(29): p. 39-40.

125.   Holmes, B., et al., *A synergistic approach to the design, fabrication and evaluation of 3D printed micro and nano featured scaffolds for vascularized bone tissue repair.* Nanotechnology, 2016. **27**(6).

126.   Zein, I., et al., *Fused deposition modeling of novel scaffold architectures for tissue engineering applications.* Biomaterials, 2002. **23**(4): p. 1169-1185.

127.   Verhulsel, M., et al., *A review of microfabrication and hydrogel engineering for micro-organs on chips.* Biomaterials, 2014. **35**(6): p. 1816-32.

128.   Potyrailo, R.A. and W.G. Morris, *Parallel high-throughput microanalysis of materials using microfabricated full bridge device arrays.* Applied Physics Letters, 2004. **84**(4): p. 634-636.

129.   Wang, Z., et al., *Nanochannel system fabricated by MEMS microfabrication and atomic force microscopy.* IET Nanobiotechnol, 2011. **5**(4): p. 108-13.

130.   Zorlutuna, P., et al., *Microfabricated Biomaterials for Engineering 3D Tissues.* Advanced Materials, 2012. **24**(14): p. 1782-1804.

131.   Voldman, J., M.L. Gray, and M.A. Schmidt, *Microfabrication in biology and medicine.* Annual Review of Biomedical Engineering, Vol 14, 1999. **1**: p. 401-25.

132.   Wolfe, D.B. and G.M. Whitesides, *3 - Rapid prototyping of functional microfabricated devices by soft lithography*, in *Nanolithography and*

Patterning Techniques in Microelectronics, D.G. Bucknall, Editor 2005, Woodhead Publishing. p. 76-119.

133. Xu, B., et al., *Fabrication of 3D metal micro-mold based on femtosecond laser cutting and micro-electric resistance slip welding.* International Journal of Advanced Manufacturing Technology, 2013. **66**(5-8): p. 601-609.

134. Naohite, T., F. Hiroshi, and N. Kazuya, *Polymers for Artificial Joints*, in *Polymeric Biomaterials*, D. Severian, Editor 2002, Marcel Dekker Inc.: Quebec, Canada.

135. Zhang, M.Y., et al., *Microfluidic environment for high density hepatocyte culture.* Biomedical Microdevices, 2008. **10**(1): p. 117-121.

136. Neeley, W.L., et al., *A microfabricated scaffold for retinal progenitor cell grafting.* Biomaterials, 2008. **29**(4): p. 418-426.

137. van Midwoud, P.M., et al., *Comparison of Biocompatibility and Adsorption Properties of Different Plastics for Advanced Microfluidic Cell and Tissue Culture Models.* Anal Chem, 2012. **84**(9): p. 3938-3944.

138. Kaihara, S., et al., *Silicon micromachining to tissue engineer branched vascular channels for liver fabrication.* Tissue Engineering, 2000. **6**(2): p. 105-117.

139. Wang, J., et al., *Biodegradable microfluidic scaffolds for tissue engineering from amino alcohol-based poly(ester amide) elastomers.* Organogenesis, 2010. **6**(4): p. 212-216.

140. Lee, S.J. and N. Sundararajan, *Microfabrication for microfluidics*. Integrated microsystems series2010, Boston: Artech House. xii, 262 p.

141. Gauvin, R., et al., *Microfabrication of complex porous tissue engineering scaffolds using 3D projection stereolithography.* Biomaterials, 2012. **33**(15): p. 3824-3834.

142. Nerem, R.M. and A. Sambanis, *Tissue engineering: from biology to biological substitutes.* Tissue Eng, 1995. **1**(1): p. 3-13.

143. Catapano, G., J.F. Patzer, 2nd, and J.C. Gerlach, *Transport advances in disposable bioreactors for liver tissue engineering.* Adv Biochem Eng Biotechnol, 2009. **115**: p. 117-43.

144. Shatford, R.A., et al., *Hepatocyte function in a hollow fiber bioreactor: a potential bioartificial liver.* J Surg Res, 1992. **53**(6): p. 549-57.

145. Gupta, S., H. Malhi, and G.R. Gorla, *Re-Engineering the liver with natural biomaterials.* Yonsei Med J, 2000. **41**(6): p. 814-24.

146. Fiegel, H.C., et al., *Hepatic tissue engineering: from transplantation to customized cell-based liver directed therapies from the laboratory.* Journal of Cellular and Molecular Medicine, 2008. **12**(1): p. 56-66.

147. Bhandari, R.N., et al., *Liver tissue engineering: a role for co-culture systems in modifying hepatocyte function and viability.* Tissue Eng, 2001. **7**(3): p. 345-57.

148. Mizuguchi, T., et al., *Enhanced proliferation and differentiation of rat hepatocytes cultured with bone marrow stromal cells.* Journal of Cellular Physiology, 2001. **189**(1): p. 106-19.

149. Booth, C., et al., *Liver bioengineering: current status and future perspectives.* World J Gastroenterol, 2012. **18**(47): p. 6926-34.

150. Alison, M.R., et al., *Hepatocytes from non-hepatic adult stem cells.* Nature, 2000. **406**(6793): p. 257.

151. Mohamadnejad, M., et al., *Phase 1 human trial of autologous bone marrow-hematopoietic stem cell transplantation in patients with decompensated cirrhosis.* World J Gastroenterol, 2007. **13**(24): p. 3359-63.

152. Pang, Y., et al., *Liver tissue engineering based on aggregate assembly: efficient formation of endothelialized rat hepatocyte aggregates and their immobilization with biodegradable fibres.* Biofabrication, 2012. **4**(4): p. 045004.

153. Demetris, A.J., et al., *Reliability and Predictive Value of the National-Institute-of-Diabetes-and-Digestive-and-Kidney-Diseases Liver-Transplantation Database Nomenclature and Grading System for Cellular Rejection of Liver Allografts.* Hepatology, 1995. **21**(2): p. 408-416.

154. Mitaka, T., et al., *Growth and maturation of small hepatocytes.* J Gastroenterol Hepatol, 1998. **13 Suppl**: p. S70-7.

155. Kazemnejad, S., *Hepatic Tissue Engineering Using Scaffolds: State of the Art.* Avicenna Journal of Medical Biotechnology, 2009. **1**(3): p. 135-145.

156. Navarro, L., et al., *Poly(polyol sebacate) Elastomers as Coatings for Metallic Coronary Stents.* Macromol Biosci, 2016.

157. Yamanaka, N., et al., *Dynamics of Normal and Injured Human Liver-Regeneration after Hepatectomy as Assessed on the Basis of Computed-Tomography and Liver-Function.* Hepatology, 1993. **18**(1): p. 79-85.

158. Bettinger, C.J., *Synthesis and microfabrication of biomaterials for soft-tissue engineering.* Pure and Applied Chemistry, 2009. **81**(12): p. 2183-2201.

159. Albertsson, A.C. and O. Ljungquist, *Degradable Polyesters as Biomaterials.* Acta Polymerica, 1988. **39**(1-2): p. 95-104.

160. Perez-Castillejos, R., *Replication of the 3D architecture of tissues.* Materials Today, 2010. **13**(1-2): p. 32-41.

161. Chen, Q.Z., et al., *An elastomeric patch derived from poly(glycerol sebacate) for delivery of embryonic stem cells to the heart.* Biomaterials, 2010. **31**(14): p. 3885-3893.

162. Gerecht, S., et al., *A porous photocurable elastomer for cell encapsulation and culture.* Biomaterials, 2007. **28**(32): p. 4826-4835.

163. Ifkovits, J.L., R.F. Padera, and J.A. Burdick, *Biodegradable and radically polymerized elastomers with enhanced processing capabilities.* Biomedical Materials, 2008. **3**(3).

164. Jaafar, I.H., et al., *Spectroscopic evaluation, thermal, and thermomechanical characterization of poly(glycerol-sebacate) with variations in curing temperatures and durations.* Journal of Materials Science, 2010. **45**(9): p. 2525-2529.

165. Kemppainen, J.M. and S.J. Hollister, *Tailoring the mechanical properties of 3D-designed poly(glycerol sebacate) scaffolds for cartilage applications.* Journal of Biomedical Materials Research Part A, 2010. **94A**(1): p. 9-18.

166. Liu, L.L., F.C. Yi, and W. Cai, *Synthesis and Shape Memory Effect of Poly (glycerol-sebacate) Elastomer.* New Materials and Processes, Pts 1-3, 2012. **476-478**: p. 2141-2144.

167. Liu, Q.Y., et al., *Preparation and characterization of a thermoplastic poly(glycerol sebacate) elastomer by two-step method.* Journal of Applied Polymer Science, 2007. **103**(3): p. 1412-1419.

168. You, Z.W., et al., *A functionalizable polyester with free hydroxyl groups and tunable physiochemical and biological properties.* Biomaterials, 2010. **31**(12): p. 3129-3138.

169. Hoogenboom, R., et al., *Microwave-assisted controlled radical polymerizations.* Abstracts of Papers of the American Chemical Society, 2005. **230**: p. U4238-U4239.

170. Hoogenboom, R. and U.S. Schubert, *Microwave-assisted cationic ring-opening polymerization of a soy-based 2-oxazoline monomer.* Green Chemistry, 2006. **8**(10): p. 895-899.

171. Nakamura, T., R. Nagahata, and K. Takeuchi, *Microwave-Assisted Polyester and Polyamide Synthesis.* Mini-Reviews in Organic Chemistry, 2011. **8**(3): p. 306-314.

172. Kersemans, K., et al., *Radiolabeled gelatin type B analogues can be used for non-invasive visualisation and quantification of protein coatings on 3D porous implants.* Journal of Materials Science-Materials in Medicine, 2012. **23**(8): p. 1961-1969.

173. Desmet, T., et al., *Double protein functionalized poly-epsilon-caprolactone surfaces: in depth ToF-SIMS and XPS characterization.* J Mater Sci Mater Med, 2012. **23**(2): p. 293-305.

174. Cheng, Z.Y. and S.H. Teoh, *Surface modification of ultra thin poly (epsilon-caprolactone) films using acrylic acid and collagen.* Biomaterials, 2004. **25**(11): p. 1991-2001.

175. Suzuki, M., et al., *Graft-Copolymerization of Acrylamide onto a Polyethylene Surface Pretreated with a Glow-Discharge.* Macromolecules, 1986. **19**(7): p. 1804-1808.

176. *Standar specification for chemical passivation treatments for stainless steel parts.* An American National Standar. ASTM International, 2001.

177.   Rohan, M. *1,3-Propanediol (PDO) Market by Applications (PTT, Polyurethane, Cosmetic, Personal Care & Home Cleaning & Others) & Geography - Global Market Trends & Forecasts to 2021*. 2015; Available from: http://www.marketsandmarkets.com/PressReleases/1-3-propanediol-pdo.asp.

178.   Helle, J., et al., *Development and applications of injectable poly(ortho esters) for pain control and periodontal treatment.* Biomaterials, 2002. **23**(22): p. 4397-404.

179.   *Ullmann's Fine Chemicals*, Wiley-VCH, Editor 2014. p. 1360.

180.   Hoogenboom, R. and U.S. Schubert, *Microwave-assisted polymer synthesis: Recent developments in a rapidly expanding field of research.* Macromolecular Rapid Communications, 2007. **28**(4): p. 368-386.

181.   Aydin, H.M., et al., *Microwave-assisted rapid synthesis of poly(glycerol-sebacate) elastomers.* Biomaterials Science, 2013. **1**(5): p. 503-509.

182.   Velmathi, S., et al., *A rapid eco-friendly synthesis of poly(butylene succinate) by a direct polyesterification under microwave irradiation.* Macromolecular Rapid Communications, 2005. **26**(14): p. 1163-1167.

183.   Li, Y., et al., *Synthesis, characterization and properties of biocompatible poly(glycerol sebacate) pre-polymer and gel.* Polymer International, 2013. **62**(4): p. 534-547.

184.   Mitsak, A.G., A.M. Dunn, and S.J. Hollister, *Mechanical characterization and non-linear elastic modeling of poly(glycerol sebacate) for soft tissue engineering.* Journal of the Mechanical Behavior of Biomedical Materials, 2012. **11**: p. 3-15.

185.   Cerruti, M., *Surface characterization of silicate bioceramics.* Philos Trans A Math Phys Eng Sci, 2012. **370**(1963): p. 1281-312.

186.   Rai, R., et al., *Biomimetic poly(glycerol sebacate) (PGS) membranes for cardiac patch application.* Materials Science & Engineering C-Materials for Biological Applications, 2013. **33**(7): p. 3677-3687.

187.   Kim, M.J., et al., *Biodegradable and Elastomeric Poly(glycerol sebacate) as a Coating Material for Nitinol Bare Stent.* Biomed Res Int, 2014.

188.   Patel, A., et al., *Highly elastomeric poly(glycerol sebacate)-co-poly(ethylene glycol) amphiphilic block copolymers.* Biomaterials, 2013. **34**(16): p. 3970-83.

189.   Patel, A., et al., *Highly elastomeric poly(glycerol sebacate)-co-poly(ethylene glycol) amphiphilic block copolymers.* Biomaterials, 2013. **34**(16): p. 3970-3983.

190.   Liang, S.L., et al., *The mechanical characteristics and in vitro biocompatibility of poly(glycerol sebacate)-Bioglass (R) elastomeric composites.* Biomaterials, 2010. **31**(33): p. 8516-8529.

191.   Cai, W. and L.L. Liu, *Shape-memory effect of poly (glycerol-sebacate) elastomer.* Materials Letters, 2008. **62**(14): p. 2171-2173.

192.   Bongaerts, J.H.H., K. Fourtouni, and J.R. Stokes, *Soft-tribology: Lubrication in a compliant PDMS-PDMS contact.* Tribology International, 2007. **40**(10-12): p. 1531-1542.

193.   Van Vlierberghe, S., et al., *Gelatin Functionalization of Biomaterial Surfaces: Strategies for Immobilization and Visualization.* Polymers, 2011. **3**(1): p. 114-130.

194.   Zhu, Y.B., et al., *Endothelium regeneration on luminal surface of polyurethane vascular scaffold modified with diamine and covalently grafted with gelatin.* Biomaterials, 2004. **25**(3): p. 423-430.

195.   Stendahl, J.C., et al., *Modification of fibrous poly(L-lactic acid) scaffolds with self-assembling triblock molecules.* Biomaterials, 2004. **25**(27): p. 5847-5856.

196.   Yuan, W., et al., *Thermo-responsive gelatin-functionalized PCL film surfaces for improvement of cell adhesion and intelligent recovery of gene-transfected cells.* Science China-Chemistry, 2014. **57**(4): p. 586-595.

197.   Weng, Y.J., et al., *Surface engineering of Ti-O films by photochemical immobilization of gelatin.* Materials Science & Engineering C-Biomimetic and Supramolecular Systems, 2008. **28**(8): p. 1495-1500.

198. Declercq, H.A., et al., *Synergistic effect of surface modification and scaffold design of bioplotted 3-D poly-epsilon-caprolactone scaffolds in osteogenic tissue engineering.* Acta Biomaterialia, 2013. **9**(8): p. 7699-7708.

199. Sales, V.L., et al., *Protein precoating of elastomeric tissue-engineering scaffolds increased cellularity, enhanced extracellular matrix protein production, and differentially regulated the phenotypes of circulating endothelial progenitor cells.* Circulation, 2007. **116**(11): p. I55-I63.

200. Baquey, C., et al., *Plasma treatment of expanded PTFE offers a way to a biofunctionalization of its surface.* Nuclear Instruments & Methods in Physics Research Section B-Beam Interactions with Materials and Atoms, 1999. **151**(1-4): p. 255-262.

201. Prystupa, D.A. and A.M. Donald, *Infrared study of gelatin conformations in the gel and sol states.* Polymer Gels and Networks, 1996. **4**(2): p. 87-110.

202. Organization, W.H. *The global burden of disease: 2004 update.* WHO Press 2008; Available from: http://www.who.int.

203. Virmani, R. and A. Farb, *Pathology of in-stent restenosis.* Current Opinion in Lipidology, 1999. **10**(6): p. 499-506.

204. Miller, J.M., et al., *Restenosis the clinical issues*. 3rd ed. Textbook of Interventional Cardiology 1999, Philadelphia: E.J. Topol.

205. Holmes, D.R., et al., *Stent thrombosis.* Journal of the American College of Cardiology, 2010. **56**(17): p. 1357-1365.

206. Serruys, P.W. and A.H. Gershlick, *Handbook of drug-eluting stents*2005, London, UK: Taylor & Francis Routledge.

207. Finn, A.V., et al., *Pathological correlates of late drug-eluting stent thrombosis: strut coverage as a marker of endothelialization.* Journal of the American Heart Association, 2007. **115**(18): p. 2435-2441.

208. Jaffe, R. and B.H. Strauss, *Late and Very Late Thrombosis of Drug-Eluting Stents:: Evolving Concepts and Perspectives.* Journal of the American College of Cardiology, 2007. **50**(2): p. 119-127.

209. Jakab in, J., et al., *The lack of endothelization after drug-eluting stent implantation as a cause of fatal late stent thrombosis.* Journal of thrombosis and thrombolysis, 2008. **26**(2): p. 154-158.

210. Goldberg, L.R. and M. Jessup, *Stage B Heart Failure* Circulation, 2006. **113**: p. 2851-2860.

211. Sojitra, P., et al., *Electropolishing of 316LVM stainless steel cardiovascular stents: an Investigation of material removal, surface roughness and corrosion behaviour.* Trends Biomater. Artif. Organs, 2010. **23**(3): p. 115-121.

212. Okazaki, Y. and E. Gotoh, *Metal release from stainless steel, Co–Cr–Mo–Ni–Fe and Ni–Ti alloys in vascular implants.* Corrosion science, 2008. **50**: p. 3429-3438.

213. Tomizawa, Y., et al., *Corrosion of stainless sternal wire after long-term implantation.* Journal of Artificial Organs, 2006. **9**(1): p. 61-66.

214. Dina O. Halwani, et al., *In-vivo Corrosion and Local Release of Metallic Ions from Vascular Stents into Surrounding Tissue.* Invasive Cardiology, 2010. **22**(11): p. 528-535.

215. Scheinert, D., et al., *Prevalence and clinical impact of stent fractures after femoropopliteal stenting.* Journal of the American College of Cardiology, 2005. **45**(2): p. 312-315.

216. Manivasagam, G., D. Dhinasekaran, and A. Rajamanickam, *Biomedical Implants: Corrosion and its Prevention-A Review.* Recent Patents on Corrosion Science, 2010. **2**: p. 40-54.

217. Shih, C.-C., et al., *Increased corrosion resistance of stent materials by converting current surface film of polycrystalline oxide into amorphous oxide.* Journal of biomedical materials research, 2000. **52**(2): p. 323-332.

218. Anderson, J.M. and M.S. Shive, *Biodegradation and biocompatibility of PLA and PLGA microspheres.* Advanced Drug Delivery Reviews, 1997. **28**(1): p. 5-24

219. Xi, T., et al., *In vitro and in vivo changes to PLGA/sirolimus coating on drug eluting stents.* Biomaterials, 2010. **31**(19): p. 5151e5158.

220.   Acharya, G., C.H. Lee, and Y. Lee, *Optimization of cardiovascular stent against restenosis: factorial design-based statistical analysis of polymer coating conditions.* Plos One, 2012. **7**(8): p. e43100.

221.   Lerouge, S., et al., *Nitrogen-rich coatings for promoting healing around stent-grafts after endovascular aneurysm repair.* Biomaterials, 2007. **28**(6): p. 1209-1217.

222.   Kang, E., et al., *Paclitaxel distribution in poly(ethylene glycol)/poly(lactide-co-glycolic acid) blends and its release visualized by coherent anti-Stokes Raman scattering microscopy.* Journal of Controlled Release, 2007. **122**(3): p. 261-268.

223.   Sundback, C.A., et al., *Biocompatibility analysis of poly (glycerol sebacate) as a nerve guide material.* Biomaterials, 2005. **26**(27): p. 5454-5464.

224.   Fidkowski, C., et al., *Endothelialized microvasculature based on a biodegradable elastomer.* Tissue Engineering, 2005. **11**(1-2): p. 302-309.

225.   Motlagh, D., et al., *Hemocompatibility evaluation of poly (glycerol-sebacate) in vitro for vascular tissue engineering.* Biomaterials, 2006. **27**(24): p. 4315-4324.

226.   Byrne, R.A., et al., *A polymer-free dual drug-eluting stent in patients with coronary artery disease: a randomized trial vs. polymer-based drug-eluting stents.* European Heart Journal, 2009. **30**(8): p. 923–931.

227.   Lamichhane, S., A. Gallo, and G. Mani, *A Polymer-Free Paclitaxel Eluting Coronary Stent: Effects of Solvents, Drug Concentrations and Coating Methods.* Annals of biomedical engineering, 2014. **42**(6): p. 1170-1184.

228.   Butruk-Raszeja, B., M. Trzaskowski, and T. Ciach, *Cell membrane-mimicking coating for blood-contacting polyurethanes.* J Biomater Appl, 2014. **29**(6): p. 801-812.

229.   Zomorodian, A., et al., *Corrosion resistance of a composite polymeric coating applied on biodegradable AZ31 magnesium alloy* Acta Biomaterialia, 2013. **9**(10): p. 8660-8670.

230. Amaravathy, P., et al., *Evaluation of in vitro bioactivity and MG63 Oesteoblast cell response for TiO2 coated magnesium alloys.* Journal of Sol-Gel Science and Technology, 2012. **64**(3): p. 694-703.

231. Zhao, L., et al., *Rational design of drug-eluting stents via electrospray and in vivo evaluation of preventing oesophageal stricture.* Rsc Advances, 2014. **4**(32): p. 16885-16892.

232. Kim, D.-M., et al., *Metal Surface Coating Using Electrospray of Biodegradable Polymers and alpha-Lipoic Acid Release Behavior for Drug-Eluting Stents.* Polymer Korea, 2010. **34**(2): p. 178-183.

233. Kim, D.-M., et al., *Metal Surface Coating Using Electrospray of Biodegradable Polymers and $\ alpha $-Lipoic Acid Release Behavior for Drug-Eluting Stents.* Polymer Korea, 2010. **34**(2): p. 178-183.

234. Kim, M.J., et al., *Biodegradable and Elastomeric Poly (glycerol sebacate) as a Coating Material for Nitinol Bare Stent.* BioMed Research International, 2014. **2014**.

235. Acton, A., *Restenosis: New Insights for the Healthcare Professional: 2013 Edition*2013, Georgia Atlanta Scholarly Editions.

236. Raval, A., et al., *Novel biodegradable polymeric matrix coated cardiovascular stent for controlled drug delivery.* Trends in Biomaterials & Artificial Organs, 2007. **20**(2): p. 101-110.

237. Samuel, J.H., *Handbook of biodegradable polymers*, ed. C. Bastioli. Vol. Chapter 9. 2005: Rapra Technology Limited.

238. Yang, F., et al., *Electrospinning of nano/micro scale poly(L-lactic acid) aligned fibers and their potential in neural tissue engineering.* Biomaterials, 2005. **26**(15): p. 2603-2610.

239. Spasova, M., et al., *Preparation of PLLA/PEG Nanofibers by Electrospinning and Potential Applications.* Journal of Bioactive and Compatible Polymers, 2007. **22**: p. 62-76.

240. Garg, K. and G.L. Bowlin, *Electrospinning jets and nanofibrous structures.* Biomicrofluidics, 2011. **5**(1).

241. Sarkar, K., et al., *Electrospinning to Forcespinning (TM).* Materials Today, 2010. **13**(11): p. 12-14.

242.   Yu, J.H., S.V. Fridrikh, and G.C. Rutledge, *Production of submicrometer diameter fibers by two-fluid electrospinning.* Advanced Materials, 2004. **16**(17): p. 1562-+.

243.   Huang, Z.M., Y.Z. Zhang, and S. Ramakrishna, *Double-layered composite nanofibers and their mechanical performance.* Journal of Polymer Science Part B-Polymer Physics, 2005. **43**(20): p. 2852-2861.

244.   Elahi, F., et al., *Core-shell Fibers for Biomedical Applications-A Review.* J Bioeng Biomed Sci, 2013. **3**(1): p. 121.

245.   Doustgani, A., *Effect of electrospinning process parameters of polycaprolactone and nanohydroxyapatite nanocomposite nanofibers.* Textile Research Journal, 2015. **85**(14): p. 1445-1454.

246.   Fallahi, D., et al., *Effect of applied voltage on jet electric current and flow rate in electrospinning of polyacrylonitrile solutions.* Polymer International, 2008. **57**(12): p. 1363-1368.

247.   Mattoso, L.H.C., et al., *Effect of relative humidity on the morphology of electrospun polymer fibers.* Canadian Journal of Chemistry, 2008. **86**: p. 590-599.

248.   Casper, C.L., et al., *Controlling surface morphology of electrospun polystyrene fibers: Effect of humidity and molecular weight in the electrospinning process.* Macromolecules, 2004. **37**(2): p. 573-578.

249.   Zhang, J.F. and J. Nie, *Transformation of complex internal structures of poly(ethylene oxide)/chitosan oligosaccharide electrospun nanofibers.* Polymer International, 2012. **61**(1): p. 135-140.

250.   Li, D. and Y.N. Xia, *Direct fabrication of composite and ceramic hollow nanofibers by electrospinning.* Nano Letters, 2004. **4**(5): p. 933-938.

251.   Xu, B., et al., *Non-linear elasticity of core/shell spun PGS/PLLA fibres and their effect on cell proliferation.* Biomaterials, 2013. **34**(27): p. 6306-6317.

252.   Moghe, A.K. and B.S. Gupta, *Co-axial electrospinning for nanofiber structures: Preparation and applications.* Polymer Reviews, 2008. **48**(2): p. 353-377.

253.   Yarin, A.L., *Coaxial electrospinning and emulsion electrospinning of core-shell fibers.* Polymers for Advanced Technologies, 2011. **22**(3): p. 310-317.

254. Zhang, Y.Z., et al., *Characterization of the surface biocompatibility of the electrospun PCL-collagen nanofibers using fibroblasts.* Biomacromolecules, 2005. **6**(5): p. 2583-2589.

255. Ravichandran, R., et al., *Poly(Glycerol Sebacate)/Gelatin Core/Shell Fibrous Structure for Regeneration of Myocardial Infarction.* Tissue Engineering Part A, 2011. **17**(9-10): p. 1363-1373.

256. Chakrapani, V.Y., et al., *Electrospinning of type I collagen and PCL nanofibers using acetic acid.* Journal of Applied Polymer Science, 2012. **125**(4): p. 3221-3227.

257. Zhang, Q., et al., *Characterization of polycaprolactone/collagen fibrous scaffolds by electrospinning and their bioactivity.* International Journal of Biological Macromolecules, 2015. **76**: p. 94-101.

258. Zang, J.T., et al., *Fabrication of Novel Scaffolds Containing Collagen-I/Polylactic Acid/Nanohydroxyapatite via Co-electrospinning Methods.* Chemical Research in Chinese Universities, 2010. **26**(4): p. 662-666.

259. Wei, K., et al., *Emulsion Electrospinning of a Collagen-Like Protein/PLGA Fibrous Scaffold: Empirical Modeling and Preliminary Release Assessment of Encapsulated Protein.* Macromolecular Bioscience, 2011. **11**(11): p. 1526-1536.

260. Park, J.S., et al., *Characterization and structure analysis of PLGA/collagen nanofibrous membranes by electrospinning.* Journal of Applied Polymer Science, 2012. **125**: p. E595-E603.

261. Lee, B.S., et al., *Anodic properties of hollow carbon nanofibers for Li-ion battery.* Journal of Power Sources, 2012. **199**: p. 53-60.

262. Hwang, T.H., et al., *Electrospun core-shell fibers for robust silicon nanoparticle-based lithium ion battery anodes.* Nano Letters, 2012. **12**(2): p. 802-7.

263. Du, P.F., et al., *TiO2/Nb2O5 core-sheath nanofibers film: Co-electrospinning fabrication and its application in dye-sensitized solar cells.* Electrochemistry Communications, 2012. **25**: p. 46-49.

264. Yang, H.F., C.R. Lightner, and L. Dong, *Light-Emitting Coaxial Nanofibers.* Acs Nano, 2012. **6**(1): p. 622-628.

265.   Liu, X., et al., *Hierarchical nanotubular titanium nitride derived from natural cellulose substance and its electrochemical properties.* Chem Commun (Camb), 2012. **48**(80): p. 9992-4.

266.   Elahi, F., et al., *Core-shell Fibers for Biomedical Applications-A Review.* J Bioeng Biomed Sci, 2013. **3**(1): p. 21.

267.   Yarin, A.L., S. Koombhongse, and D.H. Reneker, *Bending instability in electrospinning of nanofibers.* Journal of Applied Physics, 2001. **89**(5): p. 3018-3026.

268.   Qu, H.L., S.Y. Wei, and Z.H. Guo, *Coaxial electrospun nanostructures and their applications.* Journal of Materials Chemistry A, 2013. **1**(38): p. 11513-11528.

269.   Kurban, Z., et al., *A Solution Selection Model for Coaxial Electrospinning and Its Application to Nanostructured Hydrogen Storage Materials.* Journal of Physical Chemistry C, 2010. **114**(49): p. 21201-21213.

270.   Wannatong, L., A. Sirivat, and P. Supaphol, *Effects of solvents on electrospun polymeric fibers: preliminary study on polystyrene.* Polymer International, 2004. **53**(11): p. 1851-1859.

271.   Yi, F. and D.A. Lavan, *Poly(glycerol sebacate) nanofiber scaffolds by core/shell electrospinning.* Macromolecular Bioscience, 2008. **8**(9): p. 803-806.

272.   Zilberman, M., K.D. Nelson, and R.C. Eberhart, *Mechanical properties and in vitro degradation of bioresorbable fibers and expandable fiber-based stents.* Journal of Biomedical Materials Research Part B-Applied Biomaterials, 2005. **74B**(2): p. 792-799.

273.   Yuan, X.Y., A.F.T. Mak, and K.D. Yao, *In vitro degradation of poly(L-lactic acid) fibers in phosphate buffered saline.* Journal of Applied Polymer Science, 2002. **85**(5): p. 936-943.

274.   Mogosanu, D.E., et al., *Fabrication of 3-dimensional biodegradable microfluidic environments for tissue engineering applications.* Materials & Design, 2016. **89**: p. 1315-1324.

275.   Choi, C.C., et al., *Flexible optical waveguide film fabrications and optoelectronic devices integration for fully embedded board-level*

optical interconnects. Journal of Lightwave Technology, 2004. **22**(9): p. 2168-2176.

276.   Lee, S.W. and S.S. Lee, *Shrinkage ratio of PDMS and its alignment method for the wafer level process.* Microsystem Technologies-Micro-and Nanosystems-Information Storage and Processing Systems, 2008. **14**(2): p. 205-208.

277.   Moraes, C., Y. Sun, and C.A. Simmons, *Solving the shrinkage-induced PDMS alignment registration issue in multilayer soft lithography.* Journal of Micromechanics and Microengineering, 2009. **19**(6).

278.   Eddings, M.A., M.A. Johnson, and B.K. Gale, *Determining the optimal PDMS-PDMS bonding technique for microfluidic devices.* Journal of Micromechanics and Microengineering, 2008. **18**(6).

279.   Samel, B., M.K. Chowdhury, and G. Stemme, *The fabrication of microfluidic structures by means of full-wafer adhesive bonding using a poly(dimethylsiloxane) catalyst.* Journal of Micromechanics and Microengineering, 2007. **17**(8): p. 1710-1714.

280.   Ryu, W., et al., *The construction of three-dimensional micro-fluidic scaffolds of biodegradable polymers by solvent vapor based bonding of micro-molded layers.* Biomaterials, 2007. **28**(6): p. 1174-1184.

281.   Tsao, C.W. and D.L. DeVoe, *Bonding of thermoplastic polymer microfluidics.* Microfluidics and Nanofluidics, 2009. **6**(1): p. 1-16.

282.   Yu, W., et al., *A microfluidic-based multi-shear device for investigating the effects of low fluid-induced stresses on osteoblasts.* Plos One, 2014. **9**(2): p. e89966.

283.   Grayson, W.L., et al., *Effects of initial seeding density and fluid perfusion rate on formation of tissue-engineered bone.* Tissue Eng Part A, 2008. **14**(11): p. 1809-20.

284.   Shahin, K. and P.M. Doran, *Strategies for enhancing the accumulation and retention of extracellular matrix in tissue-engineered cartilage cultured in bioreactors.* Plos One, 2011. **6**(8): p. e23119.

285.   Lu, H., et al., *Microfluidic shear devices for quantitative analysis of cell adhesion.* Anal Chem, 2004. **76**(18): p. 5257-64.

286. Tanaka, Y., et al., *Evaluation of effects of shear stress on hepatocytes by a microchip-based system.* Measurement Science and Technology, 2006. **17**(12): p. 3167-3170.

287. Ostrowski, M.A., et al., *Microvascular Endothelial Cells Migrate Upstream and Align Against the Shear Stress Field Created by Impinging Flow.* Biophysical Journal, 2014. **106**(2): p. 366-374.

288. Cheung, P., K. Toda-Peters, and A.Q. Shen, *In situ pressure measurement within deformable rectangular polydimethylsiloxane microfluidic devices.* Biomicrofluidics, 2012. **6**(2).

289. Fuerstman, M.J., et al., *The pressure drop along rectangular microchannels containing bubbles.* Lab on a Chip, 2007. **7**(11): p. 1479-1489.

290. Morris, C.J. and F.K. Forster, *Oscillatory flow in microchannels - Comparison of exact and approximate impedance models with experiments.* Experiments in Fluids, 2004. **36**(6): p. 928-937.

291. Anderson, J.M., *Biological Responses to Materials.* Annual Review of Materials Research, 2001. **31**(1): p. 81-110.

292. Muller, U., *In vitro biocompatibility testing of biomaterials and medical devices.* Med Device Technol, 2008. **19**(2): p. 30, 32-4.

293. Cao, T., et al., *Comparison of different test models for the assessment of cytotoxicity of composite resins.* J Appl Toxicol, 2005. **25**(2): p. 101-8.

294. (ISO), T.I.O.f.S. *ISO 10993-5: Biological evaluation of medical devices - Tests for in vitro cytotoxicity*. 2009 [cited 2016 October]; Available from: https://www.iso.org/obp/ui/#iso:std:iso:10993:-5:ed-3:v1:en.

295. Cao, Y., et al., *Human adipose tissue-derived stem cells differentiate into endothelial cells in vitro and improve postnatal neovascularization in vivo.* Biochemical and Biophysical Research Communications, 2005. **332**(2): p. 370-379.

296. Jaafar, I.H., et al., *Improving fluorescence imaging of biological cells on biomedical polymers.* Acta Biomaterialia, 2011. **7**(4): p. 1588-1598.

297.   Chan, B.P. and K.W. Leong, *Scaffolding in tissue engineering: general approaches and tissue-specific considerations.* Eur Spine J, 2008. **17 Suppl 4**: p. 467-79.

298.   Kulig, K.M. and J.P. Vacanti, *Hepatic tissue engineering.* Transpl Immunol, 2004. **12**(3-4): p. 303-10.

299.   Hammond, J.S., I.J. Beckingham, and K.M. Shakesheff, *Scaffolds for liver tissue engineering.* Expert Review of Medical Devices, 2006. **3**(1): p. 21-27.

300.   Caliari, S.R. and J.A. Burdick, *A practical guide to hydrogels for cell culture.* Nature Methods, 2016. **13**(5): p. 405-414.

301.   Overman, J.R., et al., *Growth factor gene expression profiles of bone morphogenetic protein-2-treated human adipose stem cells seeded on calcium phosphate scaffolds in vitro.* Biochimie, 2013. **95**(12): p. 2304-13.

302.   Naaijkens, B.A., et al., *Human platelet lysate as a fetal bovine serum substitute improves human adipose-derived stromal cell culture for future cardiac repair applications.* Cell and Tissue Research, 2012. **348**(1): p. 119-130.

303.   Quinn, K.P., et al., *Quantitative metabolic imaging using endogenous fluorescence to detect stem cell differentiation.* Scientific Reports, 2013. **3**.

Curriculum Vitae

Diana-Elena Mogosanu

Education

2011 - 2016

PhD candidate in Biomedical Engineering, Ghent University, Belgium;
- Thesis: "Three-dimensional fluidic microsystems for cell culturing and tissue engineering".

A1 publications:

- ✓ Mogosanu, D.E., Verplancke, R., Dubruel, P. & Vanfleteren, J. (2016). Fabrication of 3-dimensional biodegradable microfluidic environments for tissue engineering applications. *Materials & Design*, 89, 1315-1324.

- ✓ Navarro, L., Mogosanu, D.E., de Jong, T., Bakker, A.D., Schaubroeck, D., Luna, J., Rintoul, I., Vanfleteren, J. & Dubruel, P. (2016). Poly(polyol sebacate) elastomers as coatings for metallic coronary stents. *Macromolecular Bioscience*.

Conferences:

- ✓ Mogosanu, D.E., Verplancke, R., Vanfleteren, J., Navarro, L. & Dubruel, P. (2015). Integration of membranes in 3-D biodegradable and biocompatible microfluidic bioreactors. **In**: *2nd International conference on Biomedical Engineering and Systems (ICBES 2015)*, Barcelona, Spain.
- ✓ Navarro, L., Mogosanu, D.E., Schaubroeck, D., Vanfleteren, J. & Dubruel, P. (2015). Novel bio-elastomers as coating materials for

metallic coronary stents. **In**: *2015 Annual meeting of the Belgian Polymer Group (BPG 2015)*, Houffalize, Belgium.

- ✓ Mogosanu, D.E., Boon, R., Verfaillie, C., Vanfleteren, J. & Dubruel, P. (2014). Biodegradable poly(polyol sebacate)/PLLA core/shell fiber scaffolds for liver tissue growth. **In**: *Conference on Advanced Materials for Biomedical Applications (AMBA 2014)*, Ghent, Belgium.

- ✓ Mogosanu, D.E., Vanfleteren, J. & Dubruel, P. (2014). Towards an implantable bioreactor: synthesis and surface modification strategy for a soft tissue engineered elastomer. **In**: *26th Annual conference of the European Society for Biomaterials*, Liverpool, UK.

Book chapters:

- ✓ Mogosanu, D.E., Giol, E.D., Vandenhaute, M., Dragusin, D.M., Samal, S.K. & Dubruel, P. (2014). Polyester biomaterials for regenerative medicine. **In**: Cao, S. & Zhu, H. eds. *The design, synthetic strategies and biocompatibility of polymer scaffolds for biomedical application.* Bentham Science.

- ✓ Cama, G., Mogosanu D.-E., Houben A., Dubruel P. (2016), *Synthetic biodegradable medical polyesters: Poly-ε-caprolactone*, **In** *Science and Principles of Biodegradable and Bioresorbable Medical Polymers*, Z. Xiang, Editor 2016, Woodhead Publishing.

2009 - 2011
Master's degree in Chemical Engineering, Politehnica University of Bucharest, Romania; Specialization in Pharmaceutical and Cosmetic Products;

A1 Publications:
- ✓ Chifriuc, C., Lazar, V., Bleotu, C., Calugarescu, I., Grumezescu, A. M., Mihailescu, D. E., Mogosanu, D.-E., Buteica, A. S, Buteica, E.*,* (2011), "Bacterial adherence to the cellular and inert substrate in

the presence of CoFe2O4 and Fe3O4 oleic acid-core shell", *Digest Journal of Nanomaterials and Biostructures*, Vol 6, No 1, January-March 2011, p.37-42.

✓ Grumezescu, A. M., Mihaiescu, D. E., Mogosanu, D. E., Chifiriuc, M. C., Lazar, V., Calugarescu, I., Traistaru, V., (2010) "In vitro assay of the antimicrobial activity of Fe3O4 and CoFe2O4 / oleic acid – core/shell on clinical isolates of bacterial and fungal strains", Journal of Optoelectronics and Advanced Materials, vol. 4, November 2010, p. 1798-1801.

✓ Mihaiescu, D. E., Grumezescu, A. M., Mogosanu, D.-E., Traistaru, V., Balaure, P. C., Buteica, A., (2011), "Hybrid organic/inorganic nanomaterial for controlled cephalosporins release", Biointerface Research in Applied Chemistry **-** Open Acces Journal, ISSN 2069-5837, *Volume 1, Issue 2, 2011, 041-047*

2005 – 2009
Bachelor in Chemical Engineering, Politehnica University of Bucharest, Romania; Specialization in Macromolecular compounds;

Experience

2011 – 2016
PhD Candidate, Researcher
Ghent University

2010 – 2011
Chemical Engineer, R&D department
Biotehnos SA, Otopeni-Bucharest, Romania

2009 – 2010
Chemical Engineer, Sales Department
Analytic Jena Romania, Bucharest, Romania